ISSN 1410-1675

BULLETIN OF THE MARINE GEOLOGY

VOLUME 38 • NUMBER 1 • JUNE 2023

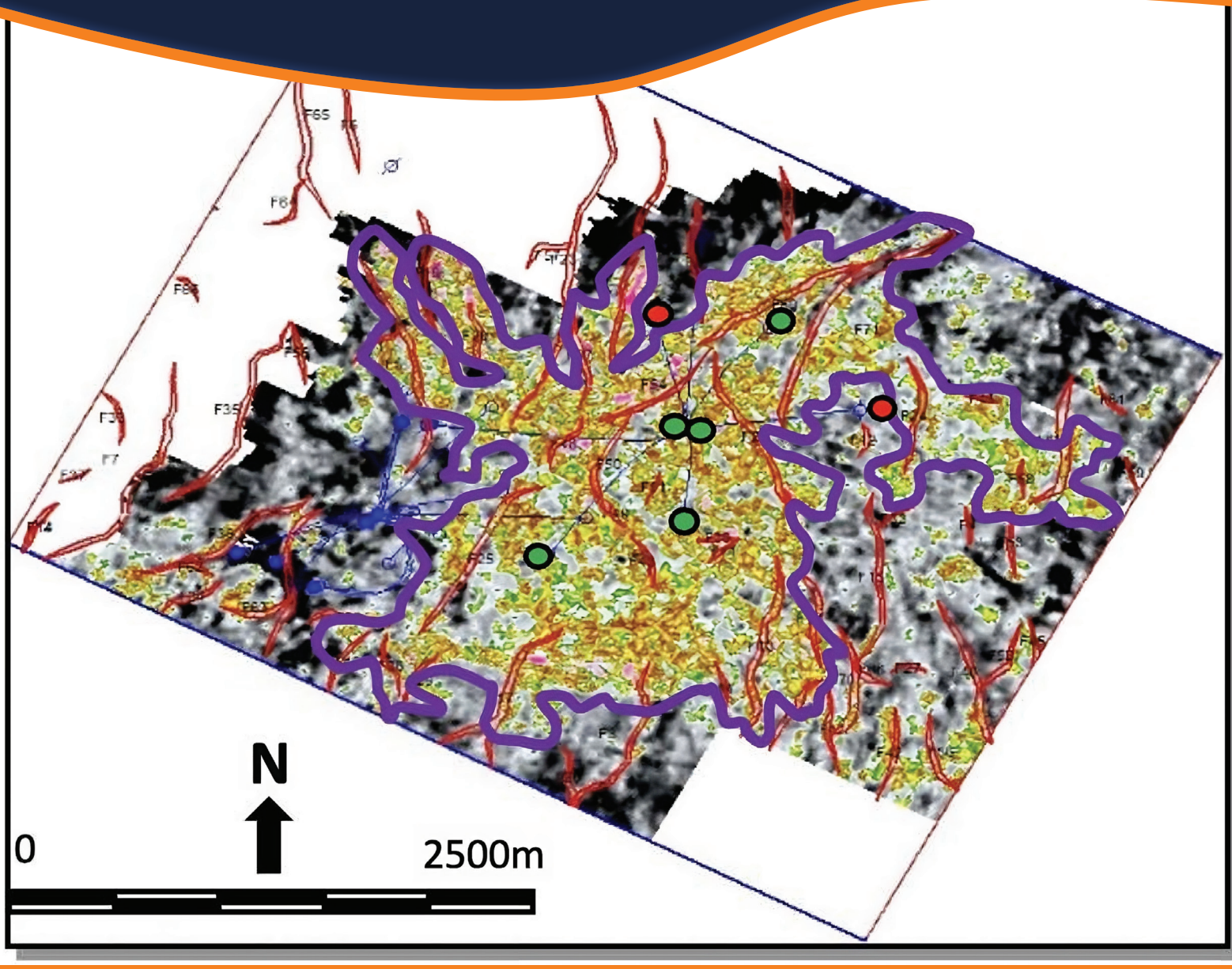

BoMG	VOL. 38	NO. 1	PAGE 1-53	BANDUNG, JUNE 2023	ISSN 1410-6175

Accredited : RISTEK-BRIN 200/M/KPT/2020

MARINE GEOLOGICAL INSTITUTE
GEOLOGICAL AGENCY
MINISTRY OF ENERGY AND MINERAL RESOURCES

BALAI BESAR SURVEI DAN PEMETAAN GEOLOGI KELAUTAN
BADAN GEOLOGI
KEMENTERIAN ENERGI DAN SUMBER DAYA MINERAL

BULLETIN OF THE MARINE GEOLOGY

Vol. 38, No. 1, June 2023

For communication of this publications, please contact :
MARINE GEOLOGICAL INSTITUTE
Dr. Junjunan 236, Bandung-40174, Indonesia
Telephone : +62-22-6032020, 6032201, Fax : +62-22- 6017887
E-mail : ejournal.p3gl@gmail.com

Cover Figure : Gravity Anomaly map overlaid on topography map of central Java (Source: Gravity data from Topex Satellite and Center for Geological Survey, Geological Agency, 2022, and Topography data from Demnas, 2022)

Preface

As the government institution for marine field survey, the Marine Geological Institute (MGI), Ministry of Energy and Mineral Resources, Indonesia, proudly presents the first publication in the year 2023 of the Bulletin of Marine Geology, Vol. 38, No. 1. The journal's scope is intended to accommodate a wide range of ideas and their scientific applications in marine geological investigation, including groundwork, fact-finding, experimentation, and exploration.

In this volume, we cover some issues regarding potential energy estimation from the OTEC system, an implementation of sidescan sonar in cable power installation, and some topics related to oil and gas reservoirs. These topics expand from the development of low resistivity for delineating reservoirs in Asri Basin to another noteworthy interpretation of Asri Basin from gravity modeling, in addition to reservoir identification based on seismic inversion at the East Lengo well.

We value the significant contributions from our outstanding authors, ranging from academics and students from Diponegoro University, Padjadjaran University, and University of Lampung, as well as professionals from Pertamina Hulu Energi Offshore Southeast Sumatra (PHE OSES) and MGI. We anticipate that their knowledge-sharing will be beneficial in advancing marine science and its implementation.

Chief Editor

ISSN 1410-6175

BULLETIN OF THE MARINE GEOLOGY

Vol. 38, No. 1, June 2023

Contents

POTENTIAL OF OCEAN THERMAL ENERGY CONVERSION (OTEC) IN THE NORTH WATERS OF LEMBATA, NTT

POTENSI KONVERSI ENERGI TERMAL LAUTAN DI PERAIRAN UTARA LEMBATA, NTT

Gisela Malya Asoka Anindita[1*], Denny Nugroho Sugianto[1], and Yani Permanawati[2]

[1] Department of Oceanography. Faculty of Fishery and Marine Science, Diponegoro University, Jl. Prof. H. Sudarto, Tembalang, Semarang

[2] Marine Geological Institute of Indonesia, Jl. Dr. Junjunan no.236, Bandung

*Corresponding author: malyaanindita8@gmail.com

(Received 03 November 2022; in revised from 11 November 2022; accepted 10 February 2023)

DOI : 10.32693/bomg.38.1.2023.789

ABSTRACT: Ocean thermal energy conversion is an attempt to convert potential energy in the variances heat content of seawater into other energy by utilizing the temperature change between the sea surface and deep sea at least 20°C. The Lembata waters is near to the equator, sea surface temperature tends to be warm and stable. This research was conducted to estimate the potential energy generated from a closed cycle OTEC system in North Lembata Waters. This study used temperature data from Global Ocean Physics Reanalysis from Copernicus Marine Environment Monitoring Service (CMEMS) for 9 years (2012-2020) in 6 stations. Validation was performed using the primary CTD Lembata OTEC Team of the Marine Geological Institute (MGI). Temperature data validation results on the MSE (Mean Square Error), RMSE (Root Mean Square Error), and MAPE (Mean Absolute Percentage Error) methods are considered to represent field temperature conditions. The variability value shows the station point in the North Lembata Waters has a temperature with slight differences. The vertical temperature change (ΔT) shows between 20.98°C to 23.44°C. Potential electric power resulting from the OTEC system using the technical estimation formula. The average net power generated from those temperature gradients ranges from 5.65 MW-7.56 MW, respectively. The Lembata waters have temperature conditions suitable for OTEC installations. Station C-4 has a power potential of 6.84 MW with a depth of 763 m and the distance of 1.86 km from the coastline. Station C-4 in the Omesuri sub-district is the best point for OTEC installation in North Lembata Waters.

Keywords: potential energy, seawater temperature, OTEC, Lembata

ABSTRAK: *Konversi energi termal lautan merupakan upaya untuk mengubah energi potensial berupa perbedaan kandungan panas/bahang air laut menjadi bentuk energi yang lain dengan memanfaatkan perbedaan suhu antara permukaan laut dan laut dalam minimal 20°C. Perairan Lembata dekat dengan garis ekuator sehingga suhu permukaan air laut cenderung hangat dan stabil. Penelitian ini dilakukan untuk memperkirakan energi potensial yang dapat dihasilkan dari sistem OTEC siklus tertutup, jika sistem tersebut dipasang di Perairan Lembata Utara. Studi ini menggunakan Global Ocean Physics Reanalysis dari data suhu Copernicus Marine Environment Monitoring Service (CMEMS) selama 9 tahun (2012-2020) dari 6 stasiun dan divalidasi menggunakan data primer CTD yang diambil oleh Tim OTEC Lembata P3GL. Hasil verifikasi data suhu pada metode MSE (Mean Square Error), RMSE (Root Mean Square Error), dan MAPE (Mean Absolute Presentage Error) dinilai dapat merepresentasikan kondisi suhu lapangan. Nilai variabilitas suhu menunjukan bahwa titik stasiun di Perairan Utara Lembata memiliki suhu dengan perbedaan yang kecil. Perbedaan suhu air laut hangat dan dingin (ΔT) berkisar 20,98°C-23,44°C. Potensi daya listrik yang dihasilkan dari sistem OTEC telah diestimasi menggunakan rumus estimasi teknis. Daya Bersih rerata yang dapat dihasilkan berkisar antara 5,65 MW-7,56 MW. Perairan Lembata diketahui memiliki perairan dengan kondisi suhu yang sesuai untuk instalasi OTEC. Stasiun C-4 memiliki potensi daya sebesar 6,84 MW pada kedalaman laut 763 m dan jarak dengan garis pantai sejauh 1,86 km. Stasiun C-4 yang terletak di kecamatan Omesuri merupakan titik terbaik untuk instalasi OTEC di Perairan Utara Lembata.*

Kata Kunci: *energi potensial, suhu air laut, OTEC, Lembata*

INTRODUCTION

Data from British Petroleum (2021) states that in 2020 the use of fossil energy in Indonesia will reach 93% with the use of coal energy (40%), oil (35%), and natural gas (18%). Although the increasing demand for public energy causes reserves of fossil energy sources to dwindle, the Ministry of Energy and Mineral Resources press release number: 311.pers/04/SJI/2020 said that efforts need to be made to maintain Indonesia's energy availability in the future, it is necessary to shift the use of fossil energy to New and Renewable Energy (NRE) and Clean Energy.

Indonesia has several energy potentials; one of the potentials for clean energy is marine energy. Yosi (2014) states that the energy that can be utilized from the sea includes ocean currents, wave energy, energy due to differences in water levels due to tides, microalgae as biodiesel, and Ocean Thermal Energy Conversion (OTEC). Some energy experts stated that the optimal use of OTEC can generate billions of watts of electrical power (Vega, 1992; Bassam et al., 2013; Syamsuddin et al., 2015; Ilahude et al., 2020). Theoretically, OTEC generates electricity indirectly from solar energy by utilizing a temperature difference of at least 20°C between the sun-warmed tropical ocean surface and calmer deep waters (Masutani and Takahashi, 2001).

The tropics always get solar heating with relatively warm and stable surface temperatures throughout the year. Lembata Island is one of the tropical areas that have the potential to use OTEC. These waters are located in the eastern part of the Flores Sea and the southwest of the Banda Sea. These waters influence the Indonesian Throughflow (ITF) and monsoon currents from the Makassar Strait. ITF has a temperature heat transported around 0°C - 4°C (Vranes et al., 2002), which can be used as an intake for cold seawater for the OTEC system in North Lembata Waters.

The morphology of the seabed in the northern waters of Lembata cannot be separated from the influence of marine geological processes. One of the effects of geological settings on oceanographic conditions causes the Indonesia Throughflow (ITF) to branch into the Indian Ocean due to the morphology of the seabed in the southern part of the Makassar Strait, the Dewakang Threshold at 680 m (Gordon et al. 2003; Atmadipoera et al. 2016). The Dewakang threshold is the barrier between the East and west canals. The condition of the Lembata waters is that one branch of the Indonesia throughflow (ITF) from the eastern canal to the Flores Sea, then the Banda Sea and exits the Timor Sea and Ombai Strait, while the other branch flows through the western canal and then to the Lombok Strait (Susanto et al. 2012; Radjawane and Hadipoetranto. 2014); Permanawati et al. 2016). The northern waters of Lembata, like waters in the tropics, are influenced by the monsoon system due to the change of seasons, so it shows that the circulation of surface layer currents occurs twice a year in the opposite direction. Therefore, under certain conditions, there are times when the mass of water from the Flores Sea meets the mass of water that comes out of the Makassar Strait and flows together into the Java Sea due to changing seasons (Ilahude & Gordon 1996; Gordon 2005; Permanawati et al. 2016).

Previous research conducted by Tim OTEC Lembata. (2017) stated that the northern waters of Lembata are generally quite deep, with a depth of 1000 meters, only about 3-7 km from the coastline. The maximum temperature is 29.48°C on the surface and a minimum of 3.58°C at a depth of 1000 m, ranging from 20.39 – 25.30°C. The temperature difference can be used to construct OTEC by calculating the gross power with the Nihous equation (2007) ranging from 1.34-0.88 MW, assuming a large cold water discharge of 2 m^3/s. OTEC analysis in Lembata waters has also been carried out by Julianto (2020) using the assumption of an open cycle OTEC that produces 2.5 MW of electrical power with a location point distance of 3 km from a coastline and a depth of 900 m.

This study will examine the potential of OTEC in the northern waters of Lembata, East Nusa Tenggara, using the Vega design (2002) through closed-cycle OTEC calculations based on the Nihous study (2007) by adjusting the value of warm water flow rate and cold water flow rate for a capacity of 5 MW. First, the condition of the waters is assessed by considering the fundamental aspects of the provisions in determining the installation location to have all concept definitions for the design of the OTEC system (Vega and Michelis, 2010; Morales et al., 2014). These primary conditions include the following aspects:

1. Sea surface temperature of at least 26 °C (annual average), in the range of 24°C - 28°C.
2. Deep sea temperature at a depth of approximately 1000 m (annual average), in the range of 4 °C - 5°C.
3. Steep topographic slope (15-20°) towards the high seas and relatively smooth seabed.
4. Significant wave height of up to 6 m (9,6 second period), wind speed of 20 m/s, and sea surface current of fewer than 1,5 m/s.
5. The probability of earthquakes, tropical storms, and other natural disasters is relatively low

CMEMS (Copernicus Marine Environment Monitoring Service) data is the GLOBAL_MULTIYEAR_PHY_001_030 which has a resolution of 1/12° (approximately 8 km) at 50 depth levels. The temperature model data is validated using the MSE, RMSE, and MAPE methods to compare values between the three methods so that validation will be more accurate. In addition, the CMEMS temperature data has a more detailed correction value than the HYCOM model, so it becomes the author's basis for using the temperature data model.

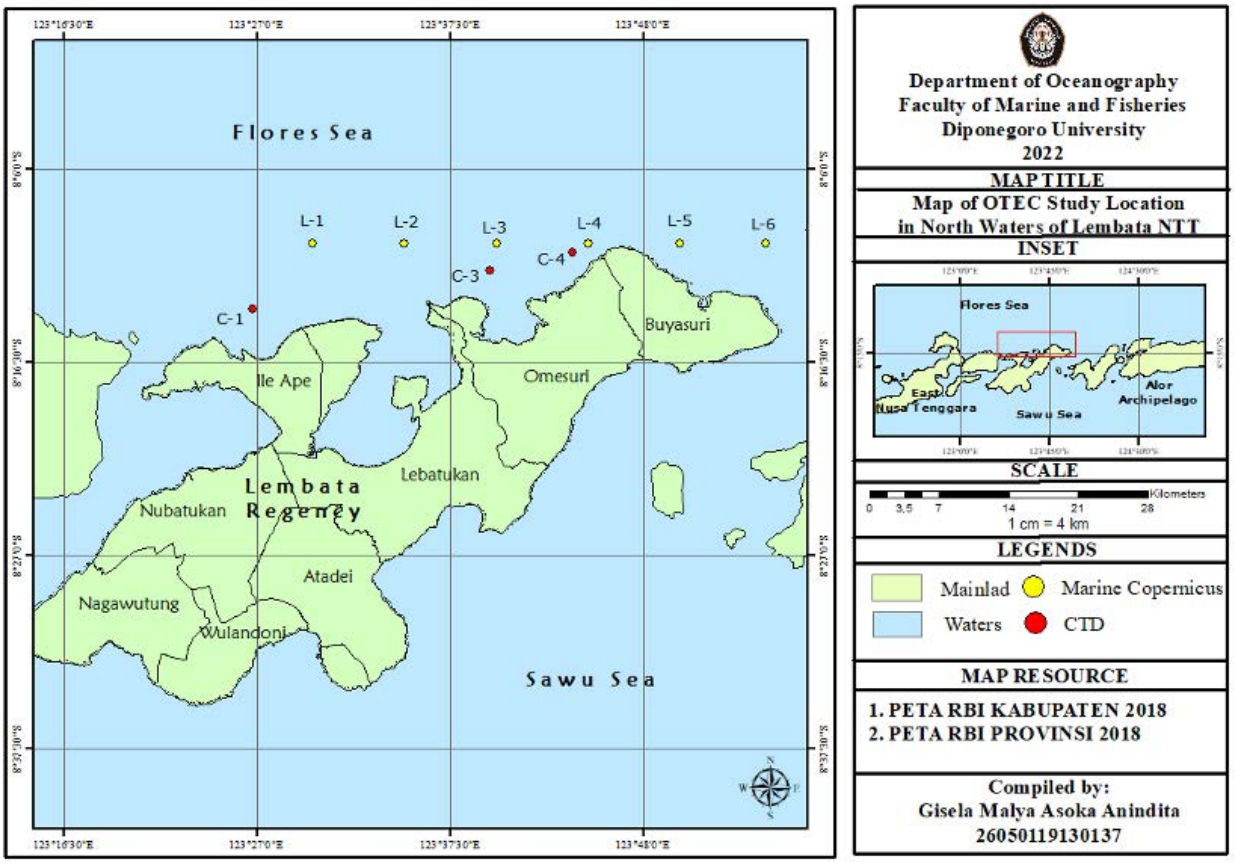

Figure 1. Map of OTEC Study Location

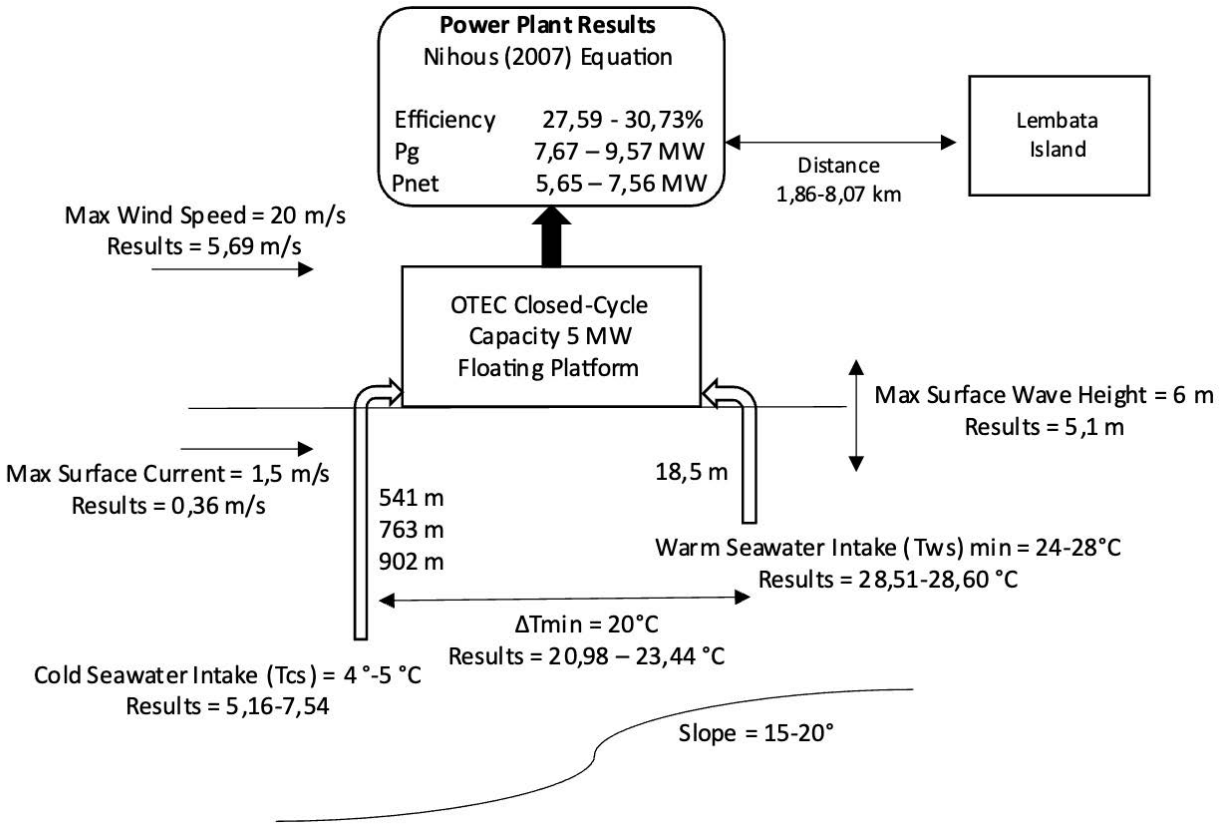

Figure 2. Graphical abstract in determining the installation location for OTEC system design

A study on the potential for Ocean Thermal Energy Conversion (OTEC) installations in the northern waters of Lembata, East Nusa Tenggara, needs to be carried out because there is yet OTEC research that examines the ideal station installation according to primary conditions of the waters including oceanographic conditions. Therefore, the study was carried out in the waters of Lembata Island, which is located at positions 8°10' - 8°11' S and 123°12' - 123°57' E through an analysis of six stations that are considered representative of the North Lembata waters (Figure 1). Figure 2 provides a graphical abstract for this study.

METHODS AND MATERIAL

The material used in the research consists of primary data sources, which are field temperature data and models, as well as secondary data used to support data processing. Temperature field data was taken with the Conductivity Temperature Depth (CTD) Sea-Bird Electronic (SBE) 19 Plus V2 instrument obtained from a survey conducted by the Marine Geological Institute (MGI) by the OTEC Team, Marine Energy Research and Development Group 2017 in the North Waters of Lembata. The vertical temperature model data for CMEMS Global Ocean Physics Reanalysis GLOBAL_MULTIYEAR_PHY_001_030 is downloaded on the website https://marine.copernicus.eu. Secondary data used in the research include the Indonesian Earth Map, bathymetry data from BATNAS BIG 2022, surface current data from CMEMS Global Ocean Physics Reanalysis GLOBAL_MULTIYEAR_PHY_001_030, Ocean significant wave data from Global Ocean Waves Reanalysis WAVERYS GLOBAL_MULTIYEAR_WAV_001_032, and wind data from ERA5 ECMWF Reanalysis.

Temperature Data Validation

Analysis of the accuracy of the field data processing results can be seen in the percentage value by calculating the relative error value.

$$MSE = \frac{\sum_{i=1}^{n}(X_{obs\,i} - X_{model\,i})^2}{n} \quad \text{.....(1)}$$

Ichsari et al. (2020) write that if the percentage value of the error results is small and the comparison of processing data is close to field data, it can be said that the processing results provide an overview of the actual situation in the field. Mignac et al. (2015) have validated the model temperature data with field data using RMSE, and the equation is as follows:

$$RMSE = \sqrt{\frac{\sum_{i=1}^{n}(X_{obs\,i} - X_{model\,i})^2}{n}} \quad \text{.....(2)}$$

Where:
$X_{obs\,i}$ is the value of the observation data,
$X_{model\,i}$ is the value of the model data,
i is the data-, and
n is the number of data.

Testing the accuracy of the model data can also be done using Mean Absolute Percent Error (MAPE). The equation can be calculated by:

$$MAPE = \sum_{t=1}^{n} \left| \frac{Xt - Ft}{Xt} \right| \left(\frac{100\%}{n}\right) \quad \text{.....(3)}$$

Where:
MAPE in presentage (%)
n the amount of data,
Xt is the actual result value, and
Ft is the forecast value

The lower the MAPE value, the better the ability of the forecasting model. According to Lewis (1982), the range of MAPE values can be seen in Table 1.

Table 1. Range of MAPE method by Lewis (1982)

Range MAPE	Interpretation
< 10 %	Highly accurate forecasting
10 - 20 %	Good forecasting
20 - 50 %	Reasonable forecasting
> 50 %	Inaccurate forecasting

Calculation of Temperature Variability

The study of temperature variability at a depth of OTEC water intake in warm and cold water was carried out by analyzing the standard deviation of the monthly average temperature for 9 years at each station as in the study conducted by Suprijo et al. (2021). The study stated that a high standard deviation indicates the area's high variation and low-temperature stability. Areas with high-temperature variations are unsuitable for OTEC installations as they can generate unstable power and may eventually not reach the minimum OTEC thermal resource requirements. The equation calculating the standard deviation of the warm water and cold water intake temperature in the study was taken at a depth of 18.5 m and a maximum depth of each station with a depth limit of 902 m. The equation is below:

$$SD = \sqrt{\frac{\Sigma x^2}{N}} \quad \text{.....(4)}$$

Where:
SD is the standard deviation,
Σx^2 is the total number of data squared, and
N is the number of data.

Efficiency and Power Plant Calculation

The calculation of the maximum thermodynamic efficiency for a Rankine cycle OTEC power system is described with technical estimation formula in Nihous (2007).

$$\mu = \frac{T_2 - T_1}{2(T_2 + 273)} \quad \text{.....(5)}$$

Where:

μ is the maximum thermodynamic efficiency

T_1 is the deep water temperature (°C)

T_2 is the sea surface temperature (°C)

Minor losses in the electrical conversion steps, such as mismatches in the expansion and compression of the working fluid, are considered to reduce the gross electrical power output, leading to gross OTEC conversion efficiency (α, in %)

$$\alpha = \varepsilon_{tg} \frac{\Delta T}{2T_2} \quad \text{..... (6)}$$

Where:

ε_{tg} is the efficiency of the turbogenerator with a value of 75%.

ΔT is the temperature difference between the sea surface and deep-sea temperature (°C)

T_2 is the sea surface temperature (°C)

The gross electric power (P_g) generated comes from the heat load of the evaporator and the thermodynamic efficiency, which the equation can calculate:

$$P_g = \frac{Q_{cw} \rho C_p 3\gamma \varepsilon_{tg}}{16(1+\gamma)T_2} \quad \text{..... (7)}$$

Where:

P_g~ Mega Watt (MW)

ρ~ 1025 kg/m^3 is the average density of seawater,

C_p~ 4 kJ/kg K is the specific heat of seawater, and

$\gamma = \frac{Q_{ww}}{Q_{cw}}$ is a ratio representing warm water's surface flow rate ($Q_{ww} = 26.4\, m^3/s$) and cold water flow rates ($Q_{cw} = 13.9\, m^3/s$). The surface flow rate of warm water is higher than the cold water flow rate to achieve performance according to the 5 MW capacity OTEC simulation. The fluid flow rate affects the performance improvement of the OTEC system, The values of Q_{ww} and Q_{cw} are used in the 5 MW OTEC system designed by Vega (2002). Furthermore, the net power (P_{net}) ~ megawatt (MW) is calculated by considering the required power consumption to drive a significant seawater flow rate through the OTEC generator ~30% of P_g with the design conditions ($\Delta T_{design} = 20$). The calculation can use the equation:

$$P_{net} = \frac{Q_{cw} \rho C_p \varepsilon_{tg}}{8T_2} \left\{ \frac{3\gamma}{2(1+\gamma)} \Delta T^2 \; - 0.18 \Delta T^2{}_{design} - 0.12 \frac{\gamma^{2.75}}{2} \Delta T_{design} \right. \quad \text{..... (8)}$$

The calculation formula in this study uses the equation belonging to Nihous (2007), which is also used in Morales' research (2014) on calculating OTEC power with a closed cycle system simulation.

RESULTS AND DISCUSSIONS

Temperature Data Validation

The model temperature data used is CMEMS (Copernicus Marine Environment Monitoring Service). Based on the results of the validation value, the data has a better value than the HYCOM model data. CMEMS GLOBAL_MULTIYEAR_PHY_001_030 data has a small regional bias value (less than 0.4 °C). Along the equator, the temperature profile is consistent with the observation data, with RMSD (Root mean square error) values generally less than 0.4 °C at the water column (Copernicus, 2021).

Table 2. Coordinate and Validation Results of CMEMS Data and CTD Data

CMEMS Station	Latitude	Longitude	CTD Station	Latitude	Longitude	MSE	RMSE	MAPE (%)	Distance (km)
C-1	-8.167	123.500	L-1	-8.227	123.445	0.67	0.82	2.53	8.79
C-2	-8.167	123.583	-	-	-	-	-	-	-
C-3	-8.167	123.667	L-3	-8.192	123.660	0.36	0.60	2.22	2.88
C-4	-8.167	123.750	L-4	-8.175	123.735	0.22	0.47	1.85	1.83
C-5	-8.167	123.833	-	-	-	-	-	-	-
C-6	-8.167	123.910	-	-	-	-	-	-	-

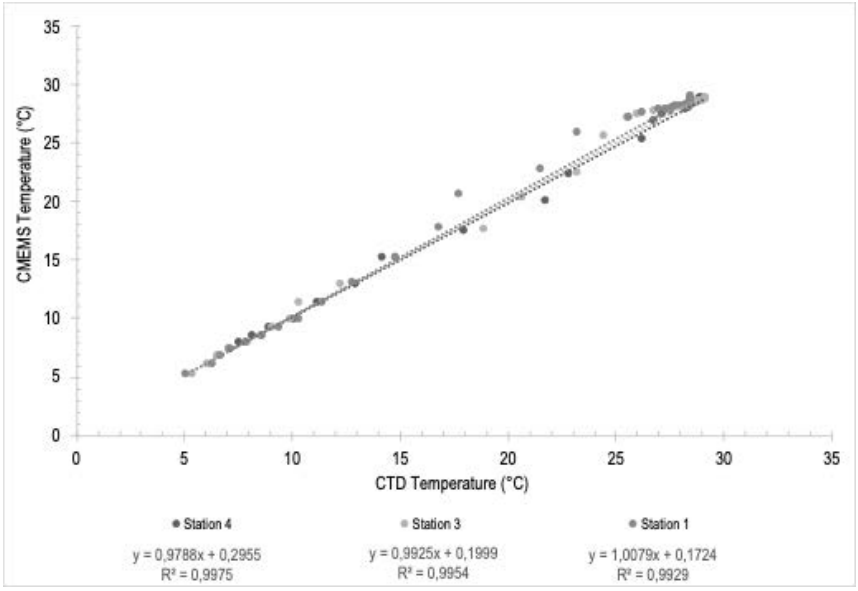

Figure 3. Correlation Between Temperature Copernicus and CTD

Validation of temperature data is carried out using the MSE (Mean Square Error), RMSE (Root Mean Square Error), and MAPE (Mean Absolute Percent Error) methods. These methods are used to measure the accuracy of the estimated results of the model data. Although validation is carried out with three station points, as seen in Table 2, the value of the results of the MSE and RMSE methods validation shows good enough results because the value is close to zero. The validation of the MAPE method produces a value of 1.85-2.53-3%, which is included in the very high accuracy category. Based on the validation values of the three methods, CMEMS model temperature data can represent field temperature data in North Lembata waters.

The graph of the correlation between the CMEMS and CTD temperature data at the three stations can be seen in Figure 2. Based on the figure, the relationship between the CMEMS temperature and the CTD temperature shows good results because the data distribution is close to a linear line.

Distribution of Vertical Temperature

The surface temperature of the CMEMS model primary daata, located at the northern waters Lembata has a range of 27-29.5 °C. This result is in accordance with the statement of Widyartono and Rahmadian (2019), which states that the temperature of surface seawater in the tropical ocean areas (coordinates between 15° N and 15° S) has a relatively constant temperature reaching the range of 28° C throughout the year. Seawater temperature tends to decrease with increasing depth; related to the reduction of sunlight intensity. The temperature characteristics described by Santoso (2005) can be influenced by topography or depth associated with sunlight penetration variability in each water layer. Based on data processing, sunlight penetration variability, directly adjacent to the Flores Sea and passed by the Indonesian Throughflow (ITF), is around 7°C at a 500 m water depth. This result similar with the statement of Raharjo (2011), which stated that Indonesian Throughflow (ITF) has a relatively constant cold seawater temperature (5°C -10°C). The distribution of vertical temperature profile is presented in Figure 4. The difference between warm and cold seawater temperatures in Lembata waters reaches 20°C at 550-600 m water depth, suggests the area is potential for OTEC installation locations.

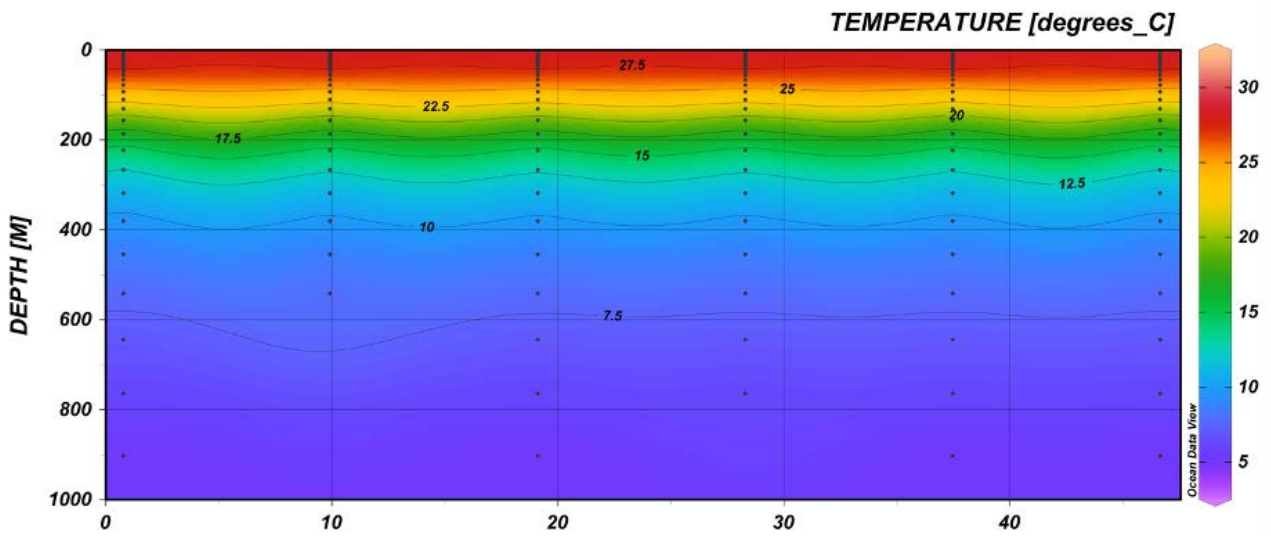

Figure 4. Distribution of Vertical Temperature

Temperature Variability of Warm Seawater and Cold Seawater

The temperature variability of warm seawater (Tws) and cold seawater (Tcs) is calculated to determine the temporal temperature change at each station. In this study, the warm seawater temperature is measured from 18.5 m water depth, while the cold seawater temperature is measured at the maximum depth of each station down to 902 m water depth. OTEC resources are sensitive to temperature changes. Therefore, it is essential to test the temperature variability to assess the feasibility of its implementation, as mentioned by Suprijo et al. (2021).

Tws variability values at each station ranged from 0.75-0.80, the highest variability value is at station C-6 with a value of 0.80 (table 3). The monsoon winds resulting the temperature variability of the warm seawater at the surface. During the East season, the easterly wind strength will increase. Stronger gusts of wind will make the turbulence in the surface layer more vital and can block sunlight penetration to the sea. Therefore, the seawater temperature during the East monsoon tends to be lower. Seawater temperature will decrease when the wind gusts are in contrast and increase when the wind gusts are weak. Cold seawater temperature variability tends to be small because monsoon winds do not affect the temperature in

Table 3. Tws and Tcs Variability from 2012-2020

Station	C-1	C-2	C-3	C-4	C-5	C-6
Tws Variability	0.75	0.76	0.77	0.78	0.79	0.80
Tcs Variability	0.06	0.16	0.06	0.09	0.06	0.06

Data source: primary data (CMEMS GLOBAL_MULTIYEAR_PHY_001_030)

the deep-sea layer—the deeper water layer, the smaller the external influence. The variability of Tcs ranged from 0.05 to 0.16; Seawater temperature will be more stable with increasing depth because it is not affected by external factors such as monsoon winds or anthropogenic activities. The value of temperature variability at each potential point in the northern waters of Lembata is quite suitable for OTEC installations because the variation value is low.

Carnot Efficiency and Potential of OTEC Power

The efficiency values and OTEC power potential of all stations are presented in Table 4 below,

which has the slightest temperature difference and efficiency. Although based on the data analysis in Table 4, the OTEC efficiency ranges from 27.28%-30.92%. This value is relatively low compared to the efficiency of other power plants.

The turbine used in the power calculation simulation in this study uses a capacity of 5 MW with the value of the warm seawater and the cold seawater rate from the Vega design (2002). The minimum requirement for temperature difference to run the OTEC system, according to Masutani and Takahashi (2001), is 20°C. In the northern water of Lembata, this delta T value can be achieved at 550 - 600 m water depth. This study's calculation of OTEC power uses

Table 4. Efficiency and Potential Power at North Lembata Waters

Station	Efficiency		Pg (MW)		Pnet (MW)	
	Min	Max	Min	Max	Min	Max
C-1	30.40%	30.88%	8.53	10.32	6.51	8.32
C-2	27.28%	27.79%	6.86	8.35	4.84	6.34
C-3	30.38%	30.88%	8.48	10.29	6.46	8.28
C-4	29.27%	29.88%	7.86	9.56	5.84	7.55
C-5	30.37%	30.86%	8.45	10.22	6.42	8.21
C-6	30.41%	30.92%	8.48	10.28	6.45	8.28

Data source: primary data (CMEMS GLOBAL_MULTIYEAR_PHY_001_030)

The calculation results of the monthly average efficiency of 2012-2020 have a maximum value of 30.92% at station C-6 and a minimum value of 27.28% at station C-2. The efficiency value relates to the temperature difference between warm and cold seawater (ΔT). The higher ΔT value, the greater the efficiency. This statement is evident from station C-6, which has the most significant temperature difference and efficiency, and station C-2,

the maximum depth of each station with a depth limit of 902 m. The calculation of the monthly average power from 2012-2020 in Table 4 shows that the Gross Electricity (Pg) production is the result of the evaporator heat load and thermodynamic efficiency with a maximum value of 10.28 MW at station C-6 and a minimum of 8.35 MW which is at station C-2. Nihous (2007) states that the net power calculation is estimated by considering the energy used to

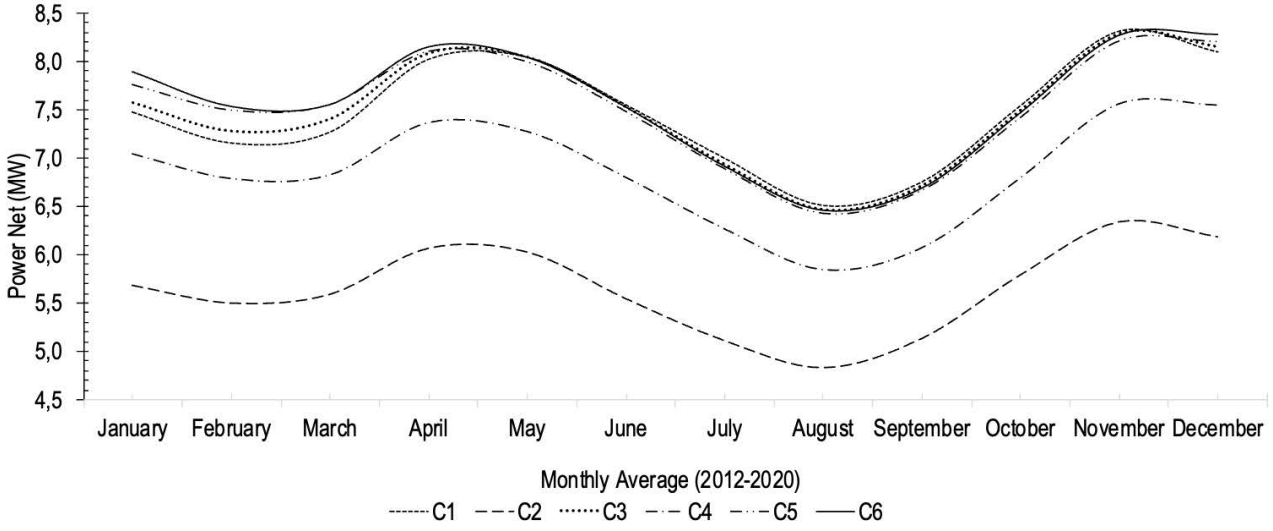

Figure 5. Monthly Average of Power Net 2012-2022

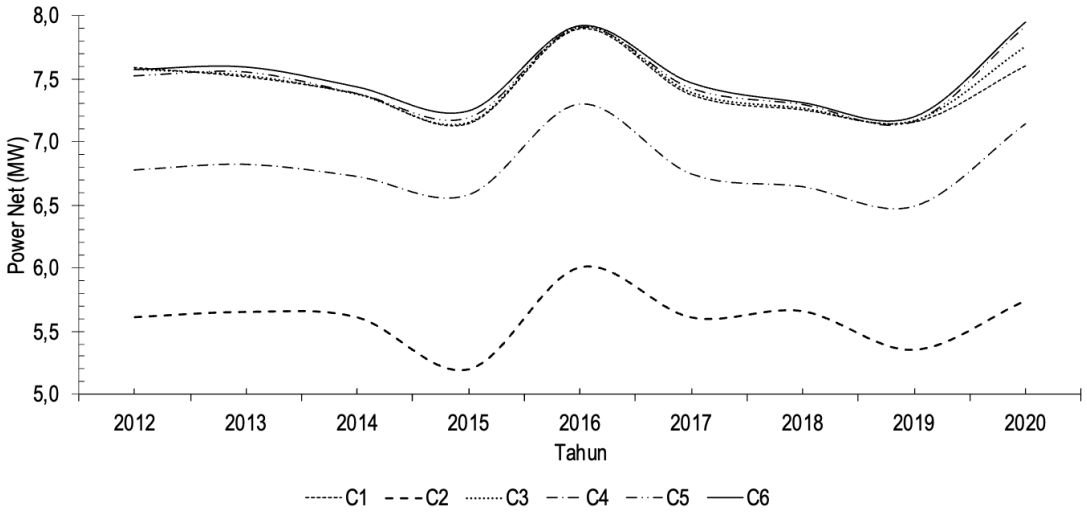

Figure 6. Annual Average of Power Net OTEC 2012-2020

run the OTEC system in pushing the large seawater flow through the OTEC system, as much as 30% of the gross power. Therefore, the maximum monthly average net power value (Pnet) is at station C-6, which is 8.28 MW, and the minimum monthly average is at station C-2, which is 4.84 MW. Figure 5 presents a graph of each station's monthly average OTEC net power for 2012-2020.

The power calculation results from 2012-2020 in Figure 6 show the power potential in the northern waters of Lembata temporally. The power potential decreased from 2012-2015, then rose again in 2016. Furthermore, the power potential decreased until 2019 and rose again in 2020. The largest power potential was in 2020, and the smallest was in 2015. The graph shows that the annual net power results did not significantly change for 9 years. The significant difference in the net power produced each year does not reach 1 MW, so it can be seen that the net power output in the North Lembata waters is relatively constant. These waters have potential in OTEC installations considering the conditions of temperature, depth, and the results of power calculations.

OTEC Installation Ideal Station

The potential point in the northern waters of Lembata Island has a fairly warm surface temperature and is relatively constant throughout the year with a range of 27.1 -29.6°C with cold sea water temperatures ranging from 5-7°C. Seawater temperature (ΔT) differences range from 20.97°C -23.44°C. According to the difference in temperature of warm seawater and cold seawater, North

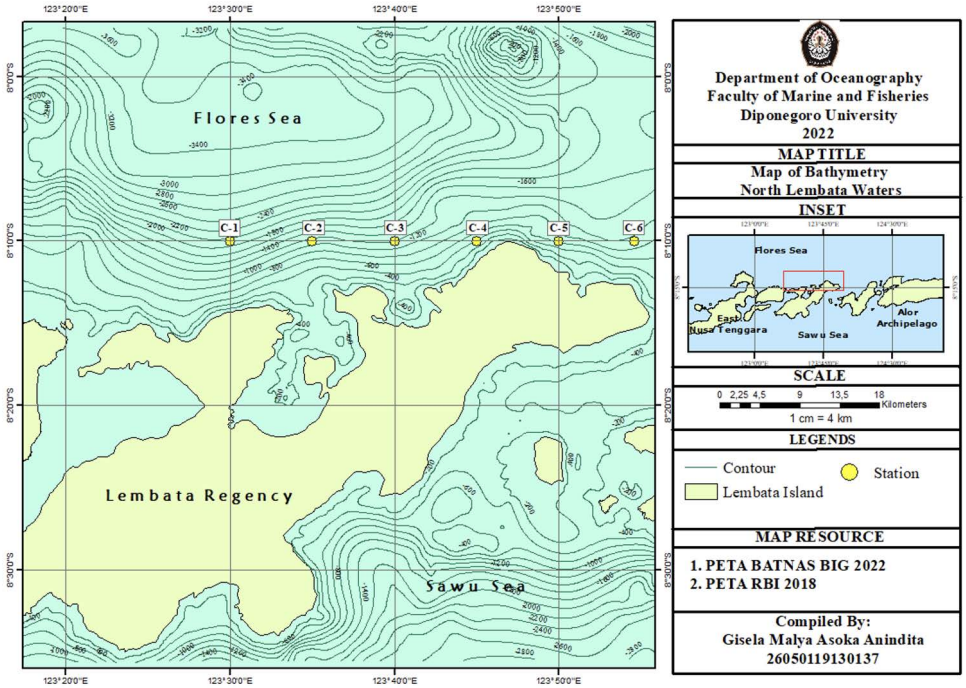

Figure 7. Map of Bathymetry Condition North of Lembata Waters

Lembata waters have great potential for utilizing the OTEC system, which has a minimum requirement of a temperature difference of 20°C.

In addition to temperature differences, the topographic slope is required to determine the appropriate location for installing the OTEC system. The topographical conditions of Lembata are mentioned in Permanawati and Hernawan's research (2018). The morphology of Lembata waters is included in the steep-very steep category, with a slope of 9-40°. Some water locations are sloping areas – slightly steep, with a slope below 9°, located around the bay area (Tim OTEC Lembata, 2017). The condition of the Lembata waters bathymetry can be seen in Figure 7. The topographical and morphological conditions in the waters are suitable for installing an OTEC system. The topography suitable for OTEC system installation is 15-20°.

Indonesia (BNPB, 2016), including earthquakes, tsunamis, and volcanic eruptions with low-risk levels in the Lembata area. Therefore, according to those parameter conditions mentioned above, the condition of the North Lembata Waters is considered to have potential in an OTEC installation it has all concept definitions for the design of the OTEC system, according to Vega and Michelis (2010) which are also mentioned in Morales et al. (2014).

The six potential station points in the northern waters of Lembata can reach the minimum requirements for the difference in warm seawater temperature and cold seawater temperature to operate the OTEC system. Table 6 displays data on potential stations for OTEC installations. Vega's design (2002) with a floating platform is an ideal OTEC system chosen in this research. The potential benefits of OTEC can only be recovered on a large scale through developing a sustainable floating-plant program.

Table 5. Maximum Surface Current, Wind, and Wave Data in North Lembata Waters 2012-2020

Parameter	Value
Maximum Surface Current	0.36 m/s
Maximum Wind Speed	5.69 m/s
Maximum Surface Wave Height	5.02 m

Data source: Secondary data (CMEMS GLOBAL_MULTIYEAR_PHY_001_030), Copernicus Reanalysis ERA 5, and Global Ocean Waves Reanalysis WAVERYS)

Table 6. Mean Data on Potential Stations for OTEC Installation

Station	ΔT (°C)	Efficiency (%)	Pnet (MW)	Max Depth(m)	Distance (km)
C-1	23.34	30.70	7.48	902	8.07
C-2	20.98	27.59	5.65	541	6.23
C-3	23.35	30.69	7.49	902	5.69
C-4	22.54	29.59	6.84	763	1.86
C-5	23.39	30.68	7.52	902	2.64
C-6	23.44	30.73	7.56	902	4.88

Oceanographic factors such as temperature, currents, and waves affect OTEC system installation. The temperature affects the OTEC system running, which utilizes the difference in surface and deep sea temperatures. Waves, wind, and currents affect the system's resistance to the surrounding aquatic environment, so a review is needed regarding the value of these parameters. Table 5 shows the processing of secondary data with the maximum values of currents, winds, and significant wave heights in the North Lembata waters. Based on the processing of wind, wave, and current data from 2012-2020, North Lembata waters have the highest significant wave height of 5.02 m and a maximum wind speed of 5.69 m/s. The most significant surface current among all station points is at station C-6, which reaches 0.36 m/s. These values are smaller than the maximum limit for the primary conditions of the OTEC installation.

Further studies are carried out by reviewing natural disasters in a study area. Rysnawati et al. (2017) stated that the level of vulnerability to earthquakes in Lembata Regency, NTT, was included in the low category. This statement in line with the map of disaster risk level in

Furthermore, an ideal station point is determined by calculating the distance of the point from the coastline, where the electricity is distributed, and the amount of net power generated under Julianto's statement (2020). If we consider the station that is closest to the shoreline, then station C-4 is the best option, with a depth of 763 m and power potential of 6.84 MW. The station with the highest net power value is station C-6, with a depth of 902 m with a power of 7.56 MW. The distance difference between the two stations is quite different. Station C-4 is 1.86 km away from the coastline, while station C-6 distance is 8.07 km away from the coast. The distance from the OTEC installation location to the coastline will affect the construction cost; as stated by Julianto (2020) and Morales et al. (2014), the closer the OTEC installation location to the coastline, the cost will be lower.

The warm seawater temperature of C-4 is between 27.15-29.55°C while the value of cold seawater temperature ranged between 5.89-6.18°C. The temperature difference (ΔT) at this station reaches the range of 21.19-23.47°C. The temperature value tends to be stable throughout the year, so the temperature variability value is small (0.74). The resulting efficiency reaches

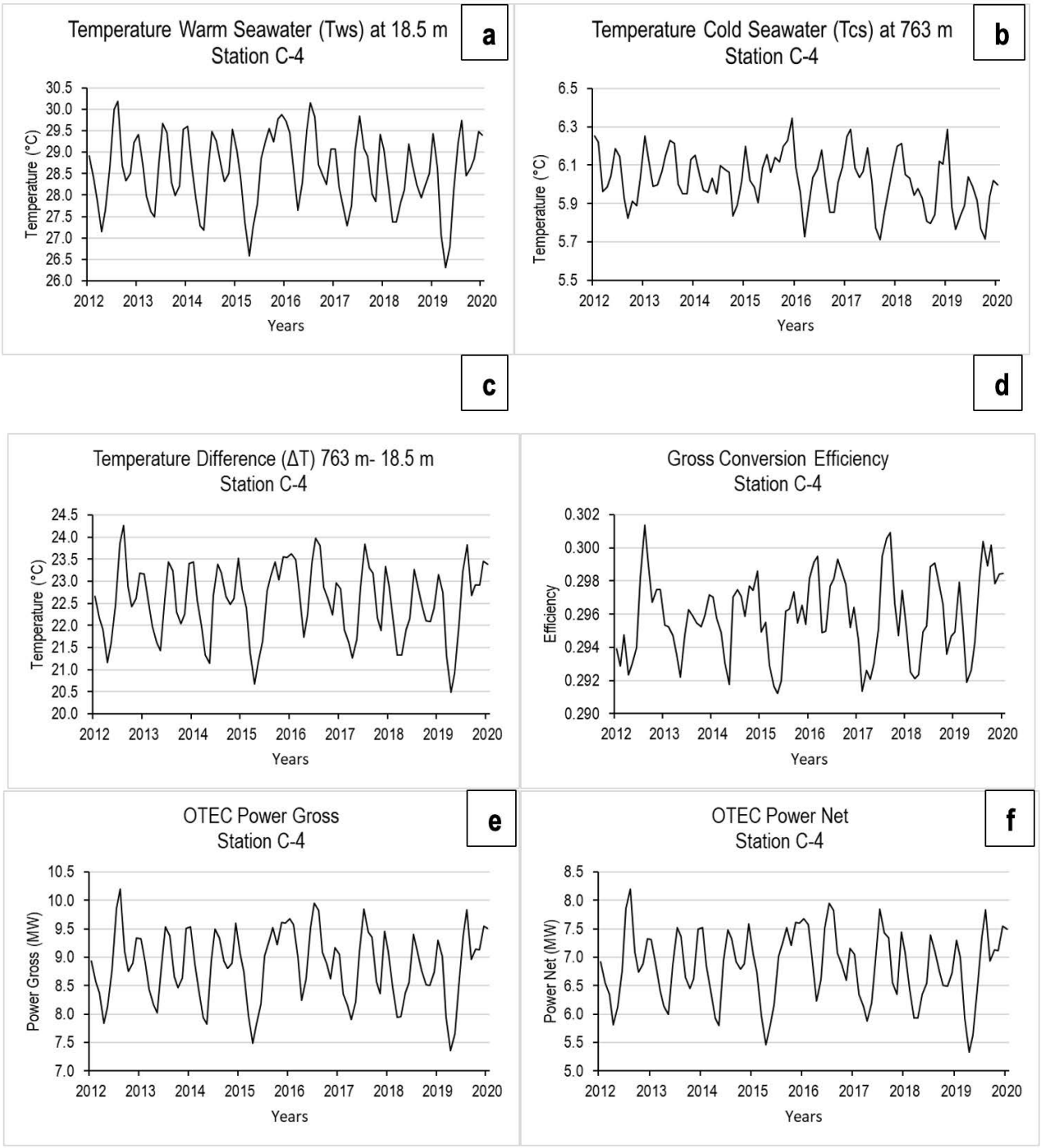

Figure 8. Result of Data Processing Analysis of Ideal Station OTEC Installation at Station C-4

29.27%-29.88%, with the gross power generated reaching a maximum value of 8.85 MW and net power reaching a maximum value of 7.55 MW. Based on the data processing results the ideal OTEC installation station is at station C-4 in Figure 8, the station reaches the minimum temperature difference requirements to run the OTEC system, according to Masutani and Takashi (2001). A small variability value indicates that the power generated tends to be stable, supporting running OTEC resources sensitive to temperature differences, as stated by Suprijo et al. (2021). The potential OTEC power generated at station C-4 has a minimum value of 5.84 MW, so it is under the simulation of a closed-cycle system with a capacity of 5 MW.

Figure 9 presents the surface current velocity at station C-4, wind speed near station C-4, and significant wave height near station C-4 for 9 years. The maximum surface current at station C-4 reaches 0.26 m/s, maximum wind speed reaches 5.69 m/s, and significant wave height reaches 5.1 m. Based on a review of ideal water conditions for the installation of the OTEC system according to Vega and Michaelis (2010), the current velocity at station C-4 is

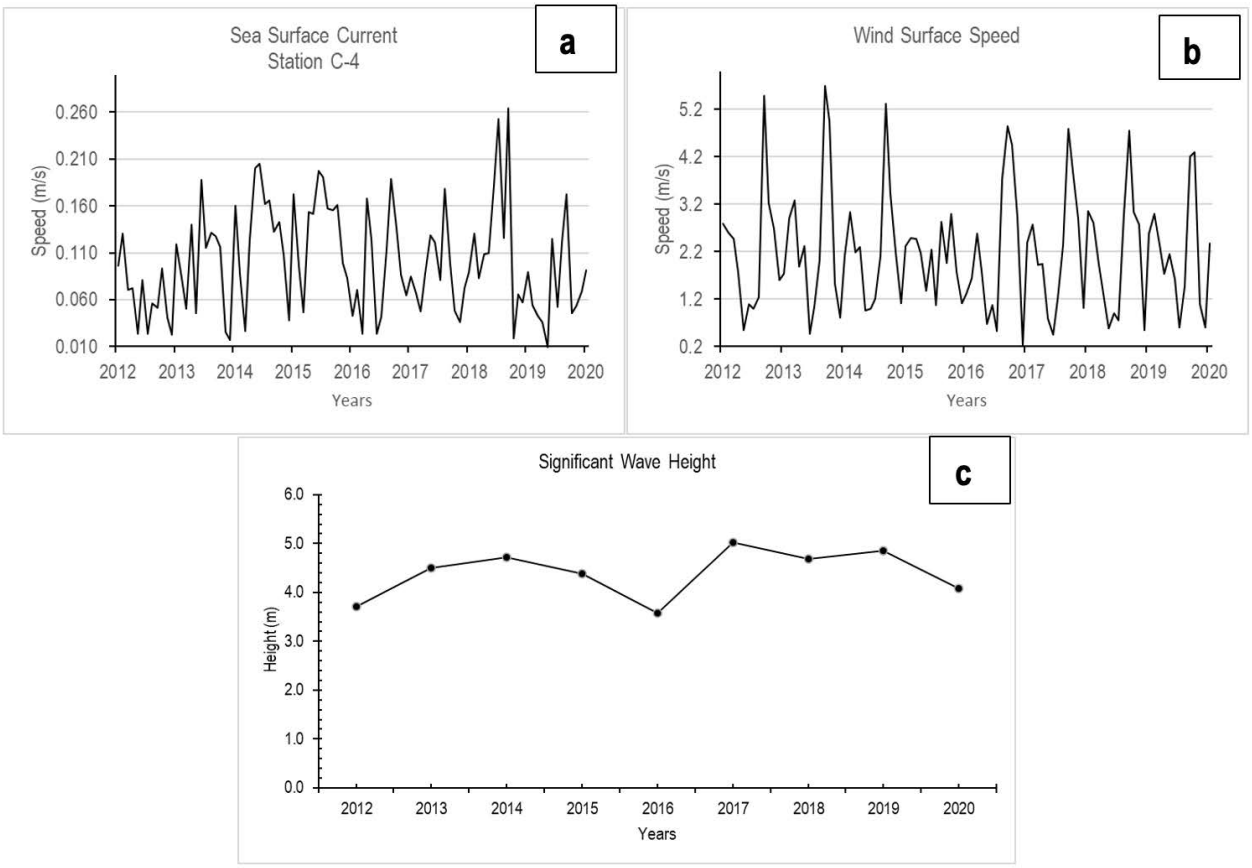

Figure 9. Sea Surface Current GLOBAL_MULTIYEAR_PHY_001_030 (a), Surface Wind Speed ERA5 ECMWF Reanalysis (b), dan Significant Wave Height WAVERYS GLOBAL_MULTIYEAR_WAV_001_032

less than 1.5 m/s, the maximum wind speed is less than 20 m/s, and significant wave heights < 6 m. Based on these data results, station C-4 has water conditions supporting the OTEC system's installation. Therefore, when considering the overall requirements for the ideal station for OTEC installations, including temperature conditions, comparison of distance to shoreline, clean power, and primary water conditions, the C-4 station located in the Omesuri sub-district is considered the most ideal for OTEC installations in North Lembata waters.

CONCLUSIONS

The water condition of Northern Lembata have a potency for the installation of an Ocean Thermal Energy Conversion (OTEC) system. The results of primary data processing include temperature data CMEMS Reanalysis produces a temperature difference value between warm seawater and cold seawater with a range of 20.97°C - 23.44°C. The variability of temperature value is relatively small, indicates relative stable throughout the year. The efficiency value that can be generated is 27.28%-30.92% with a gross power range of 6.86 MW-10.32 MW, and the net power that can be generated has a range of 5.65 MW-7.65 MW. According to the condition of bathymetry, currents, waves, and winds, and the disaster potency derived from secondary data processing, it is suggested to apply a floating platform of OTEC installation. The maximum surface current only reaches to 0.36 m/s, the wave height is 5.1 m, and the maximum wind speed is 5.69 m/s. The ideal station for the installation of the OTEC Closed-Cycle system with a capacity of 5 MW is a C-4 °C station. It has a depth of 763 m with a temperature difference (ΔT) of 21.20 °C -23.47 °C. The efficiency value at the station is 29.27%-29.88%, which can produce a net power of 5.84 MW-7.55 MW. The distance between the station and the mainland in the Omesuri sub-district is 1.86 km. This distance is considered close enough to the location of the electricity distribution.

ACKNOWLEDGEMENTS

The authors would like to thank the Department of Oceanography, Faculty of Fishery and Marine Science, Diponegoro University, and Marine Geological Institute of Indonesia (MGI) Bandung for supporting this research. This paper is part of the author's thesis, Gisela Malya Asoka Anindita, from the Department of Oceanography, Faculty of Fishery and Marine Science, Diponegoro University.

REFERENCES

Atmadipoera, A.S., Horhoruw, S.M., Purba, M., and Nugroho, D.Y., 2016. Spatial and Temporal Variation of Indonesian Throughflow in The

Makassar Strait. *Jurnal Ilmu dan Teknologi Kelautan Tropis FPIK-IPB*, 8 (1): 299-320.

Bassam, N.E., Maegaard, P., and Schlichting, M.L., 2013. *Distributed Renewable Energies for Off-Grid Communities Strategies and Technologies toward Achieving Sustainability in Energy Generation and Supply.* Elsevier Ltd. https://doi.org/ 10.1016/ B978-0-12-397178-4.00011-6.

BNPB. 2016. RBI Risiko Bencana Indonesia.

British Petroleum. 2021. Statistical Review of World Energy Indonesia's Energy Market in 2020.

Copernicus. 2021. Quality Information Document for Global Ocean Reanalysis Products GLOBAL_REANALYSI_PHY_001_030.https:// catalogue.marine.copernicus.eu/documents/ QUID/CMEMS-GLO-QUID-001-030.pdf [accessed on 1 September 2022]

Gordon, A.L, Giulivi, C.F, Ilahude, A.G., 2003. Deep Topographic Barriers within the Indonesian Seas. *Deep-Sea Research II*, 50:2205–2228.

Gordon, A.L., 2005. Oceanography of the Indonesian Seas and their Throughflow. *Oceanography*. 18:14–27.

Ichsari, L.F., Handoyo, G., Setiyono, H., Ismanto, A., Marwoto, J., Yusuf, M., and Rifai, A., 2020. Studi Komparasi Hasil Pengolahan Pasang Surut dengan 3 Metode (Admiralty, Least Square dan Fast Fourier Transform) di Pelabuhan Malahayati, Banda Aceh. *Indonesian Journal of Oceanography*, 2 (2).

Ilahude, A.G., and Gordon, A.L., 1996. Thermocline Stratification within the Indonesian Seas. *J of Geophy Res.*, 101 (C5): 12,401-12,409. doi: 0148-0227/96/95JC-03798$09.00.

Ilahude, D., Yuningsih A., Permanawati, Y., Yosi, M., Zuraida, R., and Annisa, N., 2020. Site Determination for OTEC Turbine Installation of 100 MW Capacity in North Bali Waters. *Bulletin of the Marine Geology*, 35 (1):1-12.

Julianto, C., 2020. Studi Potensi Pemanfaatan OTEC (Ocean Thermal Energy Conversion) Menggunakan Siklus Terbuka untuk Mengatasi Krisis Listrik dan Air Bersih di Pulau Lembata, Nusa Tenggara Timur. *Prosiding Seminar Nasional Teknik Kimia "Kejuangan" ISSN 1693-4393.* Pengembangan Teknologi Kimia untuk Pengolahan Sumber Daya Alam Indonesia,Yogyakarta, 14-15 Juli l 2020.

Lewis, C.D., 1982. *Industrial and Business Forecasting Methods: A Practical Guide to Exponential Smoothing and Curve Fitting*. Butterworth-Heinemann.

Masutani, S.M., and Takahashi, P.K., 2001. *Ocean Thermal Energy Conversion (OTEC)*. Academic Press: Honolulu, 1993-1999 pp.

Mignac, C., Tanajura, A.S., Santana, A.N., Lima, L.N., and Xie, J., 2015. Argo Data Assimilation into HYCOM with an EnOI Method in the Atlantic Ocean. *Ocean Sci. Discuss,* 11(17):33–51.

Ministry of Energy and Mineral Resources press release number: 311.pers/04/SJI/2020 Date: 22 October 2020 <https://ebtke.esdm.go.id/post/2020/10/22/ 2667/ menteri.arifin.transisi.energi.mutlak.diperlukan> [Accessed on 6 April 2022].

Morales, A.D., Montoya-Sanchez, R.A., Osorio, A.F., and Otero-Diaz, L.J., 2014. Ocean Thermal Energy Resources in Colombia. *Journal Renewable Energy,* 66: 759-769.

Nihous, G., 2007. A Preliminary Assessment of Ocean Thermal Energy Conversion Resources. *Journal of Energy Resources Technology,* 129 : 10-17.

Permanawati, Y., Prartono, T., Atmadipoera, A.S., Zuraida, R., Chang, Y., 2016. Rekam Sedimen Inti untuk Memperkirakan Perubahan Lingkungan di Perairan Lereng Kangean. *Jurnal Geologi Kelautan,* 14 (2) :65-77.

Permanawati, Y., and Hernawan, U., 2018. Distrbusi Karbon Organik dalam Sedimen Inti di Perairan Lembata, Laut Flores. *Jurnal Geologi Kelautan,* 16 (1) : 51-66.

Radjawane, I.M., and Hadipoetranto, P.P., 2014. Karakteristik Massa Air di Percabangan Arus Lintas Indonesia Perairan Sangihe Talaud Menggunakan Data Index SATAL 2010. *J Ilmu dan Tek Kelautan Tropis,* 6 (2):525-536.

Raharjo, N.H., 2011. *Studi Pemanfaatan Energi Panas Laut dan Gelombang Laut untuk Sistem Kelistrikan di Kabupaten Karangasem Bali.* Jurusan Teknik Elektro, Fakultas Teknologi Industri, Institut Teknologi Sepuluh Nopember (ITS).

Rysnawati, N.M., Sukarasa, I.K., and Paramarta, I.B.A., 2017. Analisa Tingkat Bahaya dan Kerentanan Bencana Gempa Bumi di Wilayah Nusa Tenggara Timur (NTT). *Buletin Fisika,* 18 (1) : 32 – 37.

Santoso, A., 2005. Pemantauan Hidrografi dan Kualitas Air di Teluk Hurun Lampung dan Teluk Jakarta. *Jurnal Teknologi Lingkungan P3TL-BPPT,* 6 (3) : 433-437.

Suprijo, T., Poerbo, P.R., Park, H., Kartadikaria, A.R., and Yosi, M., 2021. Potential Ocean Thermal Energy Conversion in Indonesian Waters Territory. *Journal of Coastal Research,* 114 : 285–289.

Susanto, R.D., Ffield, A., Gordon, A.L., and Adi, T.R., 2012. Variability of Indonesian Throughflow within Makassar Strait, 2004-2009. *Journal of Geophysical Research Oceans*, 117, C09013: 1-16. doi:10.1029/2012JC008096.

Syamsuddin, M.L., Attamimi, A., Nugraha, A.P., Gibran, S., Afifah, and Oriana, N., 2015. OTEC Potential in the Indonesian Seas. *Energy Procedia,* 65 :215-222, Elsevier Ltd.

Tim OTEC Lembata., 2017. *Laporan Penelitian Potensi OTEC di Perairan Lembata, NTT.* Laporan Kegiatan Puslitbang Geologi Kelautan. Balitbang ESDM. KESDM. Unpublished.

Vega, L.A., 1992. Ocean Thermal Energy Conversion. *Encyclopedia of Sustainability Science and Technology,*Springer : 7296-7328.

Vega, L.A., 2002. Ocean Thermal Energy Conversion Primer. *Marine Technology Society Journal,* 6 (4): 25-35.

Vega, L.A., and Michaelis, D., 2010. First Generation 50 MW OTEC Plantship for the Production of Electricity and Desalinated Water. *Offshore Technology Conference, 20957* : 1-17 pp.

Vranes, K., Gordon, A. L., Amy F., 2002. The Heat Transport of the Indonesian Throughflow and Implications for the Indian Ocean Heat Budget. *Deep-Sea Research II*, 49 : 1391–1410.

Widyartono, M., and Rahmadian, R., 2019. Potensi OTEC di Provinsi Papua Indonesia. *Indonesian Journal of Electrical and Electronics Engineering,* 2 (1): 17 – 21.

Yosi, M., 2014. Potensi Energi Laut Indonesia. *Jurnal Mineral dan Energi*, 12 (1): 54-66.

ACOUSTIC CHARACTERISTICS OF SIDESCAN SONAR ALONG PROPOSED POWER CABLE ROUTE, DUMAI – RUPAT ISLAND

KARAKTER AKUSTIK SIDESCAN SONAR SEPANJANG USULAN RUTE KABEL BAWAH LAUT DUMAI - PULAU RUPAT

Subarsyah[1*] and Sahudin[1]

[1] Marine Geological Institute of Indonesia, Jl. Dr. Junjunan no.236, Bandung

*Corresponding author: subarsyah@yahoo.com

(Received 01 February 2023; in revised from 02 February 2023; accepted 09 April 2023)

DOI : 10.32693/bomg.38.1.2023.812

ABSTRACT: Cable power installation along the route with bedforms-sediment structures sometimes potentially to have problems in the future or near future. In order to mitigate the cable from exposure because of currents, it is important to know a detailed understanding of the seabed and its mobility. Seabed characteristics, either textures or sediment structures, could be interpreted from acoustic characters, one of which is based on sidescan sonar images. An automatic interpretation to classify seabed characteristics can be done by using an image processing software. Image processing has been done on sidescan sonar images along power cable route between Dumai and Rupat Island. The image processing was using simple textures and Grey-Level Co-occurrence Matrix (GCLM) textures. Manual interpretation of sidescan sonar images classifies the acoustic characters into six; (1) fine sand waves with ripple marks, wave length 2.5-4 meters, (2) fine sands, (3) fine sand waves with ripple marks, wave length 5-9 meters, (4) fine sand with ripple-mega ripples, (5) coarse sands with ripple-trawl marks, and (6) very fine sands. The results of automatic classification show that image processing with simple textures is unable to identify the textures and structures of sediments properly, but by combining simple texture classification and GCLM types of sediment textures and sediment structures are better identified. This classification results are in agreement with the results of manual interpretation of sidescan sonar images.

Keywords: Ripple, Sonar, Image Processing and Classification

ABSTRAK*:* Pemasangan kabel listrik di sepanjang jalur dengan dasar laut yang memiliki struktur sedimen terkadang berpotensi mengalami masalah di masa mendatang atau dalam waktu dekat. Untuk mencegah kabel terekspos akibat arus laut. Penting untuk memahami secara rinci tentang dasar laut dan mobilitasnya. Karakteristik dasar laut baik tekstur maupun struktur sedimen dapat diinterpretasikan dari karakteristik akustik, salah satunya berdasarkan citra *sidescan sonar*. Interpretasi otomatis untuk mengklasifikasikan karakteristik dasar laut dapat dilakukan dengan menggunakan perangkat lunak *image processing*. Pemrosesan citra sudah dilakukan pada citra *sidescan sonar* di sepanjang jalur kabel listrik Dumai-Pulau Rupat. Pengolahan citra yang digunakan adalah *simple textures* dan *Grey-Level Co-occurrence Matrix* (GCLM) *textures*. Interpretasi manual citra *sidescan sonar* mengklasifikasikan karakter akustik menjadi enam; (1) gelombang pasir halus dengan tanda riak, panjang gelombang 2,5-4 meter, (2) pasir halus, (3) gelombang pasir halus dengan tanda riak, panjang gelombang 5-9 meter, (4) pasir halus dengan riak-mega riak, (5) pasir kasar dengan tanda *ripple-trawl*, dan (6) pasir sangat halus. Hasil klasifikasi otomatis dengan pengolahan citra menunjukkan bahwa pengolahan citra dengan *simple textures* tidak dapat mengidentifikasi tekstur dan struktur sedimen dengan baik, tetapi menggabungkannya dengan GCLM jenis tekstur sedimen dan struktur sedimen dapat teridentifikasi dengan baik, dengan hasil klasifikasi yang relatif berkorelasi dengan hasil interpretasi manual terhadap citra *sidescan sonar*.

Kata Kunci: *Riak, Sonar, Pengolahan Citra dan Klasifikasi*

INTRODUCTION

A bedform is a morphological feature formed by the interaction between a flow and cohesion less sediment on a bed (Nichols, 2009). Bedforms frequently observe in estuaries, coastal and offshore region. Bedforms can occur on cohesive and non-cohesive sediment (Poppe et al., 2002; Viekman et al., 1992; Blondel, 2009). Well-known bedforms on cohesive sediments (silt, clay and mud) is furrows and bedforms on non-cohesive (sand-gravel) that are mega ripples, ripples and sand waves. Erosional or depositional bedforms are influenced by sediment supply, current, waves or tides.

Bedforms on non-cohesive sediments is more dynamic, this meant that mobility of sediment will be easier and faster to follow the direction of current flow. Morphological changes that associated with bedforms on non-cohesive sediments have to be studied extensively because they may lead to hazards to navigation and offshore constructions.

Cable power installation along the route with bedforms sometimes potentially to have problems in the future or near future. Cable traversing a sand wave or mega-ripple field may experience a local stress build-up due to an uneven strain. It is well known that cables possibly to exposed on the seafloor may experience local scour, which in some cases may be sufficient to undermine the cable, causing a free span. When combined with sand wave migration the risk of free spanning increases. Besides a local stress build up and free span, it also experiences vortex induced vibrations (Roetert et al., 2017). Therefore, it is important to have a detailed understanding of the seabed and its mobility. Practically, morphological changes or dynamic bedforms should be considered during cable engineering in order to anticipate or mitigate power cable from exposure because of scouring and finally damage due to fishing or shipping activities.

A detailed mapping of bedforms must be carried out prior to cable laying or cable installation. Quick mapping of bedforms along the proposed cable route can be done by acoustic survey either sidescan sonar, sub bottom profiling or multibeam echosounder survey.

Proposed power cable route from Dumai to Rupat Island located in the Rupat Strait, Figure 1. The Rupat Strait is a narrow strait that separates the island of Sumatra and the island of Rupat, it was estimated that the near bottom current is quite strong. Based on bedforms classification by Morelissen et al. (2003) and Knaapen (2005), commonly near bottom current associated with existence of mega-ripples and sand waves. Because it is very important to know about the existence of bedforms for submarine cable installation then identification and mapping of bedforms have been carried out in this route by conducting an acoustic survey of sidescan sonar. Data

Figure 1. Study area of power cable route, Dumai – Rupat Island

analysis has been carried out to obtain acoustic characters of several identified bedforms.

METHODS

Acoustic characteristics related to bedforms were extracted from sidescan sonar data by using classification module on post-processing of Sonarwiz 7 software. This classification was processed with image processing that applied to sidescan sonar imagery as an output of data processing. Sidescan sonar imagery was computed from acoustic backscatter intensity that converted into pixel values, commonly 0-255, of a grayscale image (Subarsyah et al., 2021).

Classification use five parameters of image processing. Three parameters are simple textures consisting of intensity, entropy and standard deviation, while two more parameters are Grey-Level Co-occurrence Matrix (GCLM) textures (Chesapeake Technology, 2017).

The GLCM method was used to classify the sonar images into regions of different texture. This technique has been used for post-processing of sidescan sonar imagery for about 40 years (Pace and Dyer, 1979; Reed and Hussong, 1989; Keeton, 1994; Blondel et al., 1998). GLCM is an image processing technique developed by Haralick et al. (1973) which analyses texture and tone. Tone refers to the backscatter amplitude (the gray scale) of image pixels, with dark tone indicating lesser backscatter return than light tone. Texture refers to a repeating pattern, such as sand ripples. In this study only one GLCM used that is homogeneity.

RESULTS AND DISCUSSIONS

Distribution of sediment textures along Rupat Strait classified into three classifications, which is coarse silt, very fine sand, fine sand, medium sand and very coarse sand (Girsang and Rifardi, 2014). The sediment samples were taken using grab sampler. Based on this literature sediment texture along proposed power cable routes only classified into fine sand.

Manual interpretation of sidescan sonar images along power cable route in generally defined into six patterns; (1) fine sand wave with ripple marks, wave length 2.5-4 meter, (2) fine sands, (3) fine sand waves with ripple marks, wave length 5-9 meter, (4) fine sands with ripple-mega ripples, (5) coarse sands with ripple-trawl marks, and (6) very fine sands (Figure 2). Location of each character can be seen on Figure 3. Mosaic image on Figure 3, shows that dark zone has high intensity while bright zone has low intensity, or the grey color was inverted.

Detailed information about sediment textures distribution and sediment structures along proposed power cable required as consideration for cable engineering and protection. Lack of detailed information regarding the distribution of sediment textures and sedimentary

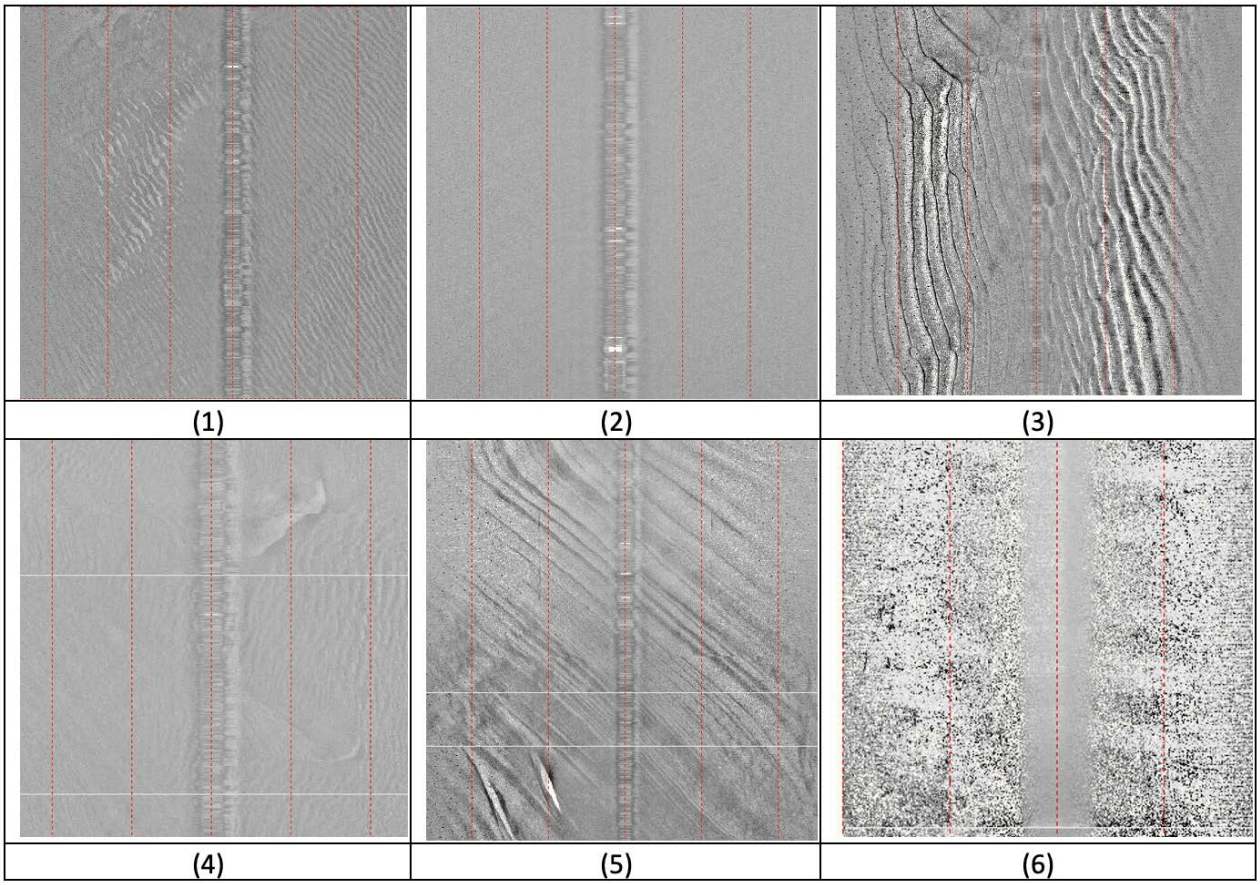

Figure 2. Acoustic patterns along proposed power cable route, Dumai - Rupat Island

structures along proposed power cable route is a challenge to carry out studies related to seabed classification, automatic classification and mapping of sediment textures and sediment structures.

Classification based on image processing with simple texture; standard deviation, entropy and intensity has classified seabed into six classes, Figure 4. Class 1 (red color) minor identified generally nearby coastal zones. This class has lowest intensity and highest entropy, and associated with coarse silt or shadow zone due to ripple marks. Class 2 (green color) has low intensity and high entropy and is distributed close to the coastal zone and shadow zone due to ripple marks. Class 3 (blue color) is a dominant class and it has medium intensity and entropy. This class is distributed on fine sand without ripple marks also fine sand with short wavelength ripple marks. Class 4 (magenta color) has high intensity and low entropy, this class distributed on coarse sand with ripple-trawl marks.

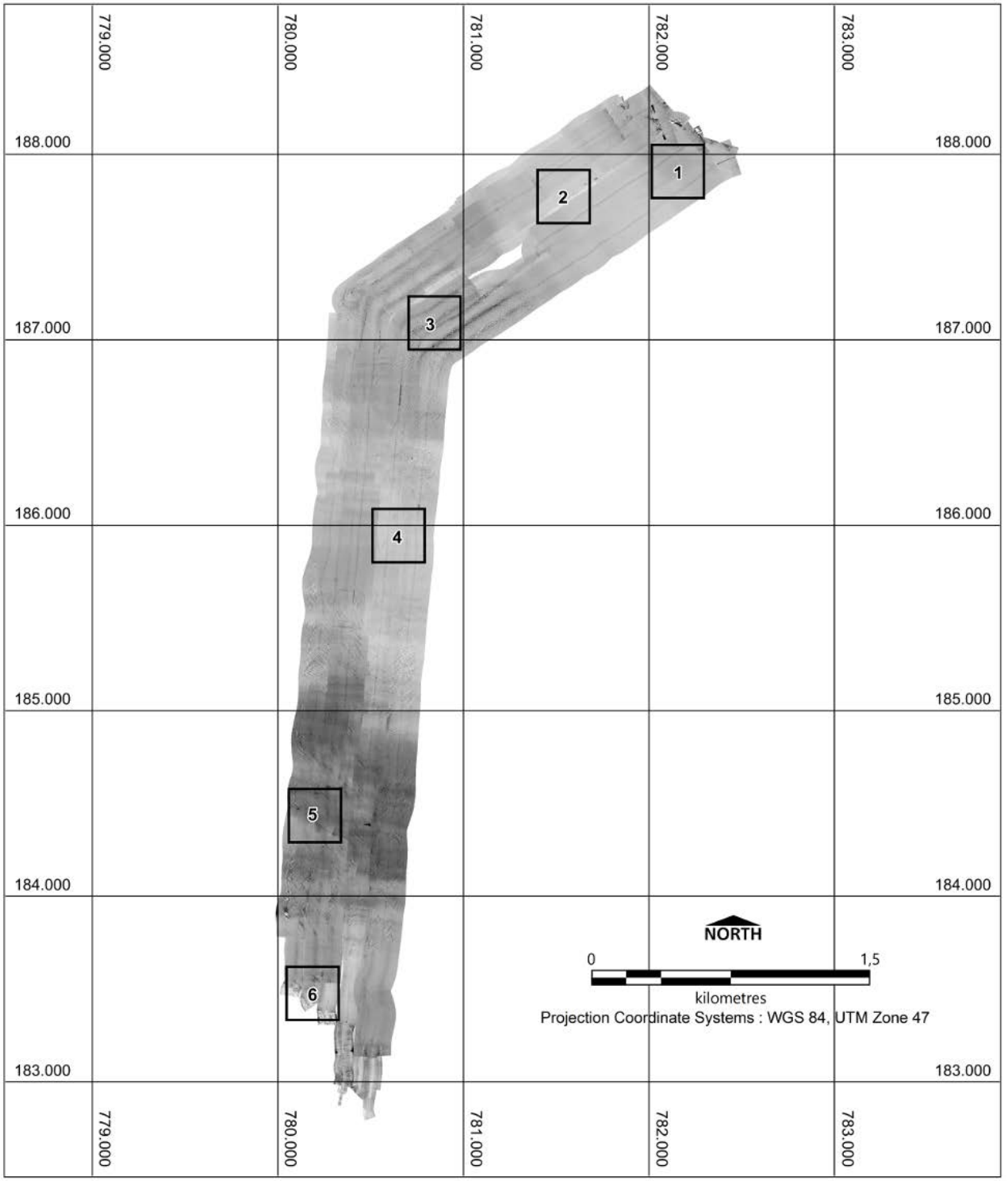

Figure 3. Mosaic of sidescan sonar images along proposed power cable route, Dumai - Rupat Island

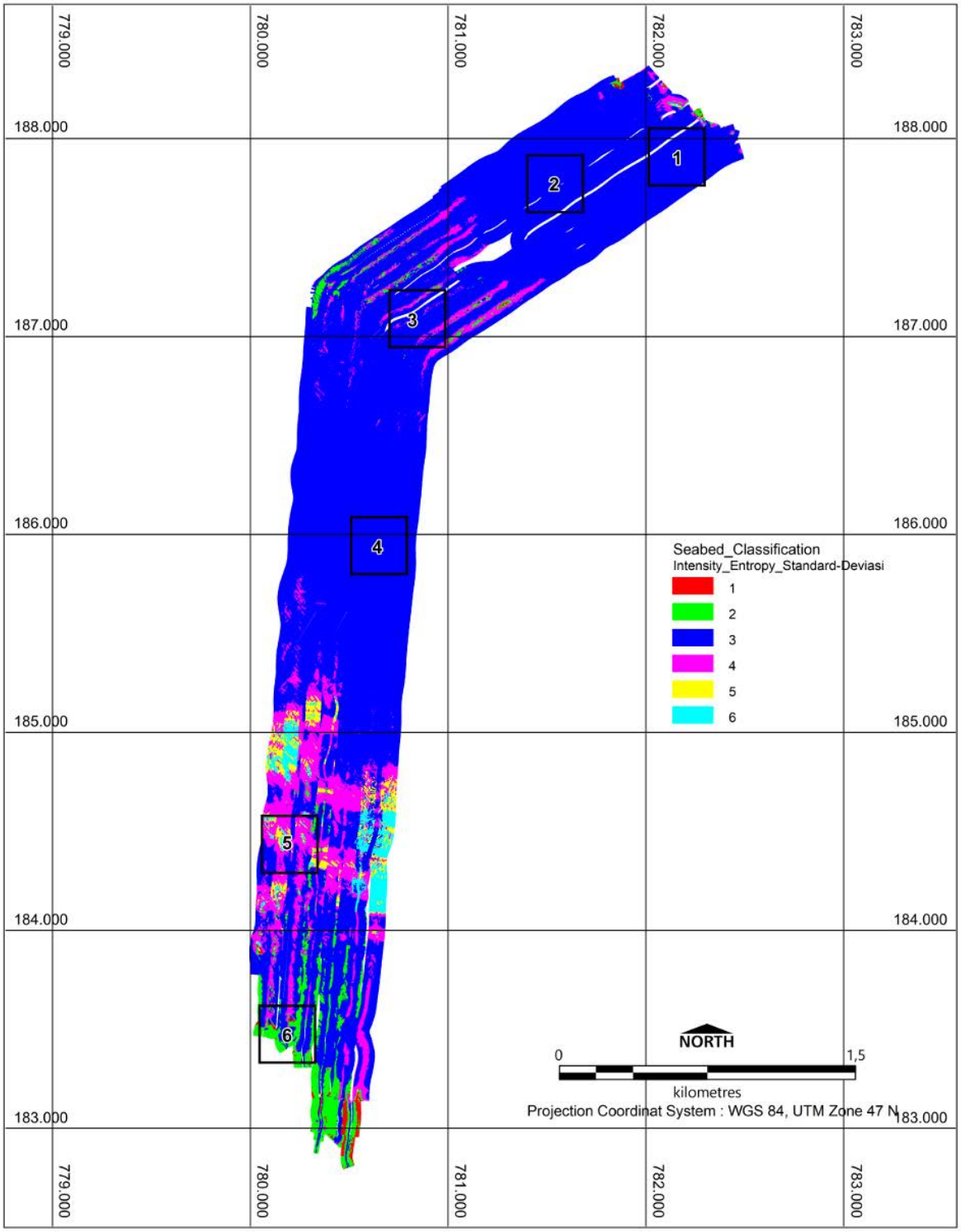

Figure 4. Seabed classification using simple textures.

Class 5 (yellow color) is distributed on coarse sand with ripple-trawl marks. This class has high intensity and low entropy. Class 6 (light blue) has high intensity and low entropy and is distributed on coarse sand with ripple-trawl marks. Class distribution has distortion at small part especially in the southern part due to artefact or acoustic distortion.

Sediment structures along the route can not be well defined by simple texture image processing, especially the short wavelength ripple marks and mega ripple. Class distribution to mapping sediment structures conducted by combining simple texture-intensity and GLCM-homogeneity image processing.

Seabed characterization by combining simple texture-intensity and GLCM-homogeneity classify seabed

into five classes, Figure 5. The first class (red color) is distributed almost in the southern part that has homogeneity on high intensity, this region associated with coarse sand. Small part of this class is distributed in the part of ripple marks which will give a high acoustic intensity value. The second class (green color) is relatively similar to the first class but has a lower intensity value. Most of this class is distributed in the southern part of the first class and at the outer region of the ripple mark with wavelength 5-9 meters. Homogeneity of the third class (blue color) is in medium intensity, this class almost found along the power cable route included in the ripple marks zone that have wavelength 2.5-4 meters. The fourth and fifth class are identified in the upper part and middle part of the power cable route. Both classes have homogeneity in low acoustic intensity.

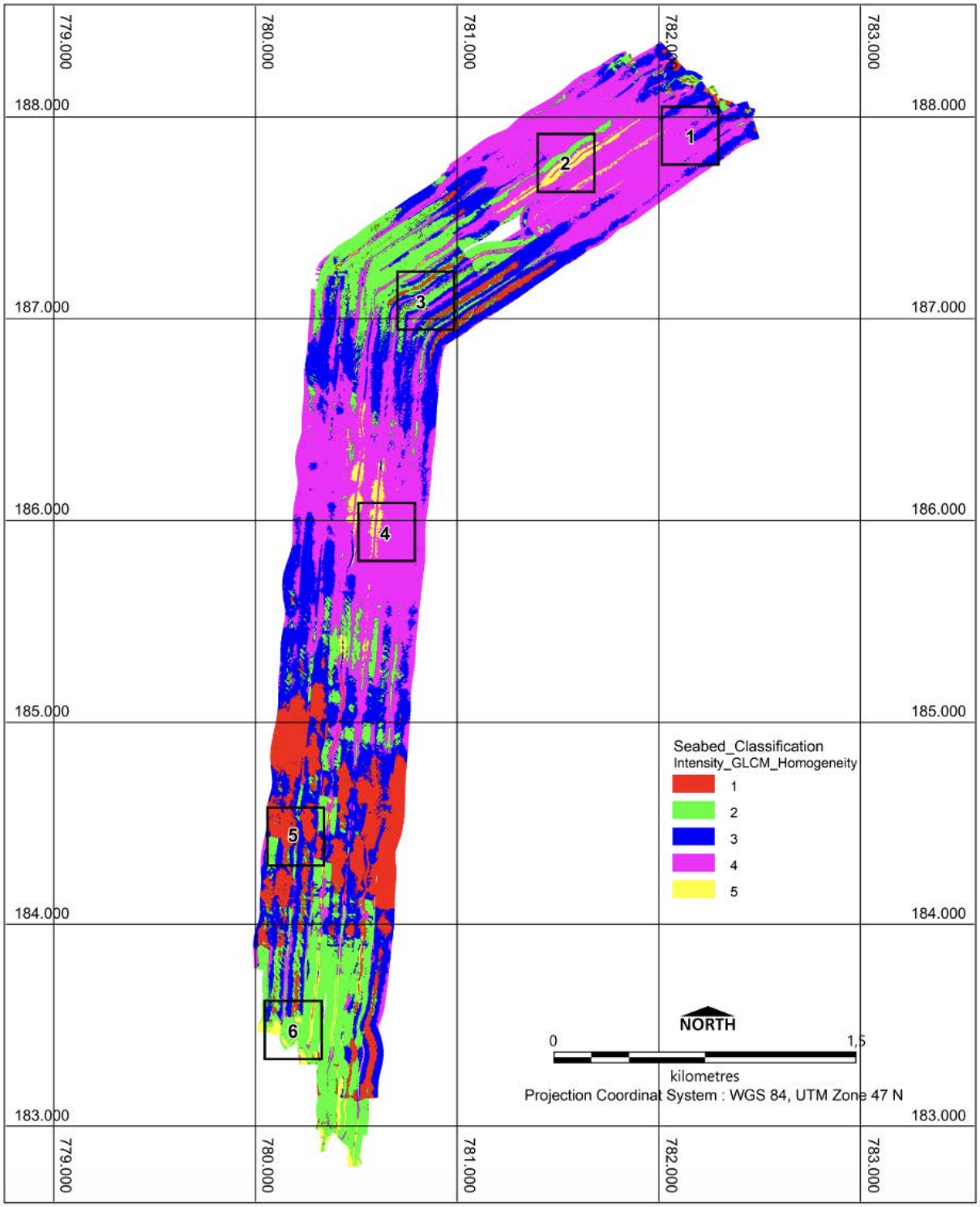

Figure 5. Seabed classification using simple texture and GLCM-homogeneity.

Based on the result of sediment structures identification through its acoustic characteristic, mapping of sediment structures affected by wave length and height of the ripple marks. These two parameters will contribute to low and high intensity distribution. Besides the two things mentioned above, the selection of parameters in image processing both window size and window step also will affect the result.

CONCLUSIONS

Manual interpretation of sidescan sonar image classifies the acoustic characters into six; (1) fine sand wave with ripple marks, wave length 2.5-4 meters, (2) fine sand, (3) fine sand wave with ripple marks, wave length 5-9 meters, (4) fine sand with ripple-mega ripple, (5) coarse sand with ripple-trawl marks, and (6) very fine sand.

Based on acoustic characteristics, automatic seabed classification of sediment textures cannot be clearly identified and its distribution does not correlate with the results of the interpretation manual. But implementation of image processing combined with simple texture and GCLM produced seabed classification that correlated with manual interpretation.

ACKNOWLEDGEMENTS

This study was supported by Marine Geological Institute (MGI) and the project is fully funded by PT. PLN Engineering. The authors would like to thank the heads of MGI and PT. PLN Engineering. Our true appreciation to MGI scientists for discussion and to all scientists and technicians who have participated on the team.

REFERENCES

Blondel, P., Parson, L.M. & Robigou, V. 1998. TexAn: Textural Analysis of Sidescan Sonar Imagery and Generic Seafloor Characterization. Proceedings 1, 419-423. OCEANS'98, IEEE-OES.

Blondel, P., 2009. The Handbook of Sidescan Sonar, Springer-Praxis.

Chesapeake Technology, Inc., 2017. SonarWiz Seabed Characterization User Guide.

Girsang, E. J and Rifardi, 2014. Characteristic and Pattern of Sediments Distribution Eastern of Rupat Strait Waters. Berkala Perikanan Terubuk. Vol. 42. No.1.

Haralick, R.M., Shanmugam, K. and Dinstein, R. 1973. Textural features for image classification. IEEE Transactions on Systems, Man, and Cybernetics 3(6), 610-621.

Knappen, M. A. F., 2005. Sandwave migration predictor based on shape information. Journal of Geophysical Research, 110, F04S11.

Keeton, J.A. 1994. The use of image analysis techniques to characterize mid-ocean ridges from multibeam and sidescan sonar data. PhD Thesis, University of Durham. http://etheses.dur.ac.uk/1620/.

Nichols, G, 2009. Sedimentology and Stratigraphy, Wiley-Blackwell, pp-419.

Morelissen, R., Hulscher, S., Knappen, M., Németh, A. and Bijker, R., 2003. Mathematical modelling og sandwave migration and the interaction with pipelines. Coastal Engineering, 48, 197-209.

Pace, N.G. and C. M. Dyer, 1979. Machine classification of sedimentary sea bottoms, IEEE Trans. Geosci. Remote Sensing GE-17, 52–56.

Poppe, L.J, Knebel, H.J, Lewis, R.S, and DiGiacomo-Cohen, M.L., 2002. Processes Controlling the Remobilization of Surficial Sediment and Formation of Sedimentary Furrows in North-Central Long Island Sound, Journal of Coastal Research, 18-4:741-750.

Reed, T.B. & D. Hussong. 1989. Digital image processing techniques for enhancement and classification of SeaMARC II sidescan sonar imagery. Journal of Geophysical Research 94, 7469-7490.

Roetert, T., Raaijmakers, T. and Borsje, B., 2017. Cable route optimization for offshore wind farms in morphodynamic areas. The 27th International Ocean and Polar Engineering Conference.

Subarsyah, Manik, H. M and Albab, A., 2021. Side-scan sonar image processing: Seabed classification based on acoustic backscattering, IOP Conf. Series: Earth and Environmental Science 944 (2021) 012001.

Viekman, B.E, Wimbush, M., Faghri, M., Asako, Y., and Van leer, J. C, 1992. Sedimentary Furrows and Flow structure: A Study in Lake Superior. Limnor. Oceanogr: 37(4). 797-812.

LOW RESISTIVITY PAY DEVELOPMENT: CASE STUDY OF TALANGAKAR FORMATION ASRI BASIN, OFFSHORE SOUTHEAST SUMATRA, INDONESIA

PENGEMBANGAN INTERVAL RESISTIVITAS RENDAH: STUDI KASUS FORMASI TALANGAKAR CEKUNGAN ASRI, LEPASPANTAI SUMATRA TENGGARA, INDONESIA

Dwandari Ralanarko[1*], Pranowo Nugroho[1], Edy Sunardi[2], Ildrem Syafri[2], and Billy G. Adhiperdana[2]

[1] Pertamina Hulu Energi OSES, Menara Standard Chartered, Jl. Prof. Dr. Satrio No.26, Karet Semanggi, Setiabudi, Jakarta Selatan, DKI Jakarta 12950

[2] Post-Graduate Program, Faculty of Geological Engineering – Universitas Padjadjaran, Jl. Raya Bandung – Sumedang KM 21, Jatinangor, Jawa Barat 45363

*Corresponding author: dwandari.ralanarko@gmail.com

(Received 23 January 2023; in revised from 24 January 2023; accepted 14 April 2023)

DOI : 10.32693/bomg.38.1.2023.803

ABSTRACT: Southeast Sumatra is a prolific oil and gas block located offshore in the Java Sea, 90 km north of Jakarta Bay. This area covers two major basins, namely Sunda Basin and Asri Basin. The initial development of the area focused on faulted and high closures and high-resistivity reservoirs. Further analysis shows that there are special low-resistivity reservoirs in Widuri Area, especially in the Aryani field. This paper will discuss the low resistivity pay zone reservoirs and fluid containment of the intervals. The paper will also include further assesment this undeveloped interval to increase oil production, considering the upside potential of the reservoirs using current geological, geophysical, and reservoir engineering approaches. Additionally, it will describe the operational challenges faced during the production period.

The low-resistivity pay zone, a hydrocarbon-bearing reservoir in the Aryani field of the Widuri area, was identified using gas readings in the daily drilling reports, complemented with mud logging data. The Basal Sand interval, which drapes above the basement, was the site of the first producing well of Basal Sand, Aryani AC-X, preceded by a hydraulic fracturing job. Lambda-mu-rho inversion was implemented to delineate this reservoir. To recognize the potency in those wells, data reconfirmation was conducted between the elan summary, sidewall core, and cutting data. Aryani AC-X has successfully drained oil using a submersible pump, with an initial production of 408 bopd and cumulative production of 240 MBO.

Keywords: Asri Basin, Indonesia, low resistivity, Oligo-Miocene, reservoir, Talangakar Formation

ABSTRAK: *Southeast Sumatra merupakan blok minyak dan gas yang produktif yang terletak di lepas pantai Laut Jawa sekitar 90 km sebelah Utara Teluk Jakarta. Daerah ini mencakup dua cekungan utama, yaitu Cekungan Sunda dan Cekungan Asri. Pengembangan awal area ini difokuskan pada lokasi yang memiliki konfigurasi struktur tinggian dan reservoir dengan resistivitas tinggi saja. Analisis lebih lanjut menunjukkan bahwa terdapat reservoir tertentu yang memiliki resistivitas rendah di Cekungan Asri, terutama lapangan Aryani. Makalah ini akan membahas tentang identifikasi reservoir resistivitas rendah dan jenis fluida hidrokarbon yang terakumulasi. Makalah ini juga membahas kelakuan reservoir menggunakan pendekatan geologi, geofisika, dan teknik reservoir, serta menjelaskan tantangan operasional produksi.*

Zona hidrokarbon dengan resistivitas rendah di Lapangan Aryani Cekungan Asri diidentifikasi menggunakan pembacaan gas pada laporan pemboran harian yang dilengkapi dengan data mud logging. Interval Basal Sand yang membentang diatas basement merupakan site sumur produksi pertama dari Basal Sand, yaitu sumur Aryani AC-X, yang didahului dengan pekerjaan rekah hidrolik sebelum produksi. Inversi Lambda-Mu-Rho diimplementasikan untuk mendelineasi reservoir ini. Rekonfirmasi data antara Elan Summary, Sidewall Core dan Cutting dilakukan untuk mengetahui potensi di sumur tersebut. Aryani AC-X telah berhasil mengalirkan minyak dengan menggunakan pompa submersible, dengan produksi awal 408 bopd dan produksi kumulatif tidak kurang dari 240 MBO.

INTRODUCTION

Southeast Sumatra Production Sharing Contract is located in Offshore Southeast Sumatra, operated by Pertamina Hulu Energi OSES. Three basins of Sunda, Asri, and Hera lie in an area of 11,046 sq. km of concession. Asri Basin was once thought to have low maturity of source rocks resulting in a low interest to be explored, during the early stage, from 1983 to 1987 (Wight et al., 1997).

A Cenozoic extensional back-arc and half-graben rift of Asri Basin (Young and Atkinson, 1993) is situated in Offshore Sumatra, Indonesia, and covers an area of approximately 3500 sq. km. It comprises thick sediment from Paleocene to Pleistocene up to 16,000 ft in thickness. The basin is bordered by a downthrown to the west, N-S trending faults to the East, and an NW-SE trending wrench system to the south (Ralanarko et al., 2020).

Three major tectonics are recognized: pre-rift, syn-rift, and post-rift, which affected the structural style and depositional systems in the Asri Basin (Ralanarko et al., 2020). Stratigraphy of the Asri Basin is influenced by moderate intra-basinal faulting and folding. Structural control on major axial drainage systems would exert tremendous influence on sand supply to any particular basin at any given time. Basin integration and the control of axial fluvial systems play an important role in fluvial deposition during basin evolution and fill. The Lower Zelda and Upper Gita Members are the main components of the Oligocene Talangakar Formation (Aldrich et al., 1995). Figure 1a shows the location of the Asri Basin, while Figure 1b illustrates the regional stratigraphy.

The main objective of this research is early syn-rift Basal Sand interval, especially in the Aryani field. The reservoir is located above the basement fault and has a distinctive character, with a thickness of about 10 ft. This interval reservoirs in the area differ from other Talangakar Formation (TAF), in which sand was deposited by a meandering river system that streamed from the northwest to the southeast within the basin (Ralanarko et al., 2021).

Resistivity log patterns in this interval appear relatively flat and do not show any contrast with the layer above. However, the density log indicates a strong contrast with the layer above. The difference in trends between the two logs is assumed to be attributed to the presence of certain minerals that affect the resistivity log readings. Several minerals that can affect resistivity log readings

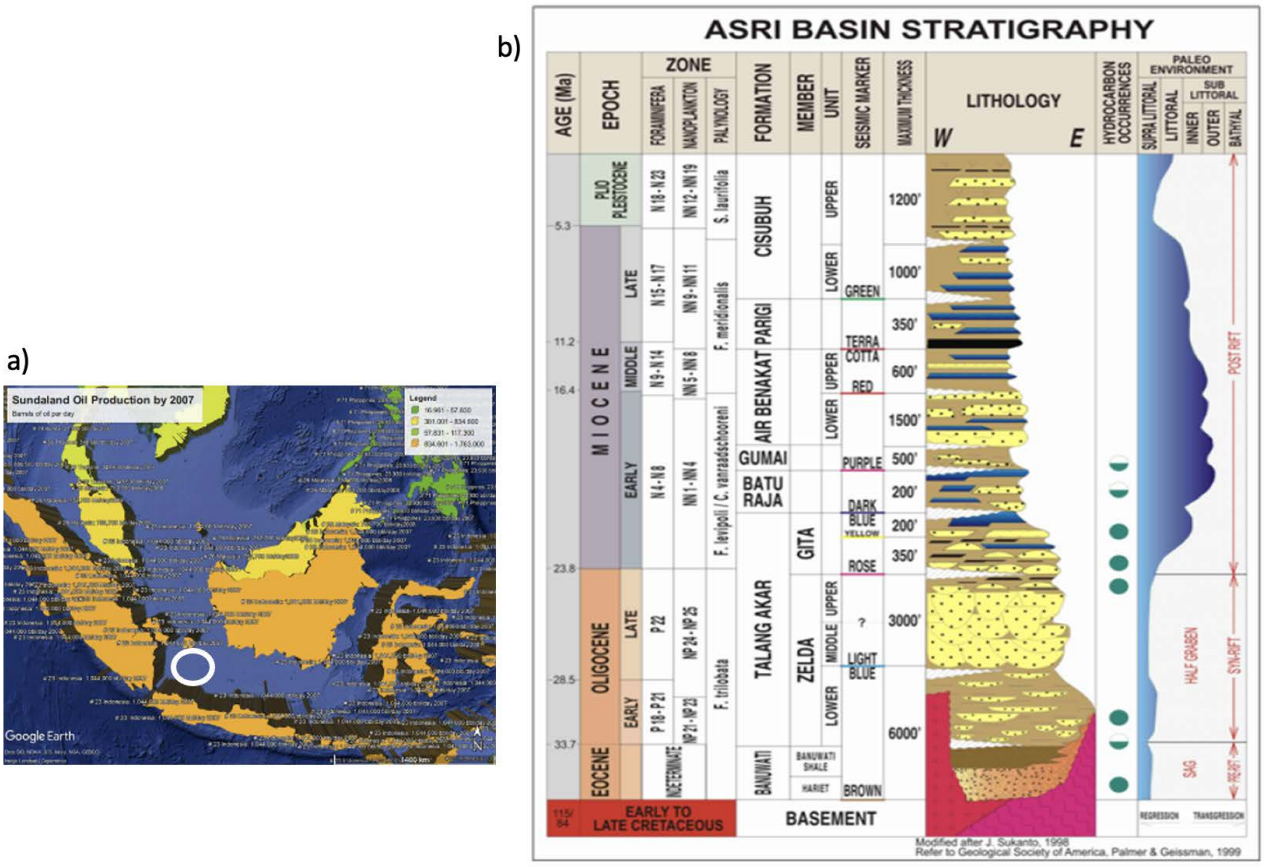

Figure 1.Asri basin location inside circle (a) and regional stratigraphy (b) (Ralanarko et al., 2020)

including clay minerals, such as clay minerals with high surface area and high cation exchange capacity, can impact the conductivity of the formation. As a result, lower resistivity readings may be observed on the resistivity log.

METHODS

The Basal Sand reservoir in the Aryani field has produced about 215 MBO from the A-05 well since it was first drilled in 2007. Based on the newest palaeogeography reconstruction conducted in this area, this interval are deposited earlier compare to the main reservoir interval in Talangakar Formation which was deposited in Upper Zelda and Gita interval (Ralanarko et al., 2021). Since only one well is currently producing from the reservoir and the average permeability is relatively low to medium, additional infill wells are needed to optimize production. The addition of well/infill drilling requires integrated reservoir characterization.

The study includes integrated geological modelling with seismic attributes to determine the lateral distribution of the Basal Sand reservoir. Vertical distribution-specific methods are needed because the Volume of Clay (VCL) and Gamma Ray (GR) logs alone are insufficient to separate thin layers in detail (Aki and Richards, 1980). In this study, we distinguished the reservoir characteristics and quality using Rock Typing (RT) methods. RT methods are used to classify an interval with similar characteristics in a particular zone (Smith and Gidlow, 1987). This process involves Cluster Analysis, which is based on statistical algorithms that classify image logs (FMI) and triple combo well logs data consisting of Gamma Ray, Neutron-Density and Resistivity that show similar characteristics. The zones along the wells were then determined based on grain size, grain shape, and sorting characteristics obtained from core data.

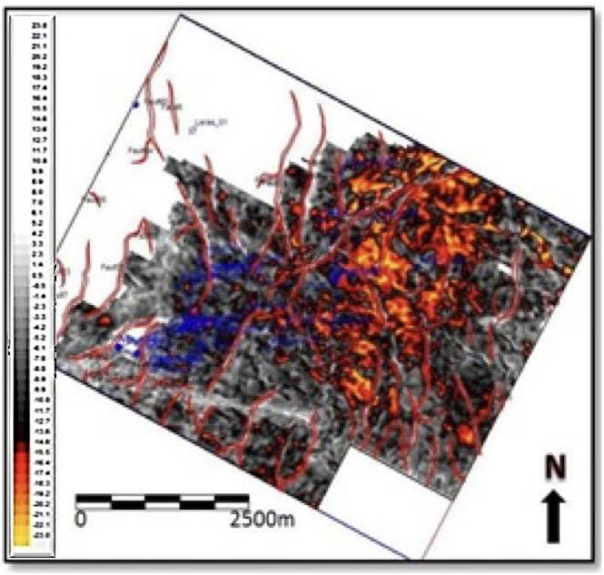

Figure 2a. Minimum amplitude attributes

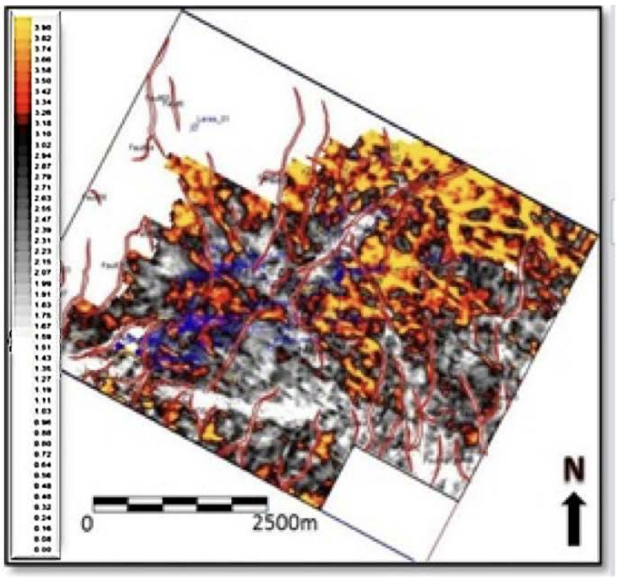

Figure 2b. Sweetness amplitude attribute

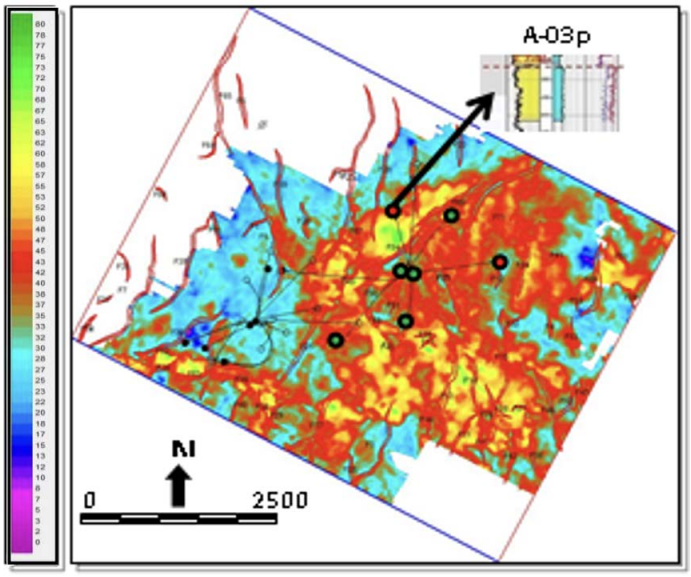

Figure 3. Isochrones interval Top Lower Zelda to the Top Basement

Geophysical Aspect

The Basal Sand is represented by a peak amplitude (a positive value indicates increased impedance) that interferes with the basement reflector. Amplitude attribute analysis was performed to determine the amplitude response of the Basal Sand. The minimum and sweetness amplitude attributes are shown in Figure 2a and Figure 2b. Unfortunately, the results were not sufficient to determine the lateral distribution of the Basal Sand.

After crosschecking with the presence of Basal Sand, many inconsistencies cannot be interpreted from the amplitude attributes. The common interpretation for predicting this Basal Sand is using isochrones from the Top Lower Zelda to the Top Basement as shown in Figure 3. These isochrones are

interpreted as the paleo-structures, especially regarding the distribution of the Basal Sand that drapes above the basement, thus controlling the depositional periods for the Lower Zelda member.

From this interpretation, the boundary of the lower Zelda member geometry has an NW–SE trend but for the Basal Sand distribution still an inconsistency between the well log and core data with the isochrones maps. An integrated geophysical analysis is needed for Basal Sand reservoir characterization.

Geological Aspect

In this case study, two commonly used Rock Typing (RT) methods, the flow-zone indicator (RQI/FZI) and the pore-throat radius (Winland's R (35)), have been applied (Guo et al., 2007). Both methods are applied to this case study.

The flow-zone indicator (RQI/FZI) method is a technique that uses the relationship between the rock quality index (RQI) and the formation factor indicator (FZI) to classify rocks into different types or zones based on their pore size distribution and permeability. The RQI measures the rock's strength and hardness, while the FZI measures of the porosity and permeability. This method is useful for identifying different flow zones within a reservoir.

The Winland's R (35) method is a technique that calculates the ratio of the volume of clay and other fine-grained minerals to the volume of pore space within a rock sample. This method is useful for determining the dominant pore-throat size and the permeability of the rock. A low Winland's R (35) value indicates that the rock has a high proportion of clay and fine-grained minerals, which can result in low permeability.

Both methods can provide valuable information about the characteristics of the rock formation, and can be used to help optimize oil and gas production. Based on the test results, the RQI/FZI is more in line with the Aryani field data. This is possible because the characteristics of clastic reservoirs in the Aryani field are most likely influenced by the texture, so permeability should correlate well with porosity.

Permeability is obtained from core data and distributed to the uncored well using the equation derived from the porosity and permeability cross plot. The ratio of RQI/FZI can be used to calculate rock typing (Amaefule et al., 1993). RQI is a rock-quality index given by:

$$RQI = 0.0314 \sqrt{\frac{k}{\emptyset_e}}$$

Where k is permeability from the Kint log, and Øe is effective porosity. Øe can be obtained from Øz, the normalized porosity index, where:

$$\emptyset_{z=(\frac{\emptyset_e}{1-\emptyset_e})}$$

So the flow zone indicator formula is:

$$FZI = \frac{RQI}{\emptyset_Z}.$$

The FZI (Formation Factor Indicator) is a measure of the porosity and permeability of a formation, and is often used in the oil and gas industry to estimate fluid flow rates and reserves. The RQI (Rock Quality Index) is a measure of the strength and hardness of the rock.

Amaefule et al. (1993) proposed a graph that relates the FZI and RQI, which can be used to estimate the reservoir properties of a rock formation. The graph shows that the FZI and RQI are inversely related, and that there are several intervals of FZI values that correspond to the same unit of reservoir quality

Based on the cutoff obtained from the FZI versus RQI graph, the intervals of FZI values that correspond to the same unit of reservoir quality can be determined. This means that within each interval, the reservoir properties are considered to be similar, and can be treated as a single

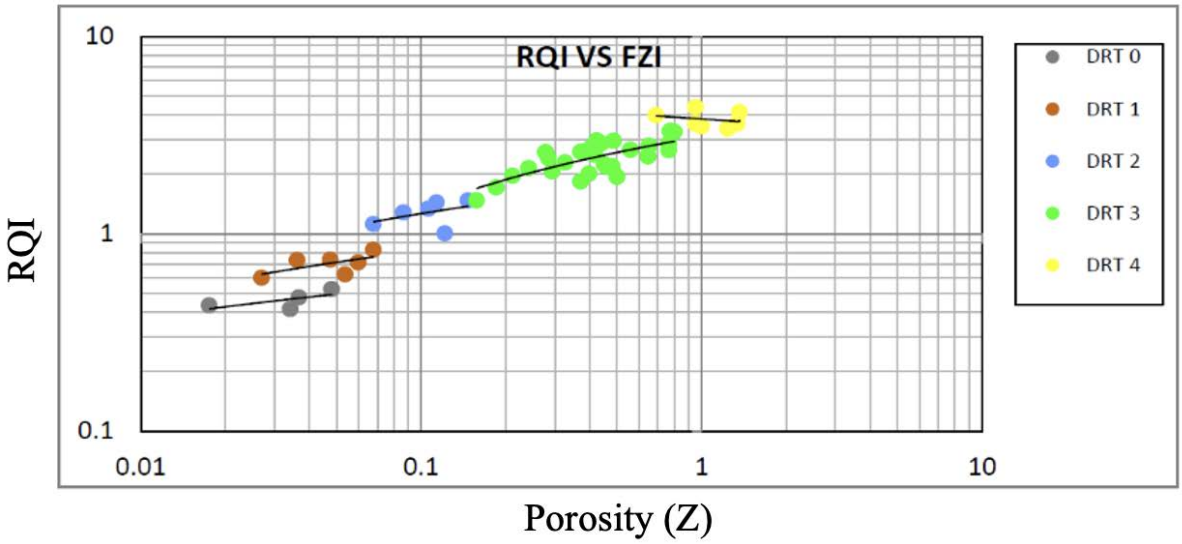

Figure 4. Correlation between RQI (Y axis) vs FZI (X axis) based on Rock Type classification

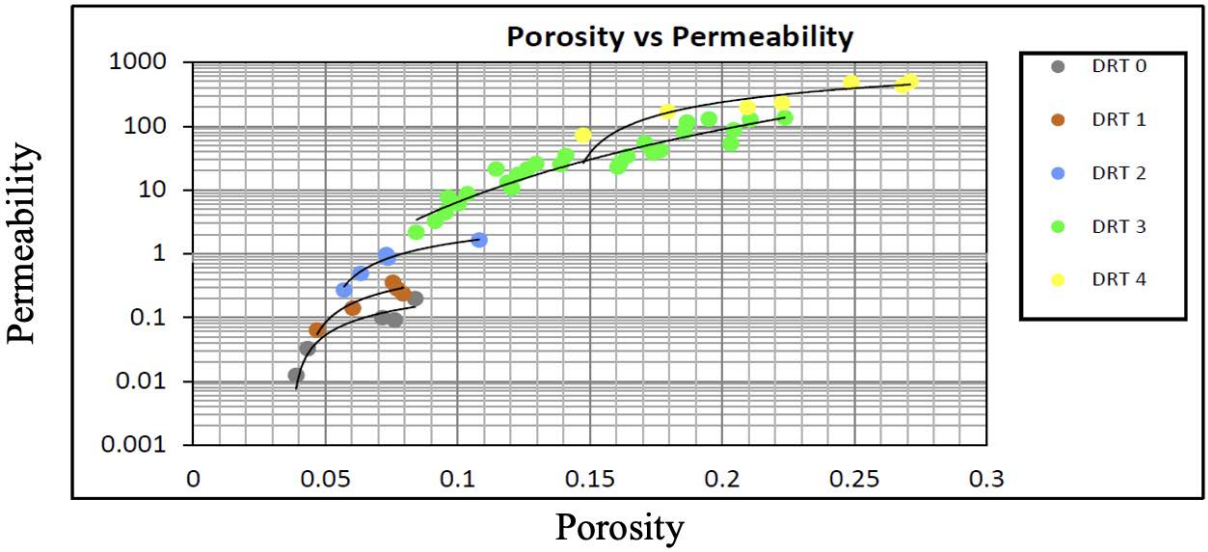

Figure 5. Correlation between porosity (X axis) and permeability (Y axis) based on RT classification

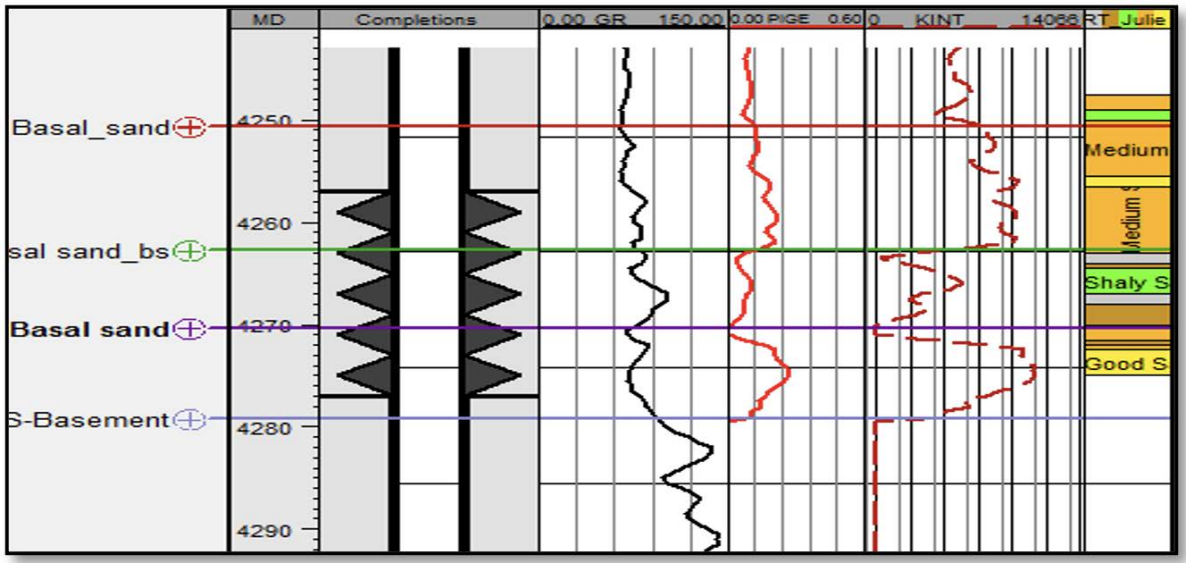

Figure 6. Correlation between porosity, permeability, RQI, and FZI based on RT classification

unit. The value of FZI is divided into several intervals, which are considered to be of the same unit based on the cutoff obtained from the FZI versus RQI graph from the A-05 well (Figure 4) and (Figure 5). Five different rock types can be classified based on the value of FZI. Different permeabilities of RT 0 to RT 4 also show the quality of each reservoir interval. The cutoff was applied to all wells in the Aryani field.

This result was used as input for the geological model. The RT method is effective enough to classify thin layers of Basal Sand. The ratio method of RQI/FZI showed a good correlation between the porosity and permeability to identify some rock types. This shows the texture of the rock has a role in distinguishing some rock types as shown in (Figure 6).

Data Analysis

Model-based inversion is one way to see the distribution of the reservoir. A feasibility study was undertaken on well A-05, showing that the crossover of AI (Acoustic Impedance) and SI (Shear Impedance) successfully separates the Basal Sand in log resolution. From the generated AI map, the Basal Sand distribution does not give a more detailed trend compared with the previous interpretation and has a poor correlation with the sand presence already known from the well data. Further analysis using the elastic properties, such as an AVO analysis and the Lame parameter, Lambda–Rho (LR), and Mu–Rho (MR), is necessary (Gray and Andersen, 2000).

The feasibility test on AI vs SI crossplot is shown in Figure 7. The AI map on the Basal Sand reservoir is displayed in Figure 8. The intercept (P) and Gradient (G) volumes can be derived from the gathered data (Castagna

et al., 1998). Near the basement, positive P values are shown in red, while negative G values are shown in blue. The results of P*G in negative values displayed in blue. Results of cross plot P vs G volume indicated by the yellow colour which indicates the distribution of Basal reservoir, indicating a similar pattern to alluvial fan deposition patterns in the NW–SE trend. These attributes are used as inputs for the geological model. The P-reflectivity (Rp) and S-reflectivity (Rs) data can also be derived from seismic data. LR and MR can be obtained by

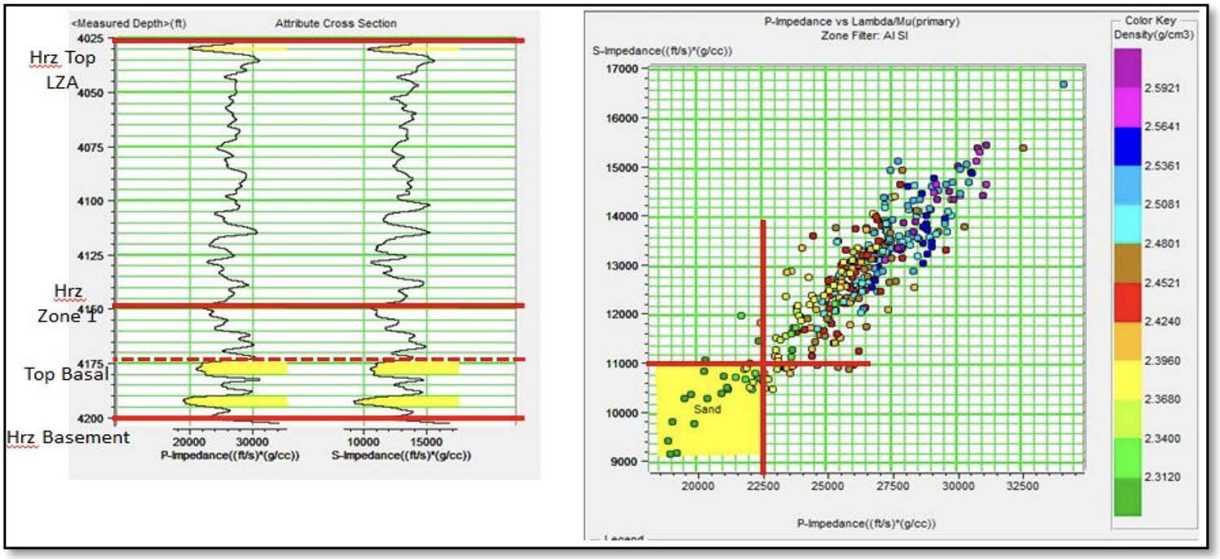

Figure 7. Feasibility test on AI vs SI crossplot

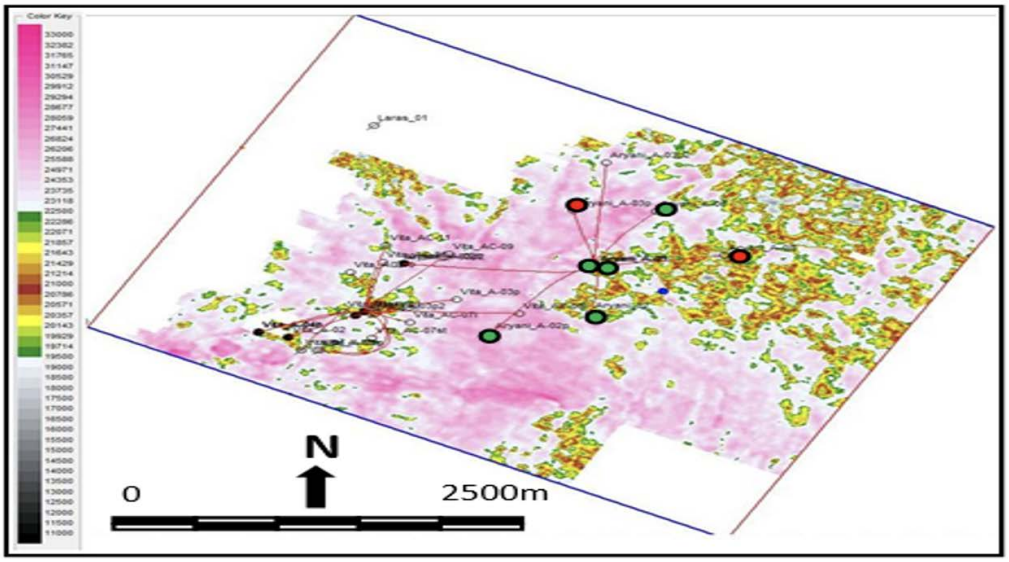

Figure 8. AI map on Basal Sand reservoir

Sand. P vs G volume is shown in (Figure 9).

The P-reflectivity (Rp) and S-reflectivity (Rs) data can also be derived from seismic data. LR and MR can be obtained by performing an AVO inversion on Rp and Rs. The cross-plot result from LR and MR from the A-05 well successfully separates the Basal Sand, with an LR cut-off ranging from 15–24 GPa*g/cc and an MR from 7.5–12.5 GPa*g/cc.

The LR section and the LR map demonstrate a good match with the well data, while the MR result is not sensitive and visibly does not match with well data. The LR map shows the lateral distribution of the Basal Sand doing an AVO inversion on Rp and Rs. The cross-plot result from LR and MR from the A-05 well successfully separates the Basal Sand, with an LR cut-off from 15–24 GPa*g/cc and an MR from 7.5–12.5 GPa*g/cc.

The LR section and the LR map show a good match with the well data, while the MR result is not sensitive and visibly does not match with well data. The LR map shows the lateral distribution of the Basal Sand reservoir similar to alluvial fan deposition patterns in the NW–SE trend. These processes are shown in Figure 10 (Intercept & Gradient Volume), Figure 11 (Feasibility test on Lambda-Rho and Mu-Rho), Figure 12 (Lambda-Rho section) and

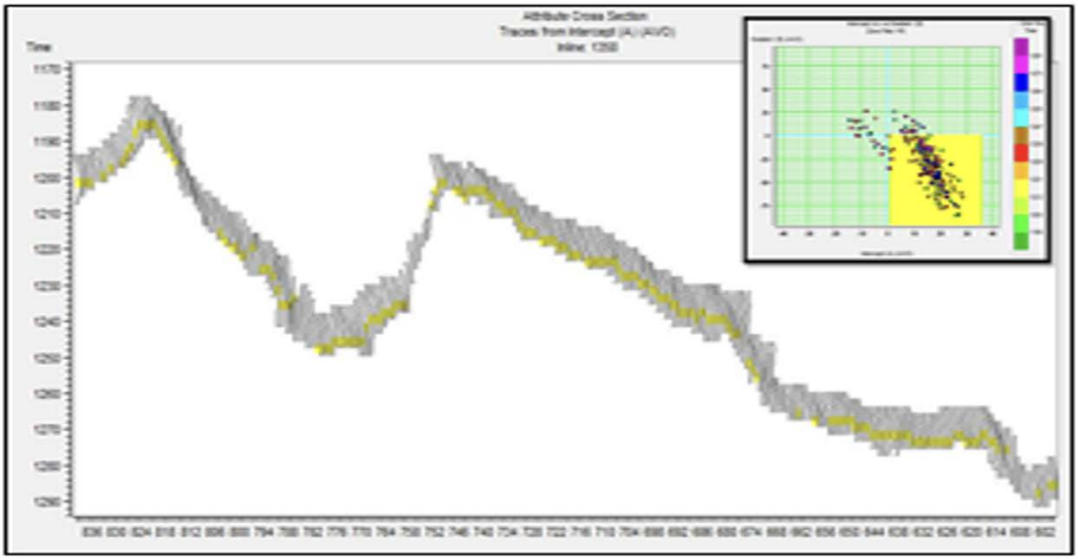

Figure 9. P vs G volume indicated by yellow colour

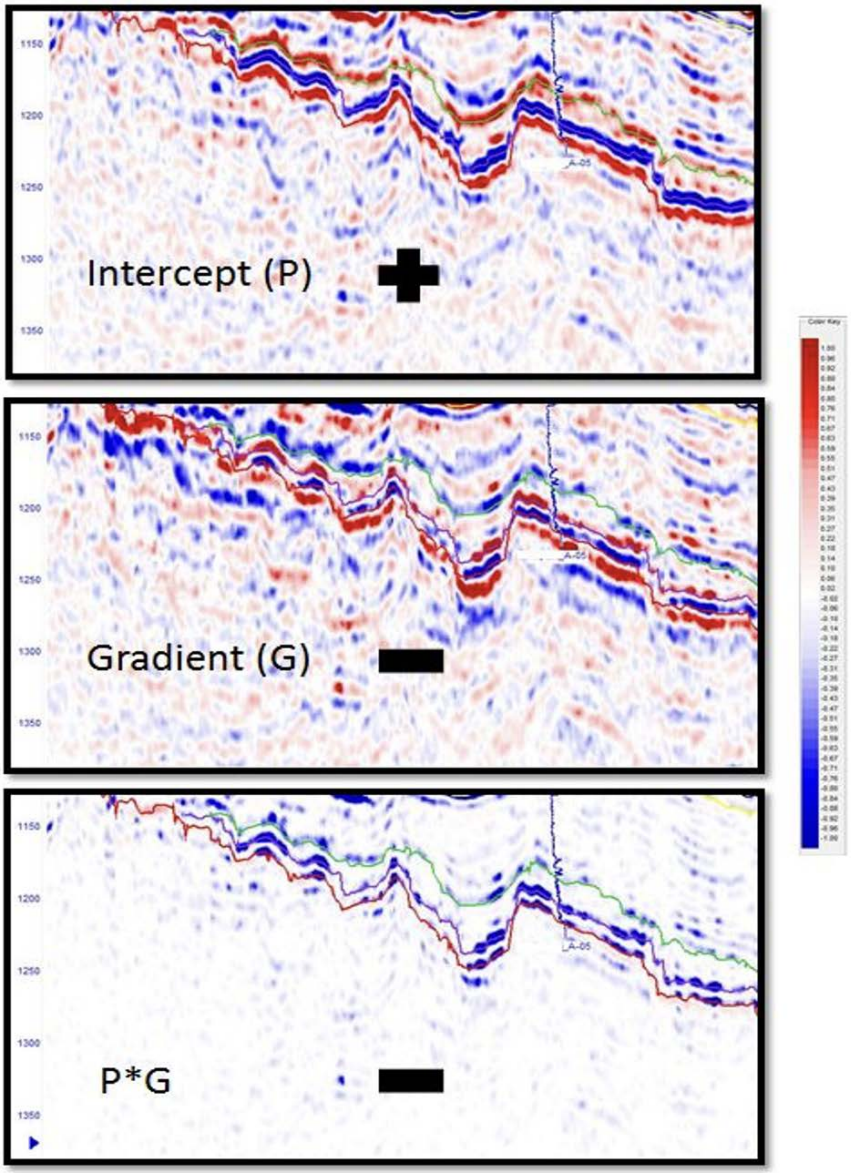

Figure 10. Intercept volume (top) shows (+) near the Basement, Gradient volume (mid) shows (-), and P*G (bottom) shows (-)

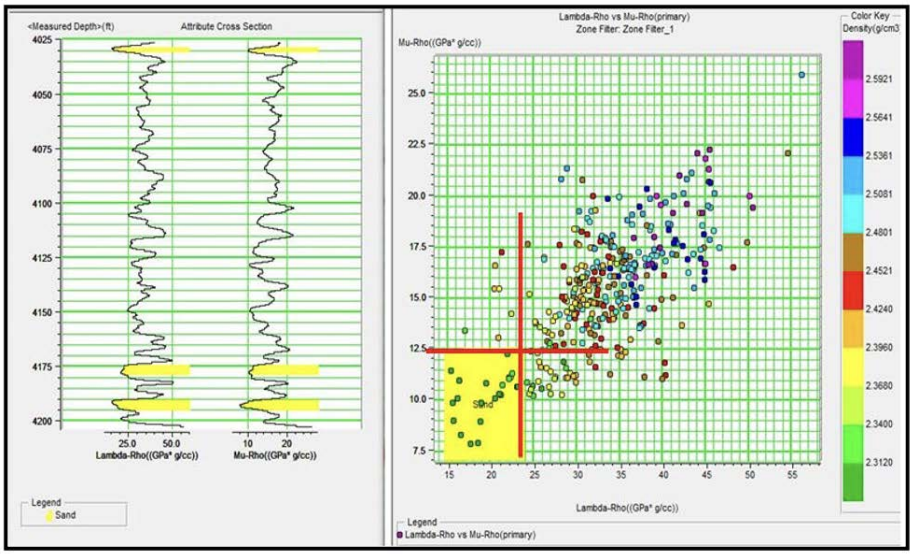

Figure 11. Feasibility test on Lambda-Rho and Mu-Rho

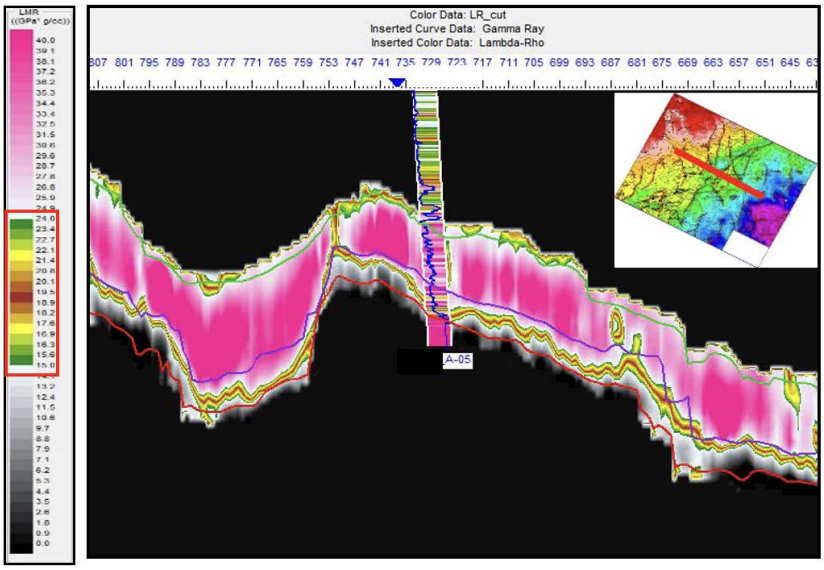

Figure 12. Lambda-Rho section that crosses on A-05 well with cut off 15-24 GPa*g/cc

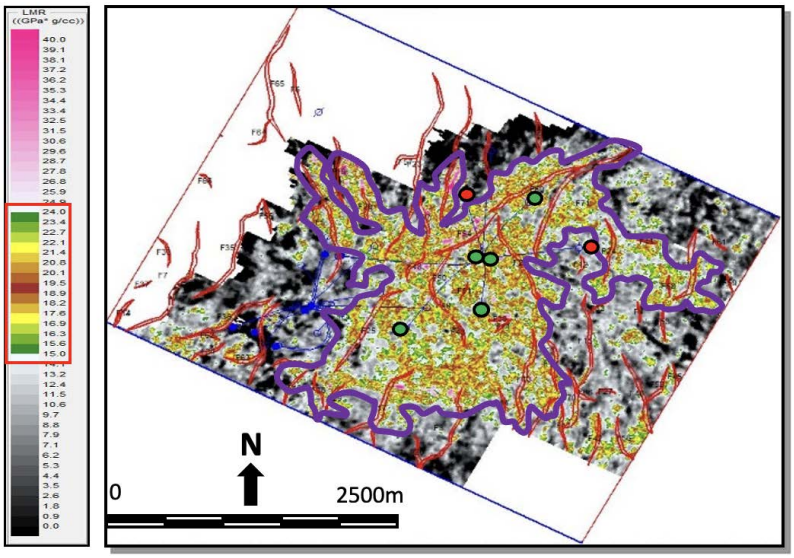

Figure 13. Lambda-Rho map shows the lateral distribution similar to alluvial fan patern

Figure 13 (Lambda-Rho map), which shows the lateral distribution similar to an alluvial fan pattern. These results were obtained from attributes that were used and utilized as an input for the geological model.

RESULTS

The four main components for constructing a static model are the seismically derived depth horizon, the fault model, layer thickness isochores, and correlated well tops. The basement horizon is the only depth horizon derived from seismic data, and other horizons are interpolated using thickness isochores. Eighteen faults are used to generate the fault model and fault segments. The facies model shown in (Figure 14) follows the conceptual depositional model for an alluvial fan system environment. Braided Channel deposits are associated with this model. Prior to facies modelling, various trends were prepared to geologically constrain the model. Data analysis of the vertical distribution of reservoir facies illustrated a common trend for most zones, where the proportion of sand generally increases towards the top of the zones. This distinct coarsening upward pattern was considered in the modelling of the reservoir facies. The total volume of clean sandstone distributed in the facies models is vertically controlled by the coarsening upward trends observed in the blocked wells. And the lateral distribution and direction of fan lobe and channels are controlled by the seismic attributes.

The distributed volume of debris-flow and mud-flow deposits is controlled by the proportions seen in the wells. It is a conceptual schematic depositional model covering the Aryani field directions within the reservoir area. It is interpreted as an alluvial fan depositional environment with both fluvial and debris flow deposits. The delineation distribution of the fan lobe follows the trend of seismic attributes.

The volume of effective porosity and permeability (Figure 15) was stochastically co-simulated with a bias towards the facies model. Each facies has its own petrophysical range, trends, and data distribution, as observed in the statistical data analysis of the upscaled well data and reflected in the model volume. Histograms, scatterplots, and data transforms were generated and analyzed for quality control of effective porosity and permeability plots. The distribution of volumes of effective porosity and permeability was compared with the stochastic output parameters to ensure consistency. Stochastic (Gaussian) conditional simulation was chosen

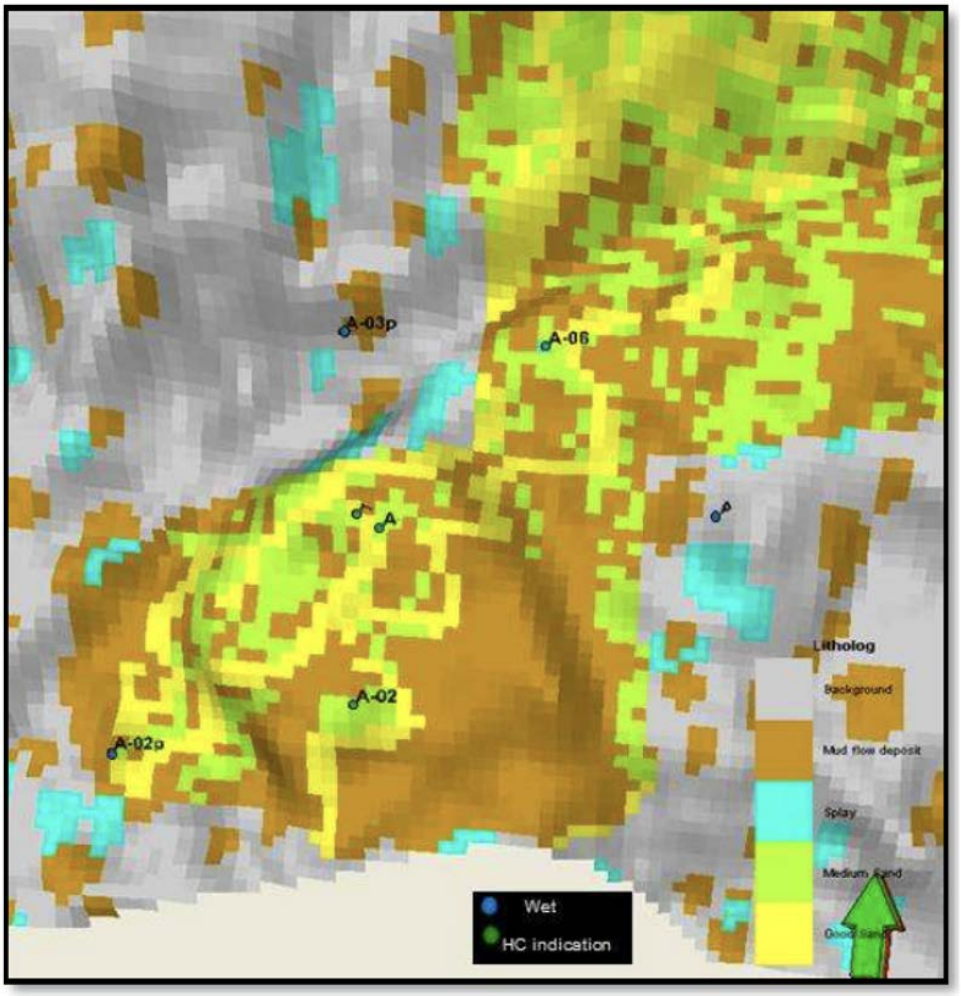

Figure 14. Facies model of Alluvial Fan deposit

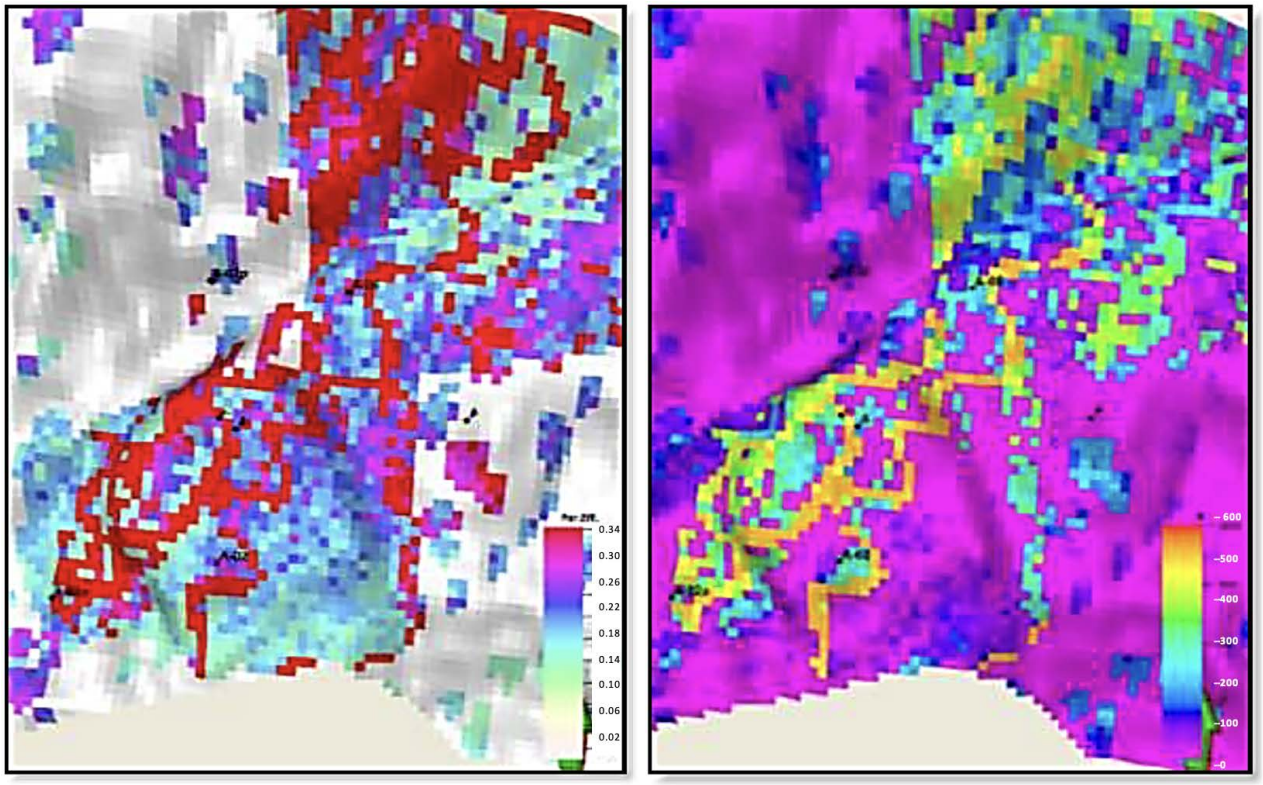

Figure 15. Porosity model (left) and permeability model (right) of Alluvial Fan deposit in Aryani Field of Widuri Area

to model the petrophysical attributes. In conjunction with the estimated variogram model, the petrophysical input parameter attributes (conditioned 100% to wells) were distributed throughout the model volume.

DISCUSSION

Based on the type of rock in the alluvial fan sediments, the interpreted Rock Type 2, which was average permeability and porosity values, is low, ranging between 6–8% and 0.1–2 mD respectively. Rock Type 3 is interpreted as mud-flow deposition and has an average permeability value of 42 mD and a porosity of 15% , indicating small channel sediment. Rock Type 4, which has a relatively high permeability average of about 280 mD and a porosity of 22%, is interpreted as the main sediment channel.

Due to the intermittent deposition process, the deposition of alluvial fans is generally not one single body but consists of several overlapping layers of sand. It is seen in the alternation of RT 0-4 which is sometimes very thin in some wells. A conceptual model of alluvial fans shows the details of the three-dimensional (3D) geometry depending on the extent of tectonic activity and the rate and volume of sediment being deposited by the streams. As indicated, alluvial fans are not generally formed as a single body but are built up over time as overlapping deposits. This is also shown in the vertical distribution of Rock Types, where the four rock types repeatedly overlap each other.

The results of the core data analysis from the A-05 well as a key well indicate that the depositional environment developing in the Aryani field is an alluvial fan as shown in Figure 16. It contains a wide range of grain sizes and many angular rock fragments. This reflects the fact that the sediments have not been transported very far from their source before being deposited. The nearest high topography is located in the northern area, and toward the south, down fan direction, the mean grain size of the sediment rapidly decreases. Alluvial fans contain a large amount of debris-flow and mud-flow deposits, leading to abrupt and erratic changes in facies, both laterally and vertically.

Alluvial fan deposits are not the result of steady deposition. Rather, a series of sporadic events, representing the discharge of an intermittent stream system is the major process. Nilsen (1982), subdivided alluvial fan deposits into two basic types. The first type consists of stream-flow deposits, which result from intermittent streams flowing in poorly defined, braided channels over the surface of the fan. Stream-flow deposits are usually coarse-grained, well sorted and stratified, with much of the clay matrix washed out. The second type consists of debris-flow and mud-flow deposits in which a saturated mass of material, often consisting of larger rocks supported in a mud-rich matrix, moves as a sediment gravity flow down the surface of the fan. As a whole, the fan body is formed through a complex interlaying of these basic types of sediment. A 3D schematic of the alluvial fan environment is shown in Figure 17.

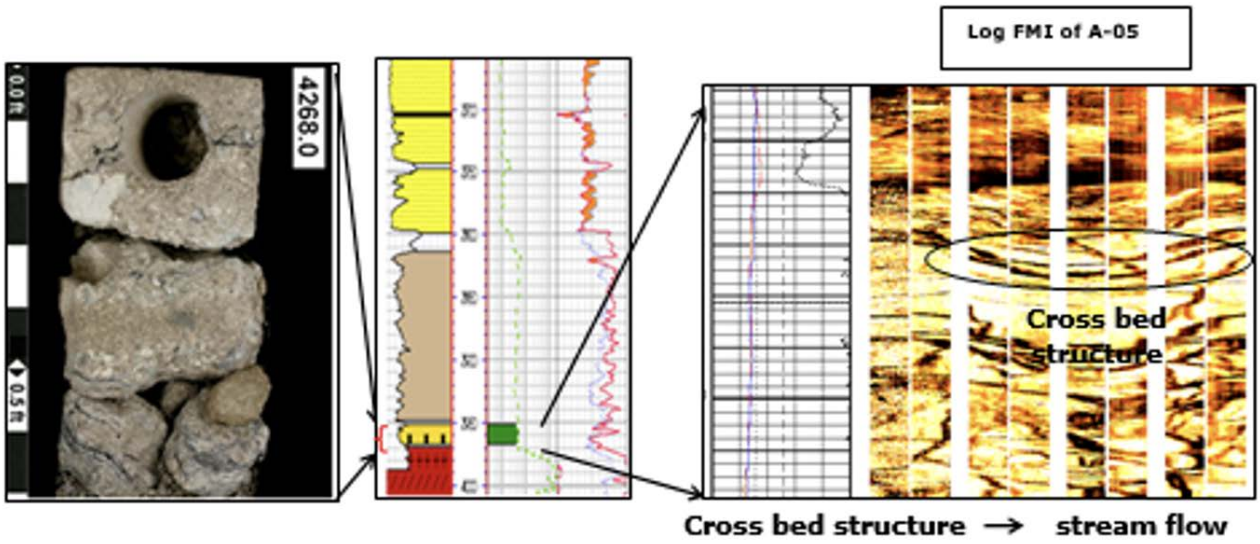

Figure 16. Core data and well logs indicate Basal Sand deposited in the Mid-Fan

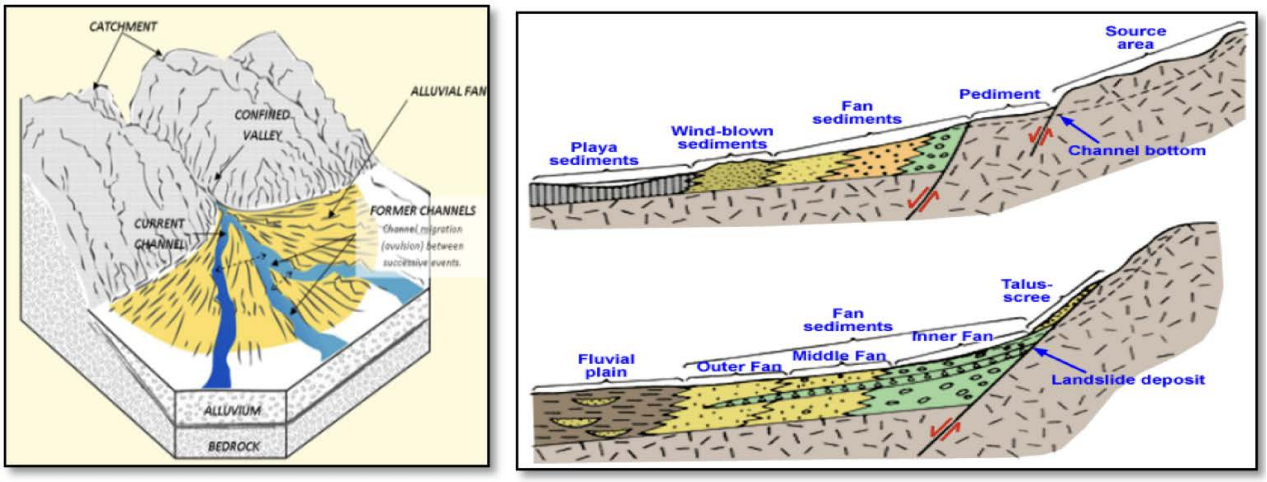

Figure 17. 3D schematic of Alluvial Fan environment (Nilsen, 1982)

CONCLUSIONS

From this research, the boundary of the Lower Zelda member geometry has defined an NW–SE trend but for the Basal Sand distribution, there is still an inconsistency between the well data and the isochrones maps. An integrated geophysical and geological analysis has been conducted for Basal Sand reservoir characterization. A low resistivity reservoir of Oligo-Miocene Talangakar Formation Basal Sand reservoir in the Aryani field of Widuri Area in Asri Basin has distinctive characteristics that require integration analysis to identify the distribution of alluvial fan sediments. By analyzing elastic properties such as Lambda Mu Rho, the lateral distribution of a thin Basal Sand reservoir has been resolved, revealing as an alluvial fan deposition pattern.

Geocellular modelling is done, using a combination of modelling methods, Truncated Gaussian for geological conditions which have lithological boundaries that are quite firm (hard boundary) and Object Model for the transition boundary (soft boundary). Rock Type and seismic attribute methods have proven to be effective in classifying thin layers of Basal Sand. The ratio method of RQI/ FZI showed a good correlation between porosity and permeability to identify different rock types. This shows the significance of rock texture in distinguishing various rock types.

ACKNOWLEDGEMENTS

The authors would like to thank the management of Pertamina Hulu Energi OSES, Pertamina EP, Pertamina Sub-holding Upstream (PHE), and SKK MIGAS, for their permission to publish this paper. Thank you to all Geosciences & Reservoir Team of the Subsurface Development Planning Department - PHE OSES, Talangakar Formation Technical Interests Group, all lecturers and civitas academica of Post-Graduate Program, Faculty of Geological Engineering, Universitas Padjadjaran for sharing beneficial, fruitful, and constructive discussions during this research and manuscript preparation.

REFERENCES

Aldrich, J.B., Pinehart, G.P., Ridwan, S., and Schuepbach, M.A., 1995. Paleogene Basin Architecture of the Sunda and Asri Basins and Associated Non-Marine Sequence Stratigraphy, *Proceedings of International Symposium on Sequence Stratigraphy, Indonesian Petroleum Association*, Jakarta, May 1995, 261-287.

Aki, K., and Richards, P.G., 1980. *Quantitative Seismology: Theory and Methods*, Vol 1, W.H. Freeman and Co.

Amaefule, J.O., Altunbay, M., Tiab, D., Kersey, D.G., and Keelan, D.K., 1993. *Enhanced Reservoir Description - Using Core and Log Data to Identify Hydraulic (Flow) Units and Predict Permeability in Un-cored Intervals/Wells,* Society of Petroleum Engineers 26436.

Castagna, J.P., Swan, H.W., and Foster, D.J., 1998. Framework for AVO Gradient and Intercept Interpretation, *Geophysics,* 63, p948-956.

Gray, F.D., and Andersen, E.A., 2000. The Application of AVO and Inversion to Formation Properties, *World Oil,* Vol. 221, No. 7.

Guo, G., Diaz, M.A., Paz, F., Smalley, J., and Waninger, E.A., 2007. Rock Typing as an Effective Tool for Permeability and Water-Saturation Modeling: A Case Study in a Clastic Reservoir in the Oriente Basin. *SPE Res Eval & Eng* 10 (6): 730-739. SPE-97033-PA.

Nilsen, T.H., 1982. Alluvial fan deposits. In Scholle, P.A. and Spearing, P. (eds.), Sandstone Depositional Environments. *Memoir: American Association of Petroleum Geologists* 31: pp. 49–86.

Ralanarko, D., Syafri, I., Abdurrokhim, and Nur, A.A., 2020. Seismic Expression of Paleogene Talangakar Formation, Asri & Sunda Basins, Java Sea, *Indonesian Journal of Sedimentary Geology,* ISSN 0853-9413, No. 46, 21-43.

Ralanarko, D., Syafri, I., Abdurrokhim, and Nur, A.A., 2021. A Success Case of Widuri Area Rejuvenation, Asri Basin, Offshore SE Sumatra Block, Indonesia, *Bulletin of Marine Geology*, DOI: http://dx.doi.org/10.32693/bomg.36.2.2021.704

Ralanarko, D., Ramadhan, M.I., Fauzielly, L., Winantris, Syafri, I., and Abdurrokhim, 2021. Facies Association and Paleogeography Reconstruction pada at Transition Zone Talangakar Formation, Asri Basin, Offshore Southeast Sumatra, Indonesia, *Journal of Marine Geology*, DOI: http://dx.doi.org/10.32693/jgk.19.2.2021.736

Smith, G., and Gidlow, P. M., 1987. Weighted Stacking for Rock Property Estimation and Detection of Gas: *Geophys. Prosp.,* 35, 993–1014.

Wight, A., Friestad, H., Anderson, I., Wicaksono, P., and Remington, C.H., 1997. Exploration History of the Offshore Southeast Sumatra PSC, Java Sea, Indonesia, in: Petroleum Geology of Southeast Asia, Fraser, Matthews, and Murphy (eds.), *Geological Society Special. Publication* No. 126, p. 121-142.

Young, R. and Atkinson, C.D., 1993. A Review of Talangakar Formation (Oligo-Miocene) Reservoirs in the Offshore Areas of Southeast Sumatra and Northwest Java. Clastic Core Workshop, *Spec. Publication of the Indonesian Petroleum Association*, 177-210.

SUBSURFACE GEOLOGICAL INTERPRETATION OF THE NORTH SUNDA ASRI BASIN BASED ON SVD ANALYSIS AND GRAVITY ANOMALY MODELING

INTERPRETASI GEOLOGI BAWAH PERMUKAAN CEKUNGAN SUNDA ASRI BAGIAN UTARA BERDASARKAN ANALISIS SVD DAN PEMODELAN ANOMALI GAYABERAT

Hayu Nurfaidah[1*], Imam Setiadi[2], Muhammad Sarkowi[1], and Ordas Dewanto[1]

[1] Department of Geophysical Engineering, Faculty of Engineering, University of Lampung, Jl. Prof. Dr. Ir Sumantri Brojonegoro, Bandar Lampung, 35141

[2] Marine Geological Institute, Jl. Djunjunan No. 236, Husein Sastranegara Bandung 40174

*Corresponding author: hayunurfaidah@gmail.com

(Received 25 May 2023; in revised from 30 May 2023; accepted 21 June 2023)

DOI : 10.32693/bomg.38.1.2023.833

ABSTRACT: The Sunda Asri Basin is dominated by normal faults and has little compressional structure. This basin consists of several depocenters with a thickness of up to 6000 m. Among the geophysical methods, gravity analysis has proven to be effective in determining the bedrock configuration and identifying sedimentary basins. This study aims to analyze sedimentary sub-basin patterns, basement height structures, faults, and bedrock configuration using trend surface analysis of polynomial filters. The analysis of polynomial filter show that a 10th-order anomaly yields optimal results. The high correlation value of 0.990925 provides the suitability of a 10th-order anomaly for qualitative interpretation. Spectral analysis results indicate an average bedrock depth of about 2.75 km within the Sunda Asri Basin. Furthermore, this analysis reveals the presence of 14 sedimentary sub-basin patterns in this area. The gravity modeling results indicate that the top layer has a density value of 2.37 g/cc, which interpreted as Pleistocene Tertiary sediment. The second layer consists of Tertiary-Miocene sediment with a density value of 2.28 g/cc, while the third layer comprises of Pre-Tertiary sedimentary rock at a density of 2.02 g /cc. The bottom layer of the model corresponds to metamorphic bedrock with a density 2.7 g/cc. SVD (Second Vertical Derivative) analysis successfully identified the presence of normal and thrust fault structures

Keywords: Gravity, Polynomial Trend Surface Analysis, Second Vertical Derivative (SVD), Sunda Asri Basin

ABSTRAK: *Cekungan Sunda Asri didominasi oleh sesar normal dan memiliki sedikit struktur kompresional. Cekungan ini terdiri dari beberapa deposenter dengan ketebalan hingga 6000 m. Di antara metode geofisika, analisis gayaberat terbukti efektif digunakan untuk menentukan konfigurasi batuan dasar dan mengidentifikasi cekungan sedimen. Penelitian ini bertujuan untuk menentukan pola sub-cekungan sedimen, struktur tinggian, patahan, dan konfigurasi batuan dasar menggunakan analisis filter permukaan dengan tren polinomial. Analisis filter polinomial menunjukkan bahwa anomali orde 10 menghasilkan keluaran yang optimal. Nilai korelasi tinggi sebesar 0,990925 memberikan bukti bahwa anomali orde 10 cocok untuk interpretasi kualitatif. Analisis spektral menunjukkan kedalaman batuan dasar rata-rata Cekungan Sunda Asri sekitar 2,75 Km. Hasil analisis juga mengungkapkan adanya 14 pola sub-cekungan sedimen di daerah ini. Pemodelan gayaberat menunjukkan bahwa lapisan teratas memiliki nilai densitas 2,37 g/cc, yang diinterpretasikan sebagai sedimen Pleistosen Tersier. Lapisan kedua terdiri dari sedimen Tersier-Miosen dengan nilai densitas 2,28 g/cc, sedangkan lapisan ketiga merupakan batuan sedimen Pra-Tersier dengan densitas 2,02 g/cc. Lapisan terbawah pada model tersusun dari batuan dasar metamorf dengan densitas 2,7 g/cc. Analisis SVD (Second Vertical Derivative) berhasil mengidentifikasi adanya struktur patahan naik dan patahan turun.*

Kata Kunci: *Gaya Berat, Polynomial Trend Surface Analysis, Second Vertical Derivative (SVD), Cekungan Sunda Asri.*

INTRODUCTION

The Sunda Basin, located about 30 miles southwest of the Asri Basin, or 30 miles northwest of Jakarta, is an offshore area in the Java Sea. The Sunda Basin extends northeastward, transforming into the Asri Basin, and is structurally separated by the Seribu Heights. In terms of regional context, the Asri Basin is positioned at the southeastern tip of the Eurasian Plate and specifically belongs to the Sunda Microplate (Todd and Pulunggono, 1971).

The Sunda Basin is an extension of the Northern Java Basin, known as the Asri Sub-basin. The Sunda Basin originates from the back-arc depocenter which is called the back-arc depocenter of Java Island. The faults trending northwest-southeast and north-south are active and act as basin boundaries (Daly, 1991).

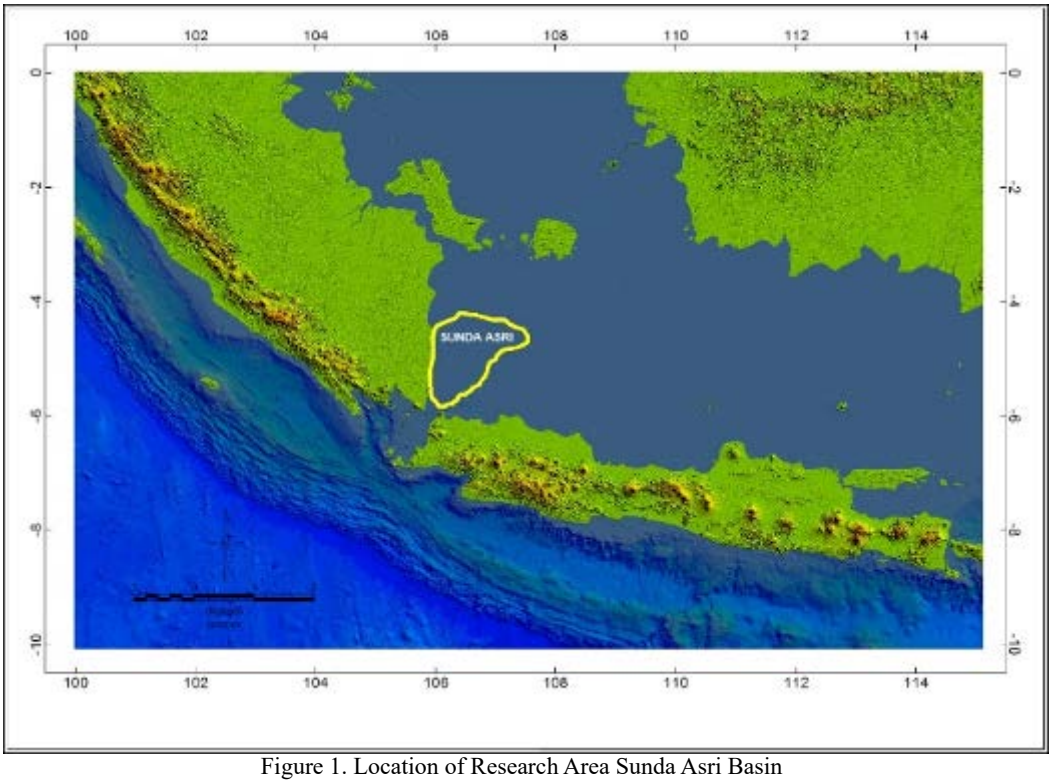

Figure 1. Location of Research Area Sunda Asri Basin

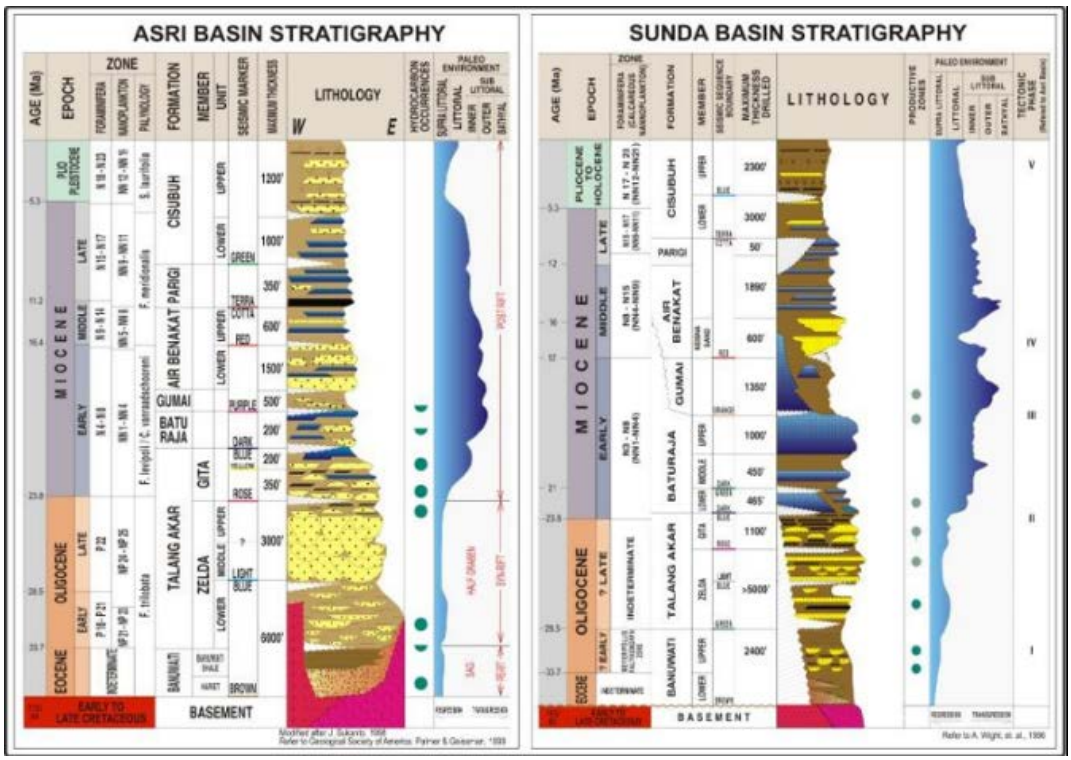

Figure 2. Stratigraphy of the Asri Sunda Basin (Wight et al., 1986)

According to Koesoemadinata (2004), the oldest rocks in the Sunda Asri Basin are bedrock consisting of metamorphic and igneous rocks. Meanwhile, according to Sukanto (1998), the stratigraphy of the Sunda Asri Basin shows a mega cycle of base level rise (Banuwati - Gumai Formation) and base level fall (Air Benakat Formation - Cisubuh).

The gravity method is a geophysical method that utilizes the Earth's gravitational field due to variations in rock mass density. The basic principle of this method is to measure the variation in the value of the gravitational acceleration caused by differences in the density of rock masses beneath the Earth's surface (Yan et al., 2020).

METHODS

The data used in this study comprises corrected Bouguer anomaly data for the Sunda Asri Basin area, collected by the Geological Agency in 2009. Data processing involved spectral analysis of corrected Bouguer anomaly data to obtain bedrock depth and window width used as a reference in modeling. Filtering uses Polynomial Trend Surface Analysis by filtering polynomials from orders 1 to 12. The selection of the optimal polynomial order was based on correlating regional anomalies derived from the polynomial results with regional anomaly references obtained from low pass filtering through spectral analysis. The correlation results show that the 10th order polynomial has the highest correlation value, so the 10th-order regional anomaly is used as the optimal filter result, which is then used to conduct a qualitative interpretation.

The gravity method is a geophysical method that utilizes the Earth's gravitational field due to variations in rock mass density. The basic principle of this method is to measure the variation in the value of the gravitational acceleration caused by differences in the density of rock masses beneath the Earth's surface (Yan et al., 2020). The 10th-order residual anomaly results are used to delineate the sedimentary sub-basin and the basement height of the study area. The residual anomaly results are also used to create cross sections for 2D modeling, which help in determining the fault structure of the study area using SVD (Second Vertical Derivative) analysis.

Spectral Analysis

The spectral analysis results obtain a graph of the wave number (k) as the x-axis with the amplitude (*ln A*) as the y-axis. In the gravity method, the spectrum is derived from the observed gravity potential in a horizontal plane (Blakely, 1996) as described by:

$$A = Ce^{|k|(z_0 - z_1)} \quad (1)$$

$$lnA = ln2\pi Gme^{|k|(z_0 - z_1)} \quad (2)$$

$$lnA = (z_0 - z_1)|k| + ln\, C \quad (3)$$

The equation is analogous to the equation of a straight line:

$$y = mx + c \quad (4)$$

Where *ln A* is the y-axis, |k| is the x-axis, and the slope of the line represents gradient. The window width is formulated as follows:

$$N = \frac{2\pi}{k_c \Delta x} \quad (5)$$

Polynomial Trend Surface Analysis

The process of separating regional and residual anomalies in research using a polynomial trend analysis filter involves utilizing the optimal order correlation results to obtain regional anomalies. The Trend Surface Analysis (TSA) equation is as follows:

$$Z_{obsi} = f(x_i, y_i) + u_i \quad (6)$$

The polynomial method can be approximated by Bouguer anomaly with the following equation:

$$G_{ij} = (ax_i + by_j + c) + e_{ij} \quad (7)$$

$$e_{ij} = G_{ij} - (ax_i + by_j + c) \quad (8)$$

Where *Gij* is the Bouguer anomaly, *xi* is the measurement coordinate in the x-direction, *yj* is the measurement coordinate in the y-direction, *eij* is the residual anomaly, and *a*, *b*, *c* are polynomial constants.

2D and 3D modeling are conducted to examine the horizontal and vertical continuity of the structure in the study area. The results of 3D inversion modeling provide an overview of subsurface conditions based on density distribution and enhance subsurface model information obtained from 2D modeling. Inversion modeling is performed using the Grablox software (Pirttijarvi, 2008).

Second Vertical Derivative (SVD) analysis was carried out to determine the boundaries of the basin or to determine the types of faults present in the study area. In the SVD graph, the line drawn at point 0 indicates the presence of a fault structure. The direction of the slope of the SVD curve can indicate the type of fault, with maximum and minimum SVD values given by the following equation:

For Thrust Fault $\left(\frac{\partial^2 \Delta g}{\partial x^2}\right)_{max} < \left|\left(\frac{\partial^2 \Delta g}{\partial x^2}\right)\right|_{min}$ (9)

For Normal Fault $\left(\frac{\partial^2 \Delta g}{\partial x^2}\right)_{max} > \left|\left(\frac{\partial^2 \Delta g}{\partial x^2}\right)\right|_{min}$ (10)

RESULTS

The Bouguer anomaly in the Sunda Asri Basin is shown in Figure 3. The figure illustrates low anomalies indicated by blue shades, while high anomalies are represented by red to purple colors. Based on the Bouguer

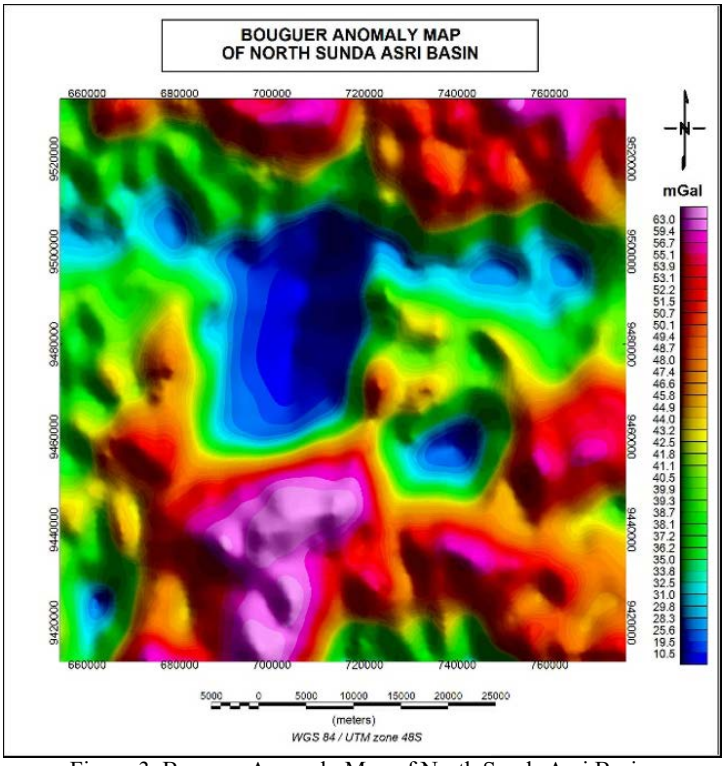

Figure 3. Bouguer Anomaly Map of North Sunda Asri Basin

anomaly map, the anomalous values range from 10.5 to 63.0 mGal. The low anomaly shown in blue ranges between 10.5 to 31.0 mGal, suggesting the presence of relatively thick sedimentary rock that occupies this area. The moderate anomaly, with values ranging from 32.5 to 48.7 mGal, is interpreted as the edge of the basin which delineating the sub-basins. The high anomaly, ranging from 49.4 to 63.0 mGal indicates the presence of uplifted high-density rocks. The Bouguer Anomaly map does not a detailed description of the local structure in the study area, as it combines both regional anomalies and residual anomalies. Therefore, it is necessary to separate these anomalies.

Spectral analysis was carried out to estimate the basement depth and window width of the study area. In this study, 8 cross-sectional tracks were created with a spacing (x) of 2 km, as shown in Figure 4. The slope or gradient of the line on the graph of *ln A* vs *k* represents the depth of the discontinuity plane. The width of the window used in the spectral analysis results is then applied in the filtering process, including lowpass and highpass filters. The separated anomalies obtained using the lowpass and highpass filters are used as a reference for the correlation process to determine anomalous pattern generated by the trend surface polynomial filter.

Anomaly separation using the trend surface polynomial filter is carried out by selecting the optimal order of the correlation results between regional anomalies from spectral analysis and polynomial trend surface analysis in the study area, as seen in Table 2. Complete data processing was carried out using Surfer software, DOS-BOX, and Matlab.

Regional and residuals anomalies of the 10th order polynomial results are shown in Figure 5. The regional anomalies of the 10th order range from 14.8 to 60.9 mGal. The low anomaly is represented by dark to light blue shades, ranging from 14.8 to 32.3 mGal. The medium anomaly, indicated by green to orange colors, has values ranging from 33.6 to 49.1 mGal. The high anomaly, shown by red to purple colors, ranges from 49.7 to 60.9 mGal.

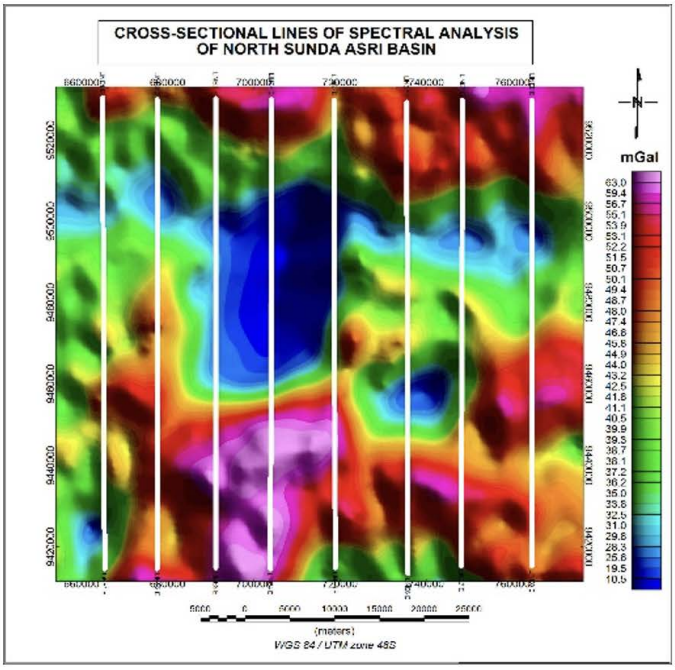

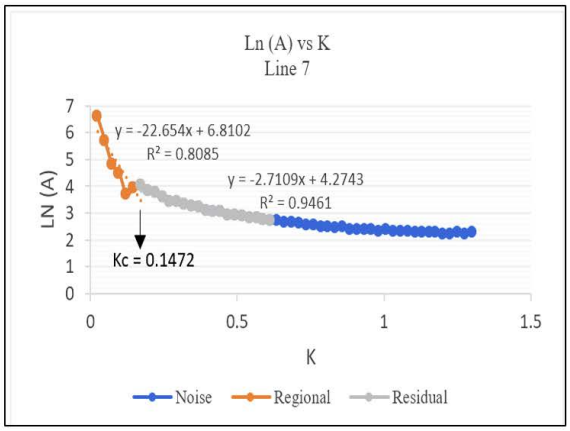

Figure 4. Cross-sectional lines of spectral analysis and the graph of ln A vs k of Line 7

Table 1. The depth of the regional and residual discontinuity planes

No	*Line*	*Regional (km)*	*Residual (km)*	*Kc*	*N*
1	Line 1	-21.467	-2.8254	0.1472	21.33
2	Line 2	-26.351	-2.8704	0.1227	25.59
3	Line 3	-13.66	-2.8876	0.1718	18.27
4	Line 4	-18.47	-2.9763	0.1472	21.33
5	Line 5	-22.259	-2.8523	0.1472	21.33
6	Line 6	-20.235	-2.6002	0.1472	21.33
7	Line 7	-22.654	-2.7109	0.1472	21.33
8	Line 8	-26.466	-2.239	0.1718	18.27
Average		**-21,45**	**-2,75**	**0,15**	**21,1**

Table 2. Regional anomaly correlation results from the spectral and polynomial analysis

No	*Order Polynomial*	*Correlation Results*
1	Polynomial Order 2	0,977892
2	Polynomial Order 3	0,986113
3	Polynomial Order 4	0,989687
4	Polynomial Order 5	0,991596
5	Polynomial Order 6	0,993682
6	Polynomial Order 7	0,996608
7	Polynomial Order 8	0,997768
8	Polynomial Order 9	0,998844
9	**Polynomial Order 10**	**0,998925**
10	Polynomial Order 11	0,998392
11	Polynomial Order 12	0,998190

The 10th order residual anomaly map shows values ranging from -8.4 to 8.0 mGal. The low anomaly ranges between -8.4 to -3.8 mGal, while the medium spans from -3.4 to 1.8 mGal. The high anomaly is observed from 2.1 to 8.0 mGal.

The regional anomaly pattern obtained using this polynomial still have a trend similar to the complete Bouguer anomaly. It reveals anomalyous sources effect at relatively shallow depths, as indicated by the presence of with both positive and negative anomalies. The North Sunda Asri Basin shows a north-south trend, likely formed by the subduction of the Indo-Australian plate to the east. This subduction process created a half-graben structure along the southern edge of the Sunda Plate during the Eocene-Oligocene period.

The lineament pattern and delineation of the Sunda Asri basin were determined based on the best filtering process of the residual anomaly, specifically utilizing the results of a 10th order polynomial filter, as shown in Figure 6. The lineament patterns of basement high have a relative north-south direction, possibly caused by the movement of the Indian Ocean crust from west to east, resulting in a high structure with a relative north-south direction. Setiadi et al. (2018) suggests that the high anomaly pattern likely caused by uplift due to tectonic events and compressional processes between plates. The analysis of residual anomalies indicates that these height patterns separate the sub-basins within the Sunda Asri basin, particularly at the blue low anomaly. The sub-basin in the Sunda Asri basin area probably formed due to openings in a relatively north-south direction, resulting in the formation of sub-basins with a similar orientation. A total of 14 sub-basins can be delineated based on the residual anomalies of the Sunda Asri basin.

Quantitative interpretation involves conducting 2D and 3D modeling to determine the shape and dimensions of the subsurface geological model. The 2D modeling is carried out along two paths, namely the AA' and BB' paths. The AA' path has a relatively northwest-southeast direction, while the cross section of the BB' path has a west-east relative direction, as shown in Figure 7.

The 2D modeling was performed using GM-SYS Oasis Montaj software, considering the stratigraphic references of the study area and depth information obtained from the spectral analysis results. Modeling process involved simplifying several formations into one-layer models based on the stratigraphic information. The first layer, consisting of the Air Benakat, Parigi, and Cisubuh formations, reveals lithologies such as claystone, sandstone, shale, and limestone, with an average density value of 2.37 g/cc. The second layer comprises the Baturaja Formation and Gumai, characterized by lithologies including limestone, claystone, shale, silt, and sandstone, with an average density value of 2.28 g/cc. The third layer consist of the Banuwati and Talang Akar formations, showing lithologies such as claystone, sandstone, and a small amount of coal content, with an average density value of 2.02 g/cc. Finally, the fourth layer represents the basement, composed of metamorphic igneous rock with an average density value of 2.71 g/cc.

The results of the SVD modeling and analysis in Figure 7 reveal the presence of normal and thrust fault

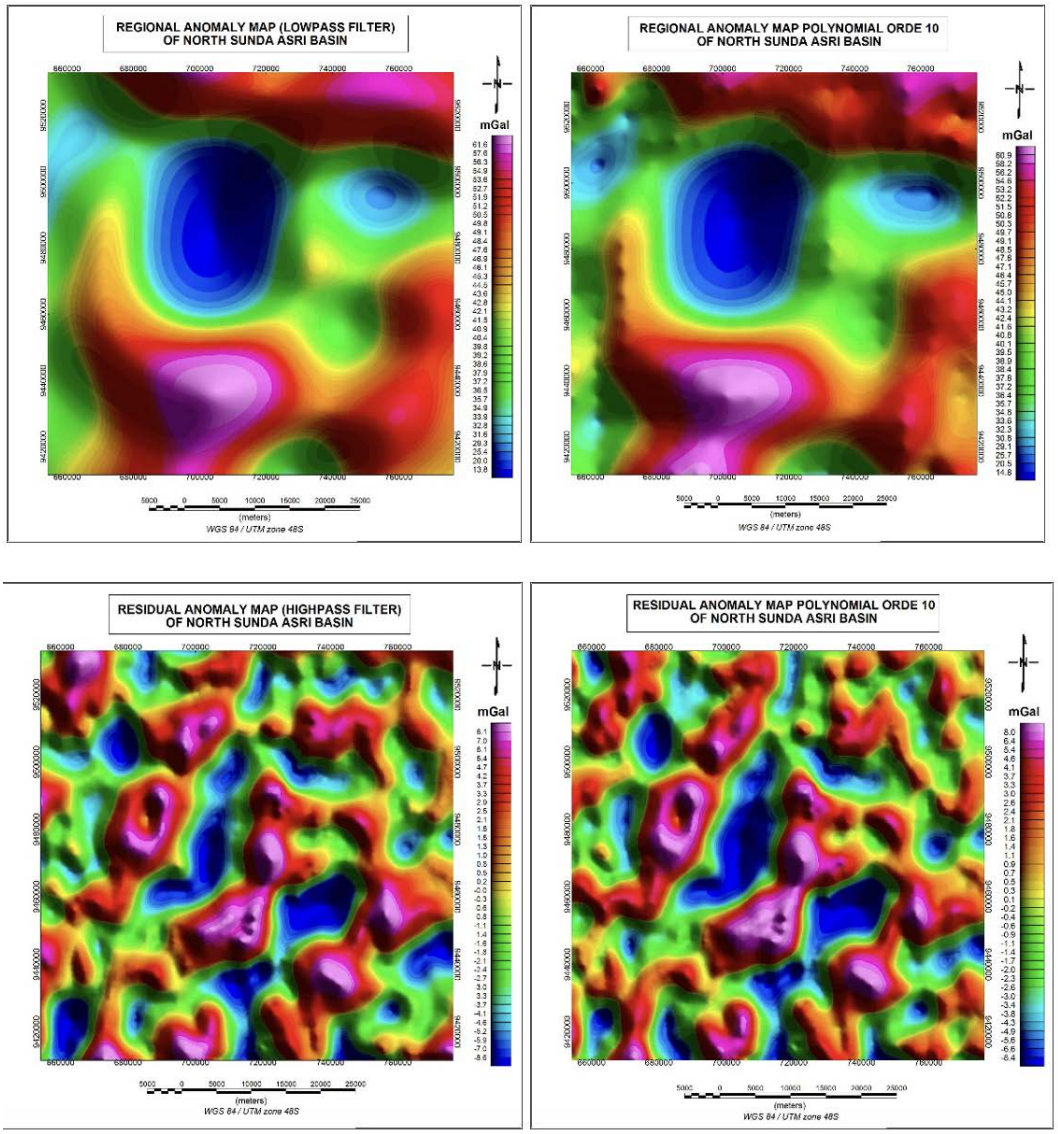

Figure 5. Regional and residual anomalies derived from polynomials of the 10th order

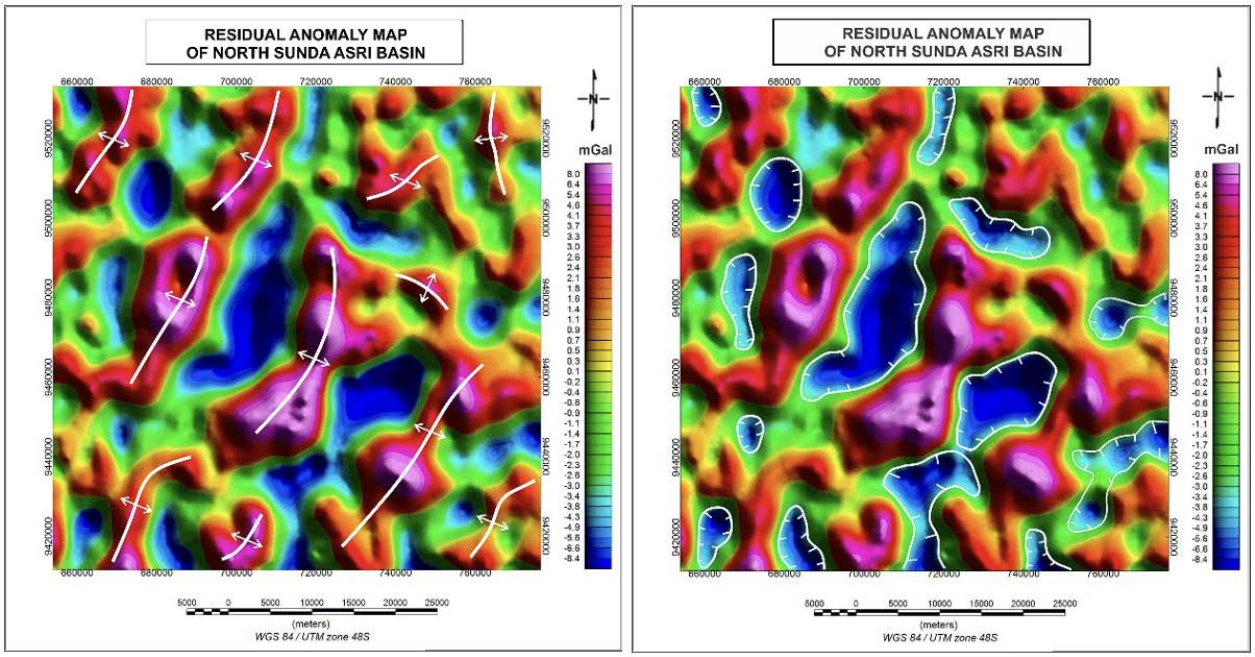

Figure 6. Lineament pattern and delineation of the Sunda Asri sub-basin

structures. The determination of the fault types in the SVD

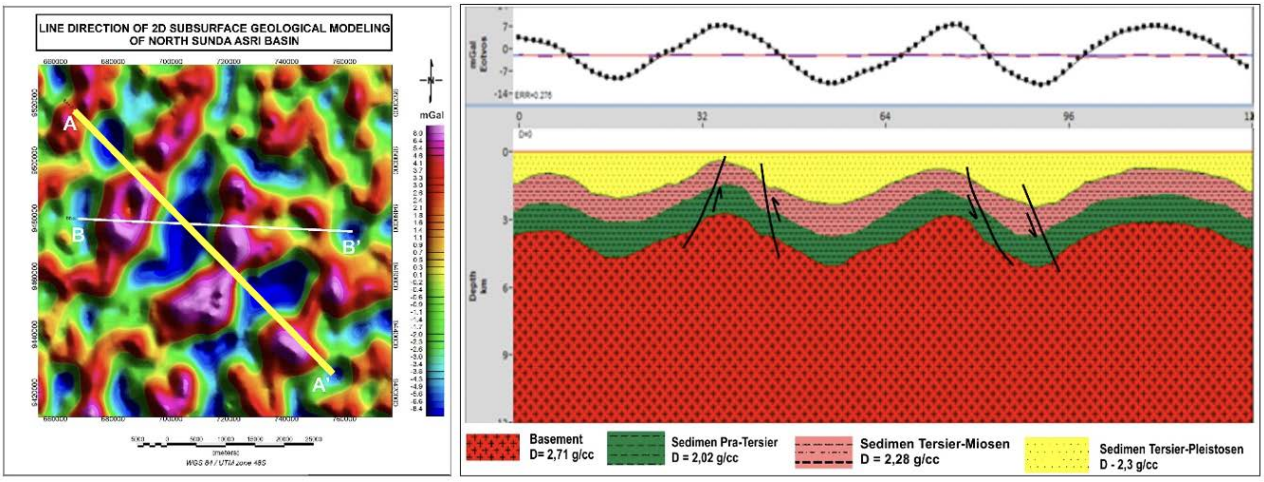

Figure 7. Line section and 2D Modeling of Line AA'

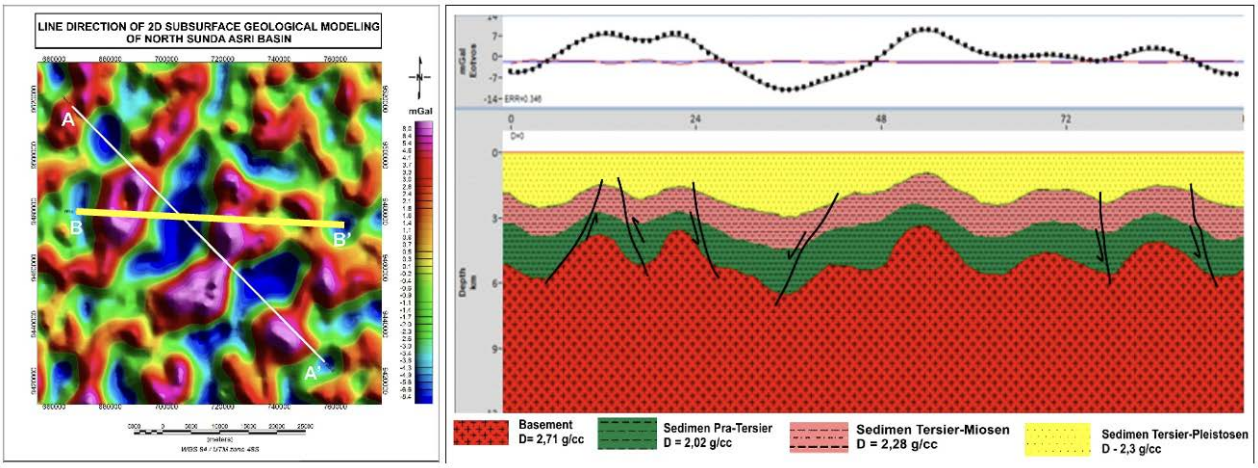

Figure 8. Line section and 2D Modeling of Line BB'

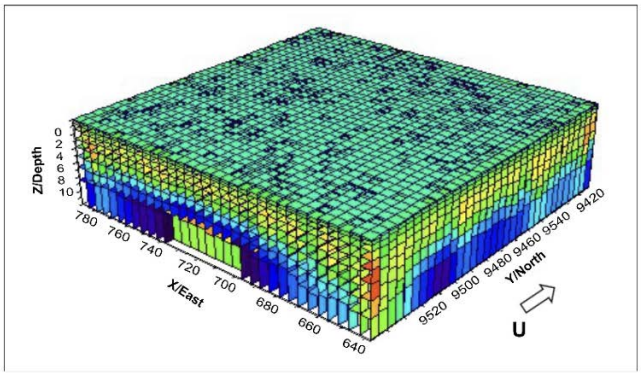

(a)

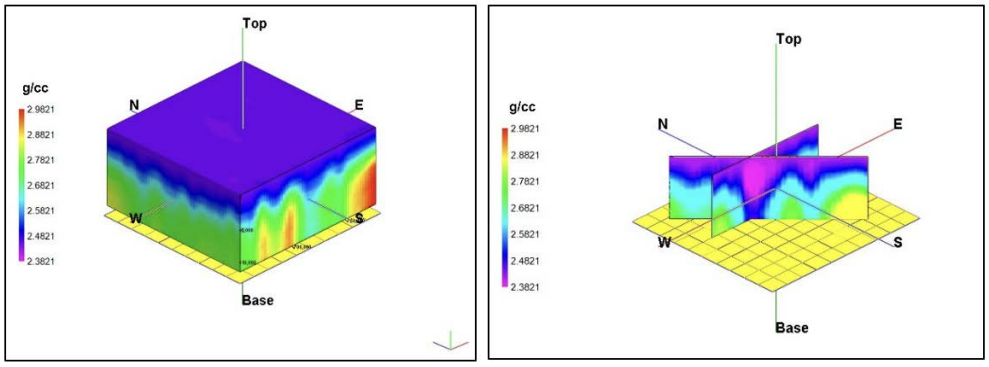

(b) (c)

Figure 9. *Rockwork* 3D Modeling

analysis is based on the second derivative having a value of zero. Along the AA' path, two types of normal faults were identified, where the maximum SVD anomaly value is greater than the minimum anomaly. It can also be identified that there are two thrust faults where the minimum SVD anomaly value is greater than the maximum anomaly.

Along the BB' path, four types of normal faults were detected, with the maximum SVD anomaly value exceeds the minimum anomaly. Furthermore, two thrust faults where the minimum SVD anomaly value exceeding the maximum anomaly.

Figure 9a display the result of 3D inversion modeling using Grablox software, while Figures 9b and 9c show the results of 3D inversion using Rockwork software. The 3D inversion modeling results indicate that sediments shown in blue are at a depth of 0 – 5000 m with a density value of 2.3 g/cc – 2.5 g/cc. Meanwhile, the basement is shown in green to red at a depth of 5000 to 12000 m with a density value of 2.6 g/cc – 2.9 g/cc. Gravity modeling aimed to identify structures in the study area and determine the depocenter depth of sub-basins in the Sunda Asri Basin. Where there are several interesting basin with a thickness of up to 6000 m.

The existence of basement height structures and several sedimentary sub-basin shows quite interesting data for the development of the existing petroleum system in the Sunda Asri Basin. Petroleum system information indicates that the study area is a hydrocarbon producing sedimentary basin, which is in the Talang Akar Formation with the main reservoir consisting of sandstones. The gravity study results in the Sunda Asri Basin provide additional geoscientific information, particularly regarding structural patterns, sedimentary sub-basins and subsurface geological models, which are expected to become additional data for the next stage of oil and gas exploration in the Sunda Asri basin.

CONCLUSIONS

The results of the spectral analysis show that the average depth of the bedrock of the Sunda Asri basin is 2.75 km. Based on the optimal polynomial filter, the delineation of sub-basins reveals the presence of 14 sedimentary sub-basins in the Sunda Asri basin. The structural pattern, as determined using qualitative analysis, demonstrates a relatively southwest-northeast and north-south direction. The first layer was modeled with an average density of 2.37 g/cc, comprising claystone, sandstone, shale, and limestone. The second layer, with an average density of 2.28 g/cc, consists of limestone, claystone, shale, silt, and sandstone. The third layer, with a density value of 2.02 g/cc, includes claystone, sandstone, and a small amount of coal. Lastly, the basement, located at the bottom, is composed of metamorphic rock with an average density value of 2.71 g/cc. The analysis of the selected paths using the Second Vertical Derivative (SVD) technique reveals the presence of normal fault structures and several thrust faults. The existence of basement high structures and several sedimentary sub-basin indicates an attractive structure for the development of the existing petroleum system in the Sunda Asri basin.

ACKNOWLEDGEMENTS

The author would like to thank the Head of the Marine Geological Survey and Mapping Center (BBSPGL) for giving permission to use the data processing facility. The author also thanks the Head of the Geological Survey Center for the use of gravity data, the editors and reviewers, as well as all parties who assisted in data processing and contributed to the writing of this scientific work.

REFERENCES

Blakely, R.J., 1996. *Potential Theory in Gravity and Magnetic Applications*. Cambridge University Press.

Daly, M.C., Cooper, M.A., Wilson, I., Smith, D.G., and Hooper, B. G. D., 1991. Cenozoic Plate Tectonics and Basin Evolution in Indonesia. *Marine and Petroleum Geology*, 8(1):2-21. https://doi.org/10.1016/0264-8172(91)90041-X.

Koesoemadinata, R.P., 2004. *Regional Setting of The Sunda and Asri Basins.* CNOOC SES Ltd. Internal Study. Jakarta.

Pirttijarvi, M., 2008. *Gravity Interpretation and Modeling Software Based on 3-D Block Models*. User's guide to version 1.6b. Department of Physics Sciences. University of Oulu. Finlandia.

Setiadi, I., Setyanta, B., and Widijono, B.S., 2018. Delineasi Cekungan Sedimen Sumatra Selatan Berdasarkan Analisis Data Gaya Berat. *Jurnal Geologi dan Sumberdaya Mineral*, 20(2):93-106.

Sukanto, J., Nunuk, F., Aldrich, J.B., Rinehart, G.P., and Mitchell, J., 1998. Petroleum System of the Asri Basin, Java Sea, Indonesia. *26th Convention and Exhibition Proceedings*. Indonesian Petroleum Association, 1998.

Todd, D.F., and Pulunggono, A., 1971. The Sunda Basinal Area, An Important New Oil Province. American Association of Petroleum Geologists Conference. Houston.

Wight, A., Sudarmono, and Imron, A., 1986. Stratigraphic Response to structural Evolution in a Tensional, Back Arc Setting and Its Exploratory Significance: Sunda Basin, West Java Sea. *15th Annual Convention Proceedings*. Indonesian Petroleum Association, 1: 77-100.

Yan, M., Zhang, Y., Bocobo, G.A., Su, Q., Zhu, K., Zhang, Q., and Tan, J., 2020. A novel tissue separation method for determining upper trunk

center of gravity in patients with thoracolumbar kyphosis using MIMICS. *Clinical Biomechanics*, 71(2020), 101–106. https://doi.org/10.1016/j.clinbiomech.2019.11.002.

LITHOLOGY AND RESERVOIR IDENTIFICATION IN THE "EL" WELL, EAST JAVA USING SEISMIC INVERSION

IDENTIFIKASI LITOLOGI DAN ZONA RESERVOIR PADA SUMUR "EL", JAWA TIMUR MENGGUNAKAN INVERSI SEISMIK

Maulana Yusuf Ibrahim[1*], Salma Dita Rysqi Puspita[1], Zhafirah Nurul Syarafina[1], Shaska Ramadhan Zulivandama[2], and Eleonora Agustine[1,3]

[1] Geophysics, Faculty of Mathematics and Natural Sciences, Padjadjaran University, Sumedang 45363, Indonesia

[2] Marine Geological Institute, Jl. Djunjunan No. 236, Husein Sastranegara Bandung 40174

[3] Center for Materials and Earth Engineering studies, Faculty of Mathematics and Natural Sciences, Padjadjaran University, Sumedang, 45363, Indonesia

*Corresponding author: maulana19004@mail.unpad.ac.id

(Received 04 March 2023; in revised from 11 April 2023; accepted 06 July 2023)

DOI : 10.32693/bomg.38.1.2023.818

ABSTRACT: The acoustic impedance inversion seismic method, carried out at the "EL" well in East Java, provides a description of the physical properties of subsurface rocks. This method involves identifying rock layers, lithology types, porosity values, the presence of hydrocarbons, and fluids in the target zone using both well data and integrated seismic data. The data processing included the cross-plotting of acoustic impedance (AI) with gamma ray logs, porosity logs, and resistivity logs. We integrated seismic and well data, picked horizons, and created AI inversion models. The based model inversion technique was used to compare the synthetic model with the seismic data, aiming to obtain an AI value that closely represents the actual model. AI seismic inversion effectively separates lithological boundaries vertically and laterally, based on the selected picking horizon and created model. To enhance understanding of the lithology and hydrocarbon prospect zone in the study area, a cross-plot analysis was used to correlate the seismic inversion model. The results reveal that the study area represents a hydrocarbon prospect zone, with reservoir rocks consist of coral and foram at a depth range of 2320 - 2430 ft.

Keywords: acoustic impedance (AI), seismic inversion, lithology, hydrocarbon prospect zone

ABSTRAK: *Metode seismik inversi impedansi akustik pada sumur "EL", Jawa Timur dapat menunjukkan gambaran sifat fisis batuan bawah permukaan melalui identifikasi lapisan batuan, jenis litologi, nilai porositas, keberadaan hidrokarbon, dan dan fluida pada zona target dari data sumur dan data seismik yang diintegrasikan. Pengolahan dibuat dengan cross plot impedansi akustik (IA) terhadap log gamma ray, log porositas, dan log resistivitas, pengintegrasian data sumur dan data seismik, picking horizon, hingga pembuatan model inversi IA. Based model inversion digunakan untuk membandingkan model sintetik dengan data seismik sehingga didapatkan nilai IA yang mendekati model sebenarnya. Hasil inversi seismik IA dapat memisahkan batas litologi secara vertikal maupun lateral berdasarkan picking horizon dan model yang dibuat. Model inversi seismik kemudian dikorelasikan dengan crosplot sehingga dapat diketahui litologi dan zona prospek hidrokarbon pada daerah penelitian. Hasil inversi seismik menunjukkan bahwa daerah penelitian merupakan zona prospek hidrokarbon dengan batuan reservoir berupa coral dan foram pada kedalaman 2320-2430 ft.*

Kata Kunci: *Impedansi Akustik (IA), seismik inversi, litologi, zona prospek hidrokarbon*

INTRODUCTION

"EL" well is an oil and gas exploration field located in East Java Province near the North Sea. Two crossover lines at the well location are used to identify the reservoir zone. Geologically, the study area is an area composed of several formations including the Ngrayong formation, Tuban formation, and Kujung formation. The Ngrayong Formation originates from the Middle Miocene period with constituent rocks in the form of sandstone, shale, lignite, calcarenite inserts, limestone, and brown carbonate-shale. The Tuban Formation originates from the Early Miocene period which is composed of clay rock, limestone, arenitic limestone inserts, coral, algae, light gray marl, and foram. The Kujung Formation originates from the Oligocene period with layers of brown clay, limestone inserts, hard coral, large foram, layered gray marl, limestone inserts, and algae (Pringgoprawiro, 1983; Triwibowo and Santoso, 2007). Stratigraphy within the study area, especially in the Kujung formation area, has potential as a hydrocarbon prospect azone for locating reserves. Seismic inversion modeling is intended to be able to identify lithology and the existence of reservoirs in the study area (Pratiwi, 2018). The result of seismic inversion model will be correlated with the references used to ensure accurate interpretation and analysis, aligning with the actual conditions of the study area.

Seismic Inversion Method

The seismic inversion method is a geophysical technique used to create a subsurface model by integrating well data with seismic data, which is used as a control and input data (Aina, 2017). The data integration is done using the seismic inversion method of Acoustic Impedance (AI). The AI method provides information about the physical properties of subsurface reservoir rocks through the results of geological cross-sections to identify lithology and the distribution of reservoir distribution in the target area (Putri and Santosa, 2014).

Acoustic impedance (AI) is determined by multiplying the seismic wave velocity with the rock density values. AI is a physical parameter that is affected by lithology, fluid content, porosity, layer depth, pressure, and temperature. This makes AI an essential tool for determining indicators such as lithology types, types of hydrocarbon, rock porosity values, lithology mapping, and distribution of hydrocarbon within the reservoir zone (Pratiwi, 2018).

$$AI = V.\rho \quad \ldots\ldots\ldots (1)$$

AI is acoustic impedance ((ft/s).(g/cc)), ρ is rock density (g/cc), and V is seismic wave velocity (ft/s). The AI value indicates the hardness level of a rock, the higher the AI value, the harder the rock will be compressed, while the lower the AI value indicates the softer and more easily compressible rock.

The study uses post-stack data with model-based inversion to obtain a synthetic geological model that represents the actual subsurface model. The synthetic model is then compared with seismic data that is iteratively updated to obtain a match close to seismic data based on error and correlation values (Abigail, 2017).

Inversion Parameters

In the model-based inversion process, the hard constraint method is used by determining the lower and upper values to minimize the error and maximize the correlation. Some other important parameters:

- Single Values, set a single value that is used as an absolute limit to review the suitability of the final result that deviates from the initial estimate. Hard constraints can also be defined as the percentage difference from the initial model (Putri, 2014).
- Average Block Size refers to a one-dimensional unit of time in the model. It represents a series of layers of equations with a thickness measured in milliseconds, controlled by the average block parameter. This model can modify how thick the layer is displayed during the inversion process. The block value will affect the appearance of the data speed structure. Smaller block intervals result in increased time and data resolution in the inversion (Arifien, 2010).
- Prewhitening, is a deconvolution step used to obtain reflection coefficient values by dividing the seismic data with the wavelets. However, the inversion process can become unstable if the result of the seismic data divided by wavelet is zero, or if the bandlimited wavelet itself has zero values. To solve this problem, the wavelet frequency's amplitude can

Table 1. Well logging of hydrocarbon rocks

Hydrocarbon Rocks	Potential identification	Shale/non-shale zone	Density (g/cm³)	Resistivity (Ω.m)	Porosity (%)
Limestone	Reservoir rock, dim spot	Non-shale	1.93 to 2.9[(a)]	50 – 4 x 10^{2}[(e)]	0 – 20[(c)]
Sandstone	Reservoir rock, bright spot	Non-shale	1.61 to 2.76[(d)]	8 – 4 x 10^{3}[(e)]	5 – 35[(c)]
Shale	Cap rock	Shale	1.77 to 3.2[(d)]	20 – 2 x 10^{3}[(e)]	0 – 10[(c)]
Clay	Maturation rock	Non-shale	1.63 to 2.6[(d)]	1 – 100[(e)]	40 – 80[(b)]

[(a)]Telford et al. (1990); [(b)]Neuzil (1994); [(c)]Jasim et al. (2018); [(d)]Arisona et al. (2018); [(e)]Ozegin and Okolie (2018)

be increased by 1% of its maximum height (Arifien, 2010).

- Number of Iterations relates to the process of creating a model that aims to minimize the error value through iteration. Increasing the number of iterations allows for achieving a smaller error value with reduced errors. While the error value differs between iteration 0 and iteration 10, there are instances where increasing the iteration value does not impact the error value (Arifien, 2010).

Petrophysics

The petrophysical analysis is one of the processes to determine the characteristics of the reservoir. This is done by determining the lithology, porosity, water saturation, and permeability of the subsurface rock layers (Maulana, 2016). Identification is carried out through the type of well logging method on well data. The gamma ray log differentiates between permeable and impermeable layers, the density log and the neutron log calculates the porosity of the rock layers, and the resistivity log determines the water saturation of the rock layers (Maulana, 2016). Petrophysical analysis is used to determine geological formations that can identify potential hydrocarbon zones in the field. The principle of this analysis involves obtaining subsurface data through the process of well logging in drill holes or exploration wells.

Well Logging

In principle, well logging works by recording the response given through a log tool as it enters the well. The recording is based on the differences in physical and fluid properties contained in the rock. This recorded response is then displayed in the form of a curve, which indicates the condition of the rock formation under the well, including lithology and fluid characteristics. These recorded curves are then interpreted to determine reservoir layers such as hydrocarbon or reservoir spreading zones (Aprilia, 2018). Determination of hydrocarbon targets needs to be done in order to identify the depth and the indications of a prospective zone. Table 1 is usually used as a reference for well logging analysis to identify reservoir target zones with rocks and log values for constructing a hydrocarbon system.

METHOD AND MATERIAL

Data

- The seismic data used is 2D post-stack time migration (PSTM) with a sampling rate of 2 ms and normal polarity which is assumed to be data that has gone through the processing step.
- Primary data includes gamma ray logs, resistivity logs, neutron logs (NPHI), and density logs (RHOB) of the "EL" wells 46A line and 59B line in northern sea, East Java.
- Secondary data consists of master log data of the Kujung "EL" formation well in the northern sea of East Java.

Data processing

The steps involved in seismic data processing include the integration of well and seismic data, followed by the construction of an inversion model, which is then analyzed and interpreted. The outcome of data processing is a 2D inversion seismic model, supported by both well data and seismic data from the "EL" well in East Java. Data processing is carried out to determine the hydrocarbon zones based on differences in AI values. The systematic work in this study is divided into several main step including sensitivity analysis, well-to-seismic tie,

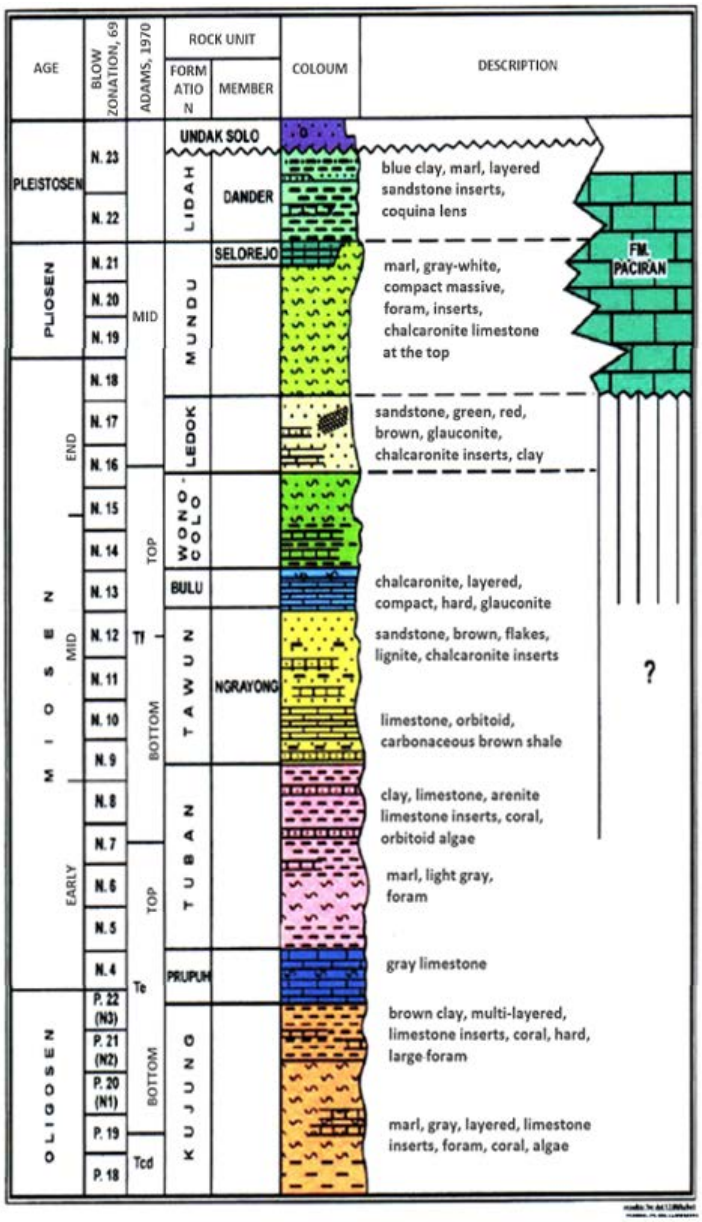

Figure 1. East Java stratigraphic column (Pringgoprawiro, 1983)

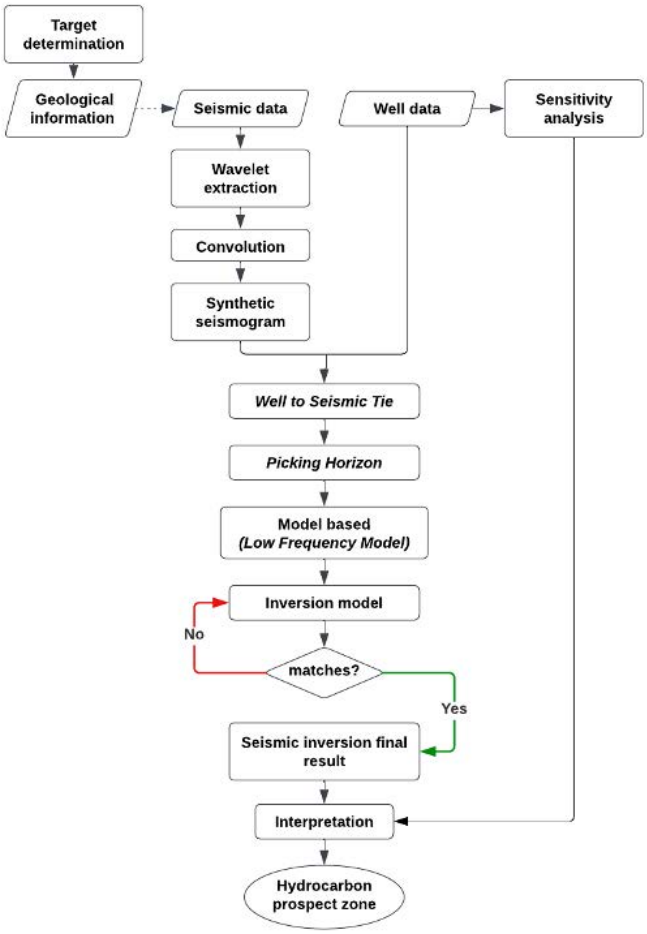

Figure 2. Research Flowchart

picking horizon, synthetic modeling, and the final seismic inversion model. The stages are shown in Figure 2.

During the sensitivity analysis, a cross plot of variables such as gamma ray, porosity, and p-impedance was conducted to observe their correlation with the type of hydrocarbon rock in the "EL" study area. These variables are indicative of the rock content in the area. This stage aids in the interpretation of seismic inversion results once the model has been created.

The well-to-seismic tie is conducted to determine seismic parameters such as phase, polarity, and frequency by binding well data based on depth to seismic data based on time (Abigail, 2017). Binding is carried out on logs used in processing including Gamma Ray (GR) logs, Density logs (RHOB), Neutron Porosity (NPHI) logs and Resistivity logs. In addition, check shot binding is carried out as an adjustment of travel time with depth which is then processed to obtain p-waves for check shot and their corrections.

Picking Horizon is utilized to create a geological cross-sectional model, which is then applied in generating maps by laterally adjusting the seismic data sections, revealing differences and inconsistencies in the sections. The process of picking involves examining the continuity of the cross-sectional layers as the boundaries of each layer.

The purpose of creating of a frequency-based model is to demonstrate the correlation between synthetic sections and bound seismic data sections. The correlation is reviewed based on error values and their corrections. A good model is shown with a small error value and high correction through both hard frequency and soft frequency review.

The final seismic inversion results will be obtained from the suitability of the model with the actual cross section. This will produce filtered colors that align with the selected picked horizons. The results are shown as a colored cross section with a corresponding color bar description indicating rock types based on the impedance value. Based on the obtained results, an interpretation of the impedance value and cross plot is carried out as to reinforce the analysis.

RESULTS AND DISCUSSION

The well data is useful for identifying the initial presumptive targeting of hydrocarbon. Figure 3 presents information on the well data in the Kujung formation. The study area exhibits a permeable (non-shale) layer, as indicated by determinating deflection of the maximum and minimum gamma ray log values in the data. In addition, the cross plot derived from the RHOB log and NPHI log indicates the presence of fluid in the Kujung formation. The resistivity log in the well data shows indications of non-resistive layers, which suggest the presence of non-resistive hydrocarbon with low resistivity values. The non-resistive layer point to the hydrocarbon target zone with a low resistivity (Table 1).

Sensitivity Analysis

Sensitivity analysis through cross plots is aimed at obtaining lithological characteristics and the distribution of reservoir zones or interest zones (Malik et al., 2018). Cross plots were performed on P-Impedance vs Gamma Ray, P-Impedance vs Porosity, and P-Impedance vs Resistivity parameters.

Figure 4 shows plot of the sensitivity analysis of the P-Impedance log to the Gamma Ray log. This cross plot is useful for identifying shale and non-shale lithologies based on the amounts of radioactive elements they contain. The P-Impedance value plays a significant role in determining the hardness or brittleness of rocks. The hardness of a rock can be identified by increasing the p-impedance value (Subakti, 2020), while decreasing the p-impedance value causes the rock to become more brittle. The determination of rock lithology in the GR log is influenced by the intensity of radioactive elements in the form of Uranium (U), Thorium (Th), and Potassium (K) (Budi and Yatini, 2021). The relationship between the

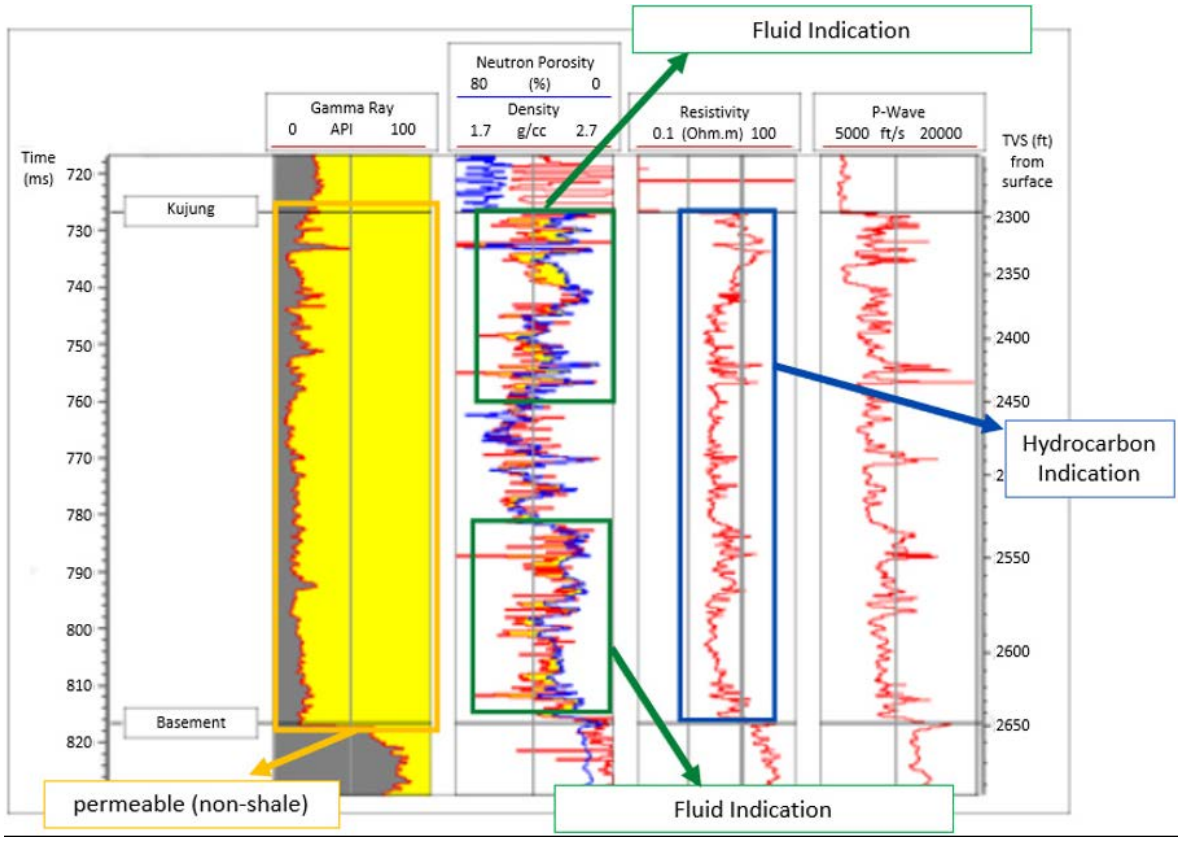

Figure 3. Well data of Kujung formation

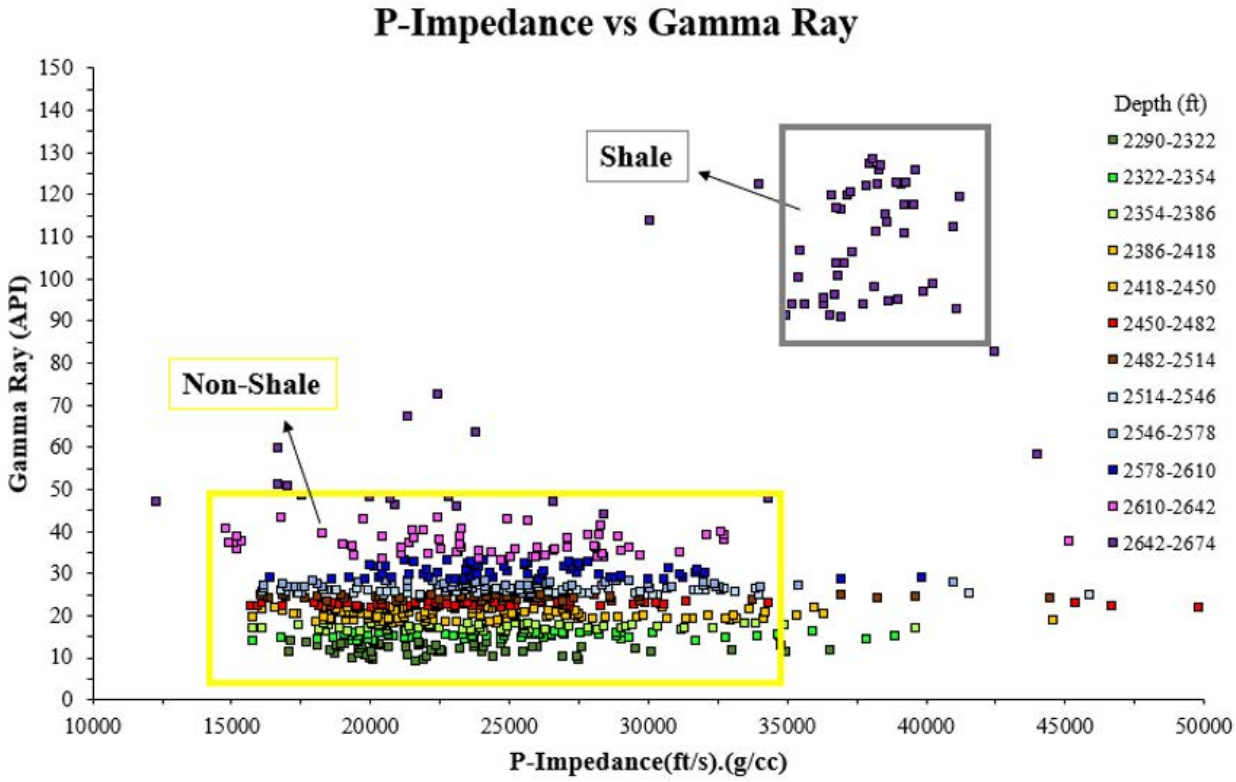

Figure 4. P-Impedance vs. Gamma Ray Cross plot of Kujung formation

intensity of radioactive elements recorded in rocks is

directly proportional to the resulting gamma ray value. Rocks containing an abundance of radioactive elements, such as impermeable layers (shale), exhibit high gamma ray values, while permeable layers (non-shale) with fewer radioactive elements have lower gamma ray values. In Figure 5, the p-impedance values are obtained in the range 15000–35000 (ft/s).(g/cc) with a GR value of 10–50 API marked in yellow. This indicates that the rock are brittle with a permeable layer, representing non-shale rock. In addition, a gray area is obtained with a p-impedance values of 35000–42500 (ft/s).(g/cc) and GR values ranging from 90–130 API which is indicated as shale rock.

The reservoir zone can be determined through a cross plot between P-Impedance and Porosity. The cross plot was carried out only in non-shale areas suspected to be potential hydrocarbon prospects (Figure 5). Porosity helps determine the volume of pore space in rocks that can be filled with fluid. The results of the p-impedance to porosity cross plot have an inverse relationship where the lower the p-impedance value, the higher the rock porosity value, so the rock may be filled with more fluid (Hapsari, 2018). Classification of effective porosity indicate a rock's ability to hold or accommodate fluid, where porosity rocks classified excellent if the values more than 25%, verry good at 20-25%, good at 15-20%, fair at 10-15%, poor at 5-10%, and negligible at 0-5% (Koesoemadinata, 1978). The relationship between p-impedance and porosity (Figure 5) shows the presence of porous prospect zones, porous zones, and tight non-prospect zones. The prospect zone on the cross plot is represents an area where the rocks are not too hard and very good porosity, making them suitable for storing fluids. The prospect zone has a P-Impedance values ranging from 15000–18000 (ft/s).(g/cc) and an effective porosity of 22–38%. In contrast, there is a porous zone with harder rocks compared to the porous prospect zone, having p-impedance values from 15000 (ft/s).(g/cc) to 28000 (ft/s).(g/cc) and effective porosity above 20%. The cross plot results also show a tight non-prospect zone with an effective porosity of 0-20% and a p-impedance value ranging from 22200-35000 (ft/s).(g/cc).

The cross plot between P-Impedance and Resistivity log is used to distinguish different rock lithologies in the Kujung formation. Cross plot is carried out on the prospect zone at specific range from 725 ms to 825 ms to simplify the interpretation of hydrocarbon zones according to Table 1. The determination of rock types is based on the effective porosity values which is can show fluid rock quality and accumulation potential in the prospect zone. The measured resistivity value on the log will be identified to determine the nature of the rock and pore fluid through its electrical resistance properties. The presence of fluid with good conductivity in the prospect zone leads to lower measured resistivity values (Aprilia, 2018). Figure 6 displays the results of the P-Impedance vs porosity cross plot which is interpreted into the lithology of rocks that comprise the Kujung formation in the study area. The cross plot allows for classification between the reservoir target, limestone, and clay based on correlations between shale/non-shale zone, porosity, p-impedance, and resistivity parameter values. The reservoir target is characterized as shale zone with good or higher porosity and low resistivity, similar to limestone, but with lower rock hardness. However, the reservoir target has lower rock hardness than limestone, whereas the tight clay characterized as non-shale zone with poor or lower porosity, dominant high resistivity, and harder rock compared to the reservoir target and

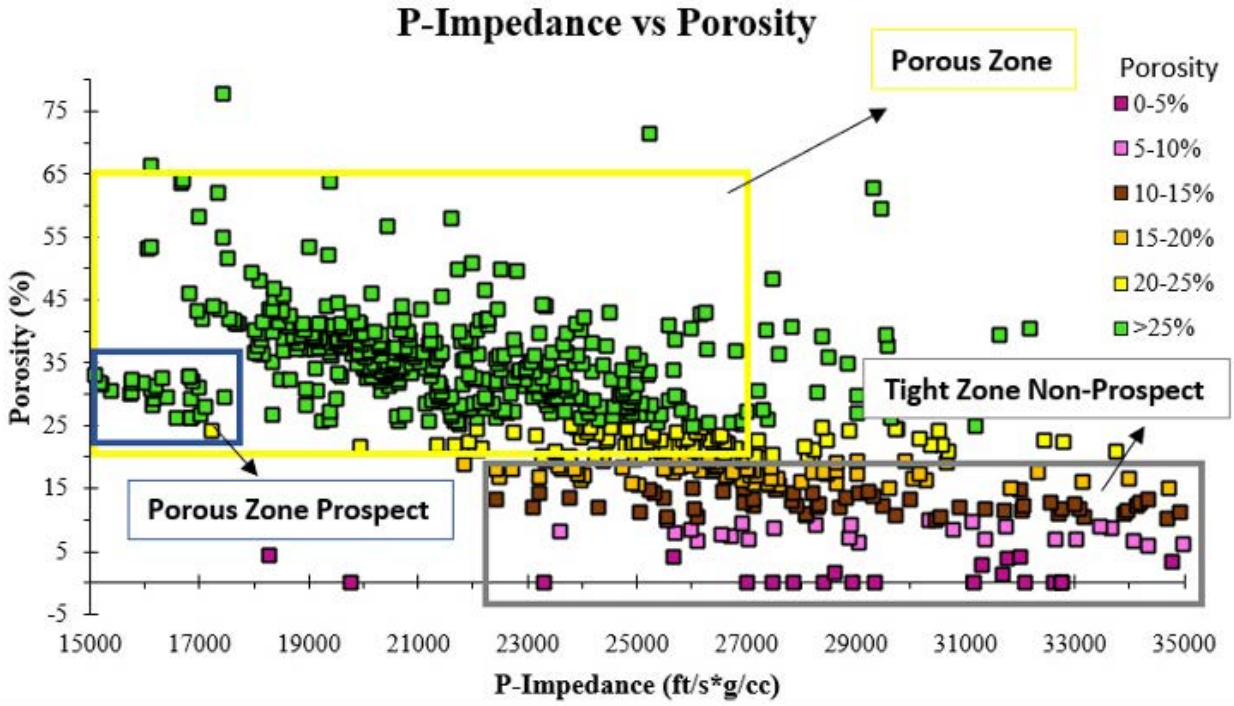

Figure 5. P-Impedance vs. Porosity Cross plot of Kujung formation

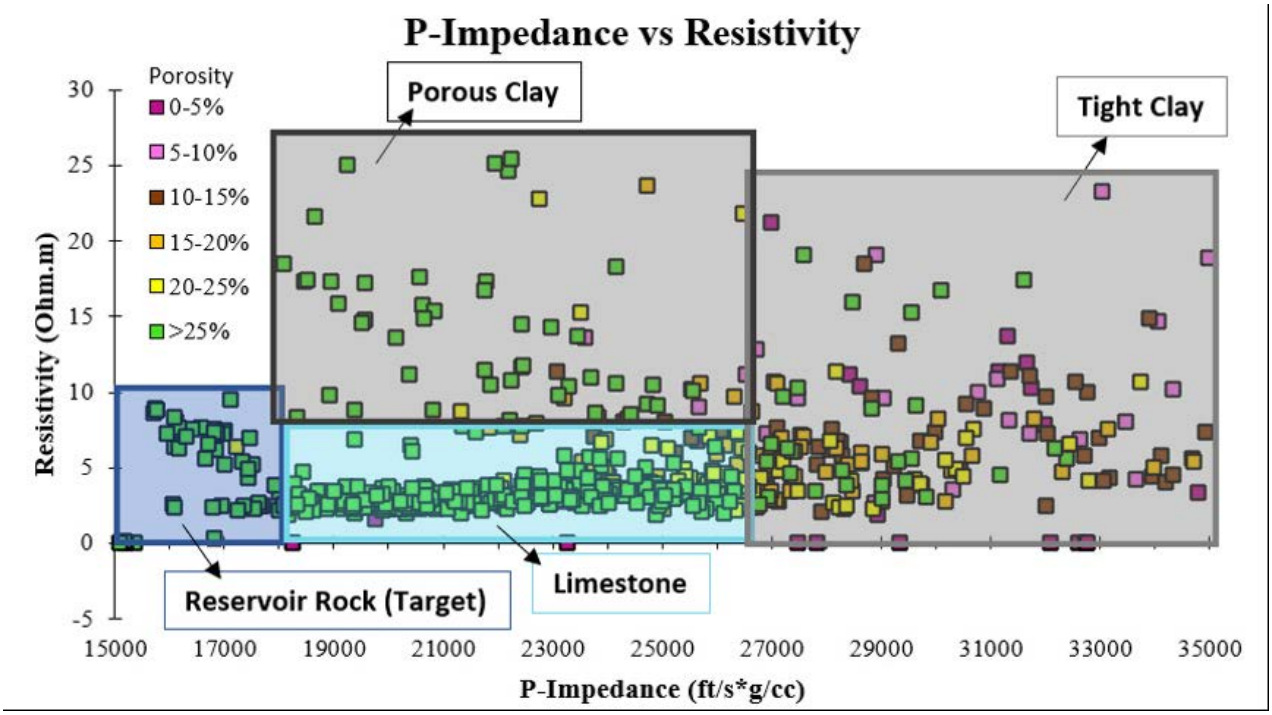

Figure 6. Cross plot of P-impedance vs. Resistivity of Kujung formation at tunning thickness area.

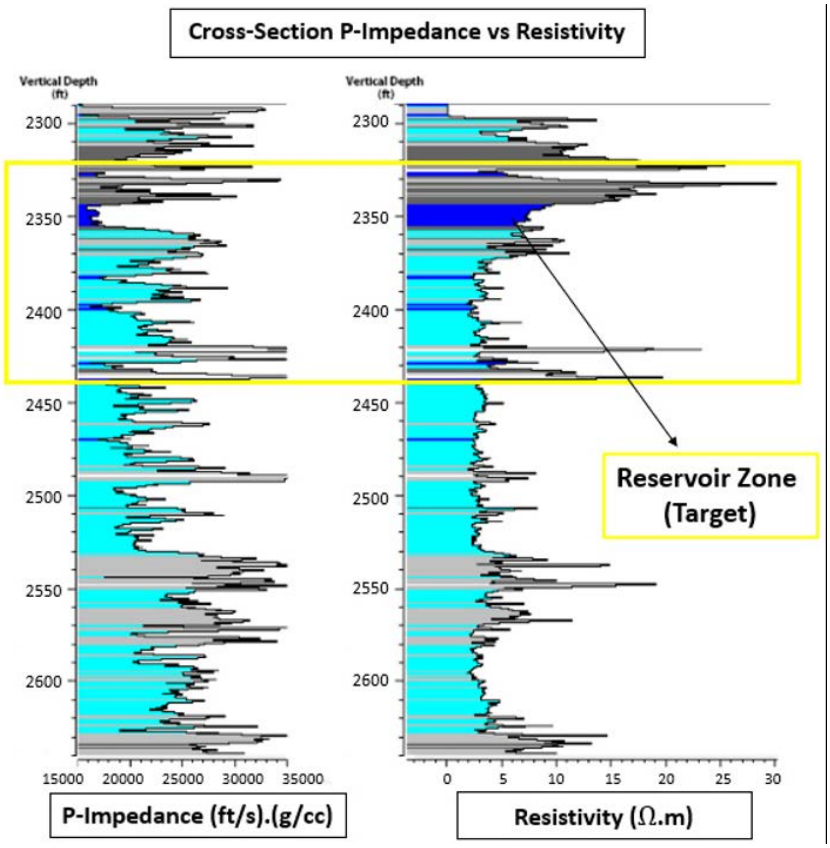

Figure 7. Cross section result of P-Impedance Vs. Resistivity cross plot

limestone. Based on the cross plot results, the lithology of the Kujung formation is composed of reservoir rock, limestone, and clay rocks. The reservoir rock in the cross plot has a resistivity value of 0–10 Ω.m and a P-Impedance of 15000-18000 (ft/s).(g/cc), including porous rock indicated by coral and foram. There are also limestones with a resistivity value of 0–15 Ω.m and a p-impedance of 18000-26500 (ft/s).(g/cc). In addition, the clay lithology is

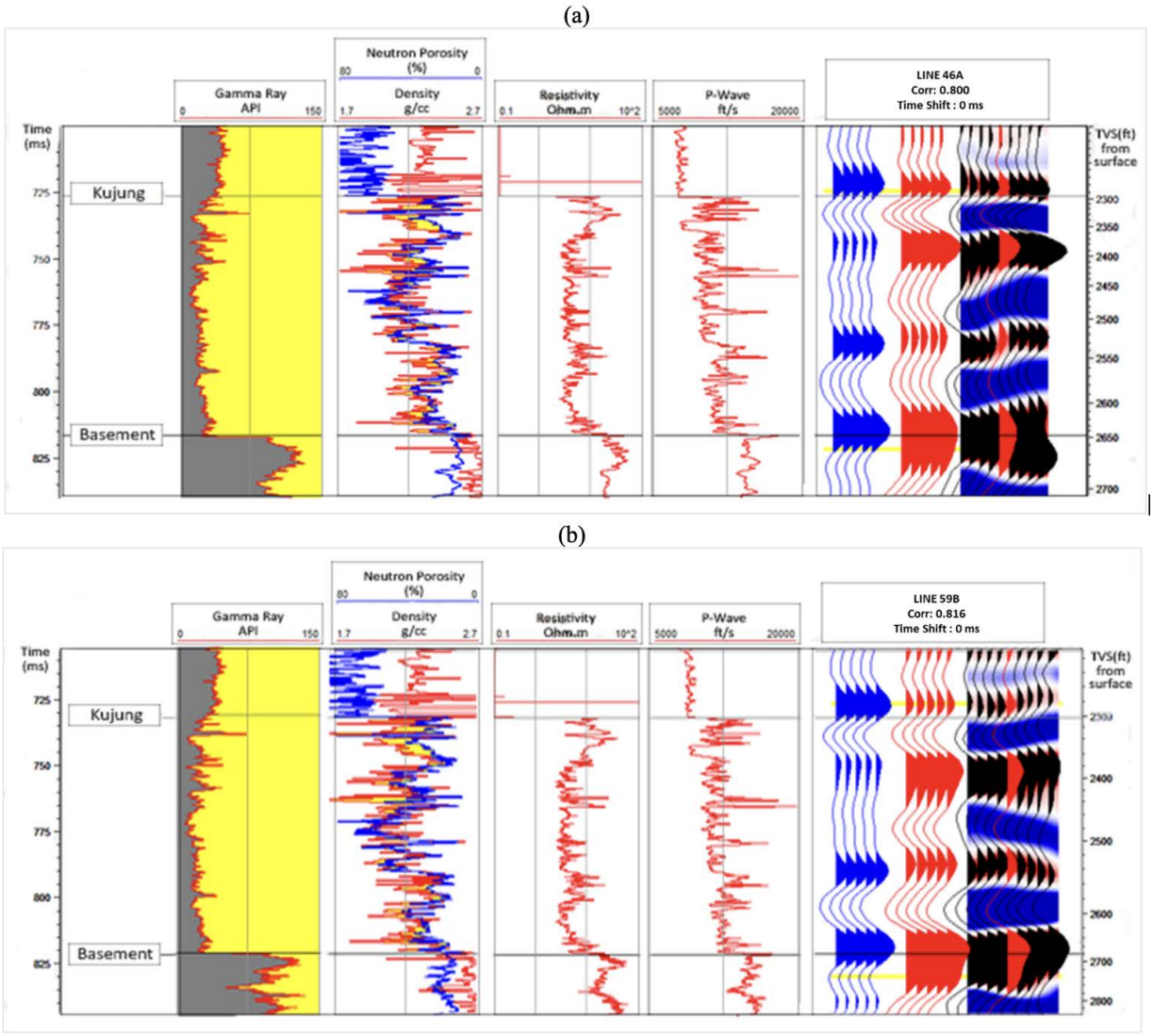

Figure 8. Well seismic result, (a) line 46A; (b) line 59B

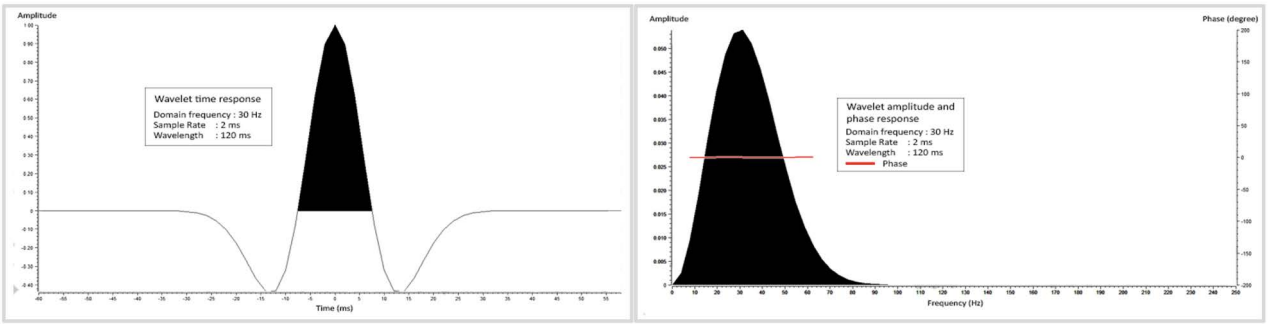

Figure 9. Estimated ricker wavelet with wavelength of 120 ms

divided into porous clay with a resistivity value of 8–26 Ω.m and a p-impedance of 18000–25000 (ft/s).(g/cc), and tight clay with a resistivity value of 0–15 Ω.m and a p-impedance of 25000–35000 (ft/s).(g/cc).

The interpretation results of the cross plot (Figure 6) are presented in Figure 7, showing the well data cross-section to determine the depth of the hydrocarbon prospect zone. The correlation between p-impedance and resistivity based on depth indicate that the reservoir target is at depth range of 2320-2430 ft.

Well to Seismic Tie

The well-to-seismic tie is carried out before the picking horizon stage to enable the integration of time-based seismic data depth-based well data. The correlation values for the well-to-seismic tie in lines 46a (Figure 8a)

and 59b (Figure 8b) using wavelet ricker with frequency domain 30 Hz and wavelength 120 ms (Figure 9) are 0.800 and 0.816, respectively.

Picking Horizon

Picking the horizon is performed once the horizon of interest has been identified by analyzing the character or polarity changes in the seismic trace. Positive polarity indicates an increase in acoustic impedance, while negative polarity indicates a decrease in acoustic impedance. The horizon is identified as a reflection marking the boundary between two materials with different acoustic properties. The picking of horizons is specifically focused on lines 46A and 59B as part of the seismic inversion processing area.

Seismic inversion model

Model-based inversion processing is used to determine error and correlation values while filtering frequency as tunning thickness. Filtering helps select frequencies within the desired range, enabling the synthetic seismic model to closely resemble actual conditions based on error values and their correlations. In this model, the frequency used for tunning thickness ranges from 725 ms to 825 ms, indicating the reservoir target zone with a minimum thickness of 83.35 ft.

The results of model-based inversion (Figure 10) for lines 46A and 59B show favorable errors and correlations. The initial modeling includes the inversion log model, synthetic and seismic models, and model error values. The inversion log error value is useful for determining the error rate of the inversion log model compared to the actual AI log. Moreover, the correlation between synthetic and seismic modeling proves to identify the compatibility

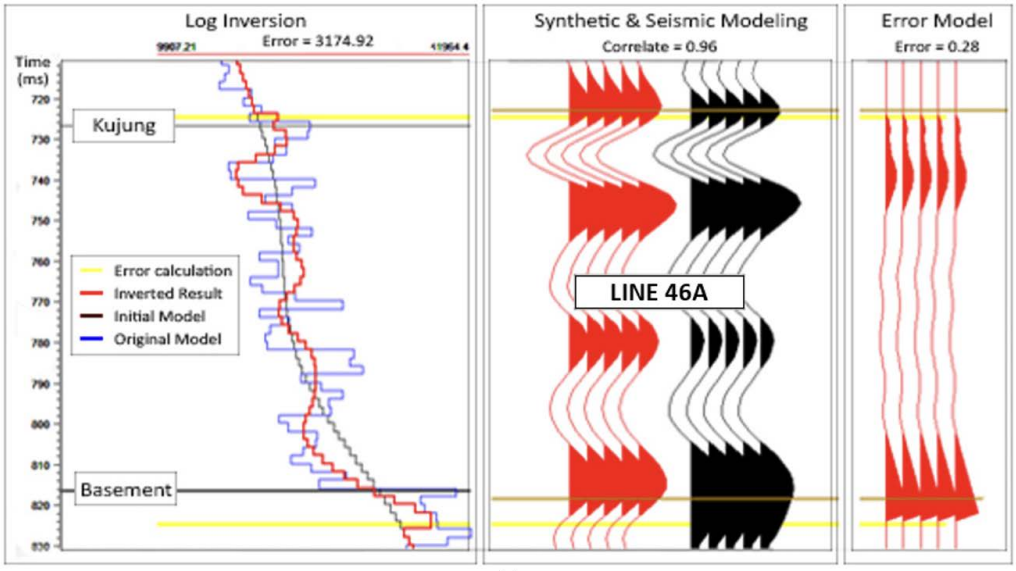

(a)

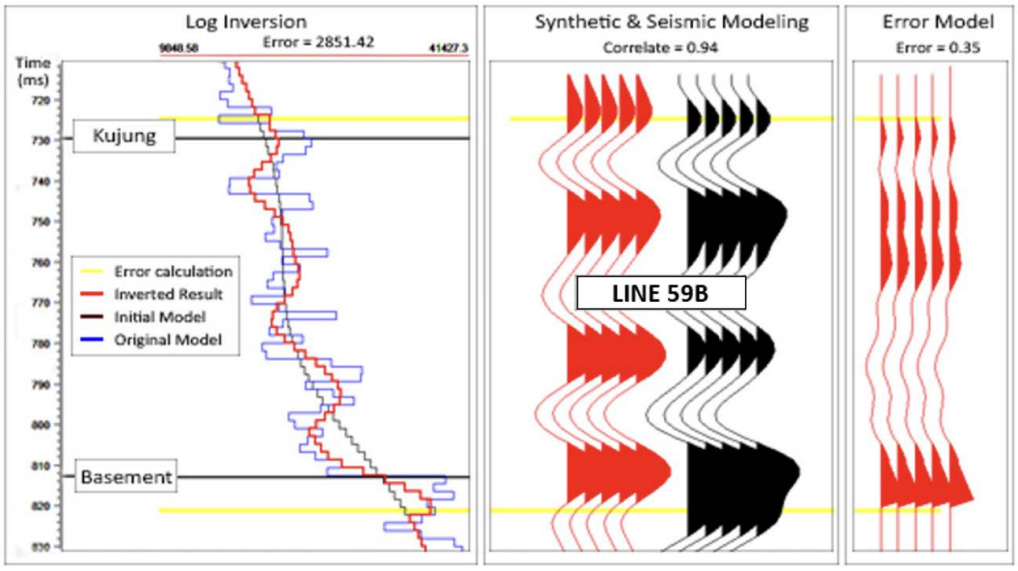

(b)

Figure 10. Model-based inversion analysis: (a) line 46A; (b) line 59B

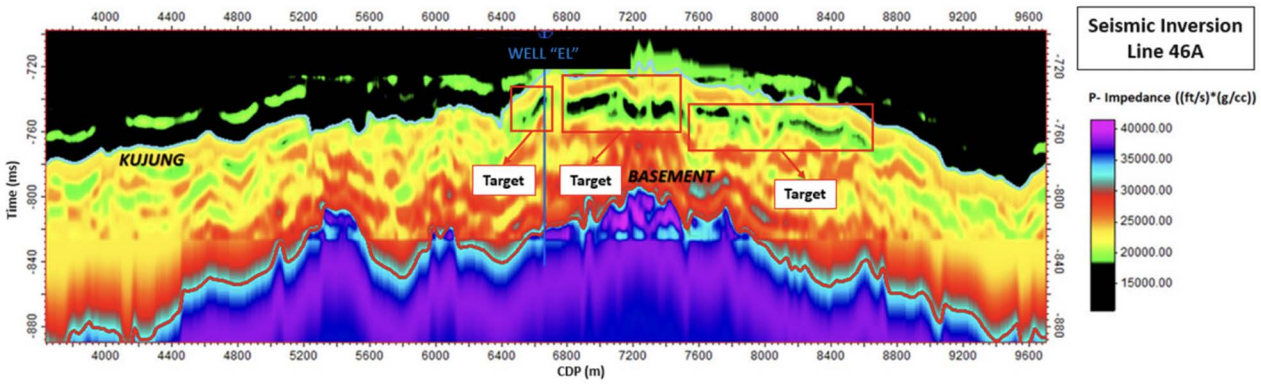

(a)

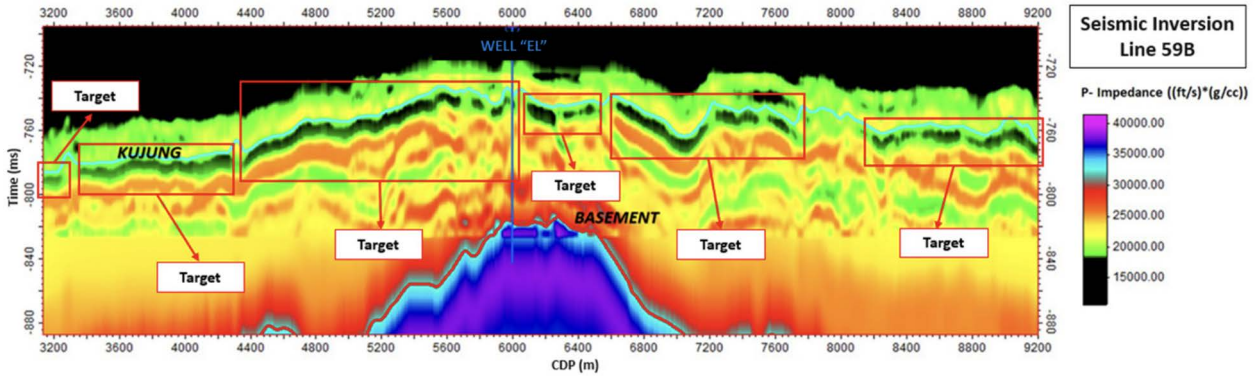

(b)

Figure 11. Acoustic Impedance Inversion (AI) with an overview of the prospect zone, (a) line 46A; (b) line 59B

between the modeling results (red color) and the actual seismic trace (black). The error model is used to determine the error level of the inversion modeling results. For line 46A (Figure 10a), the log error value was 3174.92, the model error was 0.28, and the correlation was 0.96. For line 59B (Figure 10b), the log error value was 2851.42, the model error was 0.35, and the correlation was 0.94. These values represent an optimal match between the model and the actual seismic trace. The completed model is then subjected to AI seismic inversion to accurately identify reservoir characteristics below the surface.

Seismic inversion AI is strongly influenced by changes in rock density values and seismic wave velocity. These changes will affect the value of the reflection coefficient obtained. The high or low amplitude of the seismic trace shows the value of the reflection coefficient at the layer boundary, as the seismic trace results from a convolution between the reflection coefficient and the wavelet. The amplitude shows the degree of differences in AI values derived from the velocity and rock density of each layer.

The results of AI inversion in the "EL" well, East Java on lines 46A and 59B, reveal the characteristics of the hydrocarbon reservoir in the Kujung formation. The selection is based on the correlation results of P-Impedance with Gamma Ray, Porosity, and Resistivity in the cross plot analysis with acoustic impedance values ranging from 15000–18000 (ft/s).(g/cc), indicating a porous reservoir zone, known as reservoir rock (Figure 4; Figure 5; and Figure 6). The results of seismic inversion can be seen in the distribution of acoustic impedance values (AI) in Figure 11. The character of the reservoir can be identified from the acoustic impedance values in the seismic section. The cross-section shows the inversion results based on the picked and correlated seismic data of the Kujung formation layer with the "EL" well. The P-Impedance values from the inversion results are correlated with cross plot analysis and well data to determine the litho logy and characteristics of the hydrocarbon. Correlation results in lines 46A (Figure 11a) and 59B (Figure 11b) are marked in black, distinguishing the rock lithology and fluid content in the formation. The black color represents the prospective zone of hydrocarbon contained in the Kujung Formation. The correlation at well log interpretation (Figure 3), p-impedance cross plot correlation (Figure 4, 5, 6), cross-section p-impedance vs resistivity at tunning thickness (Figure 7), and AI inversion model (Figure 11) show the indication of a hydrocarbon prospect zone in the Kujung formation at a depth of 2320–2430 ft with a P-Impedance value of 15000–18000 (ft/s).(g/cc). The correlation demonstrates the similarities between processing data results and geological regional at Kujung Formation. In addition, the very good effective porosity and low resistivity values

suggest that the rock is part of the reservoir rock and has very good fluid storage capabilities. The correlation of well and seismic data shows that the hydrocarbon prospect zone in the Kujung formation is interpreted as a reservoir rock with coral and foram as the other constituent rocks.

CONCLUSIONS

Cross plot analysis of P-impedance, gamma ray, porosity, and resistivity parameters iusing well data allows for the differentiation of shale, non-shale, porous zone, and tight zone layers. This analysis helps in determining the lithology characteristics and distribution of hydrocarbon reservoirs. The lithology of study area composed of shale, clay, limestone, coral, and foram. Seismic inversion AI results obtained from the correlation of well data and seismic data on the Kujung formation reveal the presence of a reservoir prospect zone with coral and foram lithology with impedance value ranging from 15000-18000 (ft/s).(g/cc) at a depth of 2320–2430 ft.

ACKNOWLEDGEMENTS

This study was conducted using data from the Marine Geological Institute. The author would like to thank to Marine Geological Institute for providing the opportunity to conduct this study. Special thanks go to the team members for their cooperation in working on the article and processing seismic data.

REFERENCES

Abigail, N., 2017. *Identifikasi Persebaran Litologi Reservoir menggunakan Analisis Multi-Atribut Seismik pada Lapangan Stratton, Texas Selatan.* Thesis. Institut Teknologi Sepuluh Nopember, Surabaya. 108p.

Aina, Z., 2017. *Karakterisasi Reservoir Dengan Menggunakan Inversi Simultan Dan Analisis Lambda-Mu-Rho Untuk Mengidentifikasi Persebaran Zona Potensial Reservoir Karbonat Formasi Baturaja Lapangan "Sukses" Cekungan Sumatra Selatan.* Thesis. Universitas Brawijaya, Surabaya.75p.

Aprilia, R., Dewanto, O., Karyanto., and Ramadhan, A., 2018. *Analisis Petrofisika dan Penyebab Low Resistivity Zone berdasarkan data Log, SEM, XRD, dan Petrografi pada Lapangan X Sumatera Selatan*. Jurnal Geofisika Eksplorasi, 4(2), 144-158.

Arifien, H., 2010. *Inversi Seismik Berbasis Model untuk Karakterisasi Reservoir: Studi Kasus Haurgeulis.* Thesis. Universitas Indonesia, Jakarta. 43p.

Arisona, A., Nawawi, M., Khalil, A.E., and Abdulrahman, A., 2018. *Assessment of Microgravity Anomalies of Soil Structure for Geotechnical 2D Models.* Journal of Engineering, Environment, and Technology, 3(3), 151-154. https://doi.org/10.24273/jgeet.2018.3.3.2058.

Budi, Y.S., and Yatini, Y., 2021. *Korelasi Log dan Data Laboratorium untuk menentukan Kualitas Batubara di daerah Bangko Barat, Tanjung Enim, Sumatera Selatan.* Jurnal Geosaintek, 7(1), 1-8.

Hapsari, H.E., Lestari, I., and Samsidar, 2018. *Interpretasi Akustik Impedansi (AI) menggunakan Data Seismik dan Data Sumur untuk menentukan Zona Prospek Hidrokarbon.* Komunikasi Fisika Indonesia, 15(2), 135-138.

Jasim, A., Hemmings, B., Mayer, K., and Scheu, B., 2018. *Groundwater Flow and Volcanic Unrest.* https://link.springer.com/chapter/10.1007/11157_2018_33.

Koesoemadinata, R.P., 1978. Geologi minyak dan gas bumi. ITB, Bandung. 296 p.

Malik, R., Mulyatno, B.S., and Dewanto, O., 2018. *Karakterisasi Reservoar menggunakan Metode Inversi AI (Acoustic Impedance) dan Metode Seismik Multiatribut Pada Lapangan "RM", Formasi Talang Akar Cekungan Sumatera Selatan.* Jurnal Geofisika Eksplorasi. 3(1).

Maulana, M.I., 2016. *Analisis Petrofisika dan Perhitungan Cadangan Lapangan "Kaprasida" Formasi Baturaja Cekungan Sumatera Selatan*. Thesis. Institut Teknologi Sepuluh Nopember, Surabaya. 73p.

Neuzil, C.E., 1994. *How Permeable are clays and shales?*. Water Resour. 30, 145-150.

Ozegin, K.O., and Okolie, E.C., 2018. *Application of Combined Electrical Resistivity Techniques for Subsurface Characterisation and Groundwater Resource Development in Okpella, Edo State Nigeria.* Nigerian Institute of Physics. 69-83.

Pratiwi, I.W., 2018. *Aplikasi Atribut Seismik dan Inversi Acoustic Impedance (AI) untuk Prediksi Penyebaran Reservoar Batupasir pada Lapangan "Kanaka" Formasi Bekasap Cekungan Sumatra Tengah.* Thesis, UPN "Veteran" Yogyakarta, Yogyakarta. 95p.

Pringgoprawiro, H., 1983, *Cekungan Jawa Timur Utara Suatu Pendekatan Baru.* Doctor Disertation, Institut Teknologi Bandung, Bandung. 239p. Unpublished.

Putri, I.A., 2014. *Integrasi Seismik Inversi Acoustic Impedance (AI) dan Elastic Impedance (EI) untuk Karakterisasi Reservoir Studi Kasus Lapangan "MUON".* Thesis. Institut Teknologi Sepuluh Nopember, Surabaya. 101p.

Putri, S.H., and Santosa, B.J., 2014. *Aplikasi Inversi Seismik untuk Karakterisasi Reservoir lapangan "Y", Cekungan Kutai, Kalimantan Timur.* Jurnal Sains dan Seni Pomits, 3(2), 55-59.

Subakti, P.A., 2020. *Interpretasi Data Seismik 2d Formasi Kais Lapangan "X", Cekungan Bintuni, Papua, Indonesia*. Thesis. Universitas Pertamina, Jakarta. 36p.

Triwibowo, B., and Santoso, K., 2007. *Potensi dan Kualitas Batuan Formasi Kujung sebagai Batuan Induk, pada lintasan Kali Wungkal, Tuban, Jawa Timur.* Proceeding Simposium National IATMI, UPN "Veteran" Yogyakarta.

Telford, W.M., Geldart, L.P., and Sheriff, R.E., 1990. *Applied Geophysics, Second Edition.* Cambridge University Press. 770 p.

Guide for Authors - Geoscience Publications
Bulletin of the Marine Geology

Writing should be submitted according to the following restrictions:

1. Manuscript should be written in English and be submitted online via journal website http://ejournal.mgi.esdm.go.id. Online Submission will be free. The author must login in order to make submission.
2. Manuscript should contains at least 2.000 words and at least 8 pages of manuscript that including embedded figures and tables, without any appendix, and the file should be in Microsoft Office (.doc/.docx) format. It should be prepared in A4 paper (21cm x 29.7cm) using 2.5 cm for left and right margins and 2 cm for top and bottom margins, additionally the paragraph should be used 1 line spacing, 11 TNR.
3. Title, Abstract, and Keywords should be written in English
   - Abstract should be written in English and Bahasa Indonesia version
   - Title should be less than 15 words, title case, small caps, centered, bold, font type Times New Roman (TNR), font size 16, and single spaced.
   - Abstract contains neither pictures nor tables, justified, in 11 TNR, single spaced, and should not exceed 250 words.
   - Keywords contain four to six words/phrases separated with coma and should be justified, 10 TNR and single spaced.
   - Please provide all email address of all authors for our database concern, however, in the published version, only the email address of the first author will be appeared.
4. Manuscript body consists of: Introduction, Method, Result, Discussion, and Conclusion completed by Acknowledgment and References in capital and bold.
5. Heading should be made in four levels. Level five cannot be accepted.
   - Heading 1: title caps, left aligned, bold, 14 TNR, single spaced
   - Heading 2: title case, left aligned, bold, 11 TNR, single spaced
   - Heading 3: title case, left aligned, italic, 11 TNR, single spaced
   - Heading 4 is not recommended, however, it could still be accepted with the format of: sentence case, left indent 5 mm, hanging indent 5 mm, italic, 11 TNR, single spaced
   - Heading 5 cannot be accepted in the manuscript.
6. Figure and table can be either in black and white or in color, they should be clearly readable and in a proportional measure to the overall page. Caption should be numbered, in 9 TNR and single spaced. For lay outing purpose, please provide the respective captioned figure/table with extension .tif/.jpg/.jpeg within a particular folder apart from the manuscript. Please note the figure source/citation/reference if it is taken and/or modified from previous publication.
7. Mathematical equation should be clearly written, numbered orderly, and accompanied with any information needed.
8. Header and footer including page number must not be used. All hypertext links and section bookmarks will be removed from papers. If you need to refer to an Internet email address or URL in your paper, you must type out the address or URL fully in Regular font.
9. Citation and Reference. Following are the detail organization of the references guidelines:
   a. References are written in alphabetical order according to the family name of the first author.
   b. If there is more than one references made by similar author, References are arranged in order of time, and then in alphabetical order.
   c. All the references should be cited in the text. In the text, reference is cited with author family name and the year of publication. If it is written by 2 authors, the family name of both authors are noted, followed by the year of publication, if it is written by more than 2 authors, the reference is cited with the first author family name, followed by *et al.,* and the year of publication. For example: (Kennett, 1981); (Usman and Panuju, 2013); (Susilohadi *et al.*, 2009). Several references are written in alphabetical order, for example: (Kennett, 1981; Susilohadi *et al.,* 2009; and Usman and Panuju, 2013).
   d. References are consist of paper, proceeding, or book that are published, or unpublished report including internal report, dissertation, or thesis.
   e. References can be taken from website, by writing the hyperlink, and the time when it is accessed. Wikipedia, personal blog, or non scientific website is not allowed to be taken into account.

f. References should be ten references in minimum, at least two of them were published in the last five years.

g. Only the family name of the authors are written, followed by the abbreviation of their first name and middle name (if available). If the reference is written by more than one author, all authors should be written, abbreviation (e.g. dkk, *et al,* or drr) is not allowed..

h. All the information of the references must be noted, including publisher, journal volume, number (if available), and page number.

- For book, the book title should be written in italic, for example:

  Kennett, J.P., 1981. *Marine Geology.* Prentice Hall, 813p.

- For periodicals, the name of the journal should be written in italic, for example:

  Susilohadi, S., Gaedicke, C., and Djajadihardja, Y.S., 2009. Structures and sedimentary deposition in the Sunda Strait, Indonesia, *Tectonophysics,* 467 (1): 55-71.

- (Tectonophysics is the name of the journal, 467 is the volume, 1 is issued number, 55 – 71 is page number)

  Usman, E., and Panuju, 2013. Study of Gas Potency Based on Gravity Anomaly Modeling And Seismic Profile Analysis at Banggai-Sula Basin. *Bulletin of the Marine Geology,* 28 (2): 51-60.

- For edited symposia, special issues, etc. published in periodical:

  Kenneth, S. J., 2009. Marine biogeochemistry in 2025. In: D. Glickson (Editor), *Oceanography in 2025: Proceedings of a workshop.* The National Academic Press, Washington D. C.: 130 – 134.

- For websites:

  <http://palaeo-electronica.org/2003_1/benthic/issue1_03.htm> [Accessed on 30 November 2011].

- Unpublished references:

  Darlan, Y., Kamiludin, U., Kurnio, H., Rahardian, R., Hutagaol, J. P., Sianipar, A. H., and Sinaga, A. C., 2005. *Eksplorasi prospektif gas biogenik kelautan di Perairan Muara Kakap dan sekitarnya - Kalimantan Barat.* Pusat Penelitian dan Pengembangan Geologi Kelautan, Bandung, Badan Penelitian dan Pengembangan Energi dan Sumberdaya Mineral, Departemen Energi dan Sumberdaya Mineral. Internal report, 104p. Unpublished.

SERTIFIKAT

Direktorat Jenderal Penguatan Riset dan Pengembangan,
Kementerian Riset, Teknologi, dan Pendidikan Tinggi

RISTEKDIKTI

Kutipan dari Keputusan Direktur Jenderal Penguatan Riset dan Pengembangan,
Kementerian Riset, Teknologi, dan Pendidikan Tinggi Republik Indonesia
Nomor: 21/E/KPT/2018, Tanggal 9 Juli 2018
Tentang Hasil Akreditasi Jurnal Ilmiah Periode I Tahun 2018

Nama Jurnal Imiah

Bulletin of the Marine Geology

E-ISSN: 2527-8843
Penerbit: Puslitbang Geologi Kelautan, Kementerian ESDM

Ditetapkan sebagai Jurnal Ilmiah

TERAKREDITASI PERINGKAT 2

TERAKREDITASI

Akreditasi berlaku selama 5 (lima) tahun, yaitu
Volume 31 Nomor 1 Tahun 2016 sampai Volume 35 Nomor 2 Tahun 2020

Jakarta, 9 Juli 2018
Direktur Jenderal Penguatan Riset dan Pengembangan

Dr. Muhammad Dimyati
NIP. 195912171984021001

MARINE GEOLOGICAL INSTITUTE

GEOLOGICAL AGENCY
MINISTRY OF ENERGY AND MINERAL RESOURCES
Jalan Dr, Junjunan No. 236, Bandung-40174, Indonesia
http://www.mgi.esdm.go.id, E-mail: ejournal.p3gl@gmail.com

ISSN 1410 - 6175
9 771410 617003